2022-12

STEADY STATE MODELING OF WET STEAM IN A PIPING SYSTEM

Axelsson, Bror E., IV

Monterey, CA; Naval Postgraduate School

NAVAL POSTGRADUATE SCHOOL

MONTEREY, CALIFORNIA

THESIS

STEADY STATE MODELING OF WET STEAM IN A PIPING SYSTEM

by

Bror E. Axelsson IV

December 2022

Thesis Advisor:	Walter C. Smith
Co-Advisor:	Anthony J. Gannon
Second Reader:	Garth V. Hobson

THIS PAGE INTENTIONALLY LEFT BLANK

REPORT DOCUMENTATION PAGE	*Form Approved OMB No. 0704-0188*

1. AGENCY USE ONLY *(Leave blank)*	**2. REPORT DATE** December 2022	**3. REPORT TYPE AND DATES COVERED** Master's thesis

4. TITLE AND SUBTITLE STEADY STATE MODELING OF WET STEAM IN A PIPING SYSTEM	**5. FUNDING NUMBERS**
6. AUTHOR(S) Bror E. Axelsson IV	
7. PERFORMING ORGANIZATION NAME(S) AND ADDRESS(ES) Naval Postgraduate School Monterey, CA 93943-5000	**8. PERFORMING ORGANIZATION REPORT NUMBER**
9. SPONSORING / MONITORING AGENCY NAME(S) AND ADDRESS(ES) NAVSEA 08T, Washington, DC, N/A 20003	**10. SPONSORING / MONITORING AGENCY REPORT NUMBER**

11. SUPPLEMENTARY NOTES The views expressed in this thesis are those of the author and do not reflect the official policy or position of the Department of Defense or the U.S. Government.

12a. DISTRIBUTION / AVAILABILITY STATEMENT Approved for public release. Distribution is unlimited.	**12b. DISTRIBUTION CODE** A

13. ABSTRACT (maximum 200 words)

Current designs for steam piping systems are predicated on conservative deterministic design approaches to prevent the admission of moisture. This design approach may result in excess conservatism and larger, more inefficient components. During normal steady-state operations, the steam system operates with high-quality saturated steam, and moisture admission is not a concern. However, implementing design parameters for possible transient conditions can lead to components whose potential may never be fully utilized, adding inefficiencies. This effort seeks to identify features and physics of the piping system that can be used to challenge previous design criteria and show that off-design conditions for short durations can be mitigated. These types of features include the locations of piping bends and steam traps. This effort focuses on a steady state analysis of a wet saturated steam piping system and develops and implements a computational fluid dynamics (CFD) model for qualitatively evaluating the effect of droplet size and inlet quality on the behavior of a two-phase saturated steam flow. Additional modeling using TRAC/RELAP Advanced Computational Engine (TRACE) was performed to determine the code's suitability for modeling a saturated steam system. The models developed in this effort will be used as the foundation for follow-on research of transient conditions.

14. SUBJECT TERMS computational fluid dynamics, CFD, CFX, two-phase, wet steam, steam quality, wall superheat, heat transfer, condensation, TRAC/RELAP Advanced Computational Engine, TRACE	**15. NUMBER OF PAGES** 203
	16. PRICE CODE

17. SECURITY CLASSIFICATION OF REPORT Unclassified	**18. SECURITY CLASSIFICATION OF THIS PAGE** Unclassified	**19. SECURITY CLASSIFICATION OF ABSTRACT** Unclassified	**20. LIMITATION OF ABSTRACT** UU

NSN 7540-01-280-5500

Standard Form 298 (Rev. 2-89)
Prescribed by ANSI Std. 239-18

THIS PAGE INTENTIONALLY LEFT BLANK

Approved for public release. Distribution is unlimited.

STEADY STATE MODELING OF WET STEAM IN A PIPING SYSTEM

Bror E. Axelsson IV
Lieutenant, United States Navy
BS, Worcester Polytechnic Institute, 2015

Submitted in partial fulfillment of the
requirements for the degree of

MASTER OF SCIENCE IN MECHANICAL ENGINEERING

from the

NAVAL POSTGRADUATE SCHOOL
December 2022

Approved by: Walter C. Smith
Advisor

Anthony J. Gannon
Co-Advisor

Garth V. Hobson
Second Reader

Brian S. Bingham
Chair, Department of Mechanical and Aerospace Engineering

THIS PAGE INTENTIONALLY LEFT BLANK

ABSTRACT

Current designs for steam piping systems are predicated on conservative deterministic design approaches to prevent the admission of moisture. This design approach may result in excess conservatism and larger, more inefficient components. During normal steady-state operations, the steam system operates with high-quality saturated steam, and moisture admission is not a concern. However, implementing design parameters for possible transient conditions can lead to components whose potential may never be fully utilized, adding inefficiencies. This effort seeks to identify features and physics of the piping system that can be used to challenge previous design criteria and show that off-design conditions for short durations can be mitigated. These types of features include the locations of piping bends and steam traps. This effort focuses on a steady state analysis of a wet saturated steam piping system and develops and implements a computational fluid dynamics (CFD) model for qualitatively evaluating the effect of droplet size and inlet quality on the behavior of a two-phase saturated steam flow. Additional modeling using TRAC/RELAP Advanced Computational Engine (TRACE) was performed to determine the code's suitability for modeling a saturated steam system. The models developed in this effort will be used as the foundation for follow-on research of transient conditions.

THIS PAGE INTENTIONALLY LEFT BLANK

TABLE OF CONTENTS

LIST OF FIGURES

THIS PAGE INTENTIONALLY LEFT BLANK

LIST OF TABLES

LIST OF ACRONYMS AND ABBREVIATIONS

$\bar{\alpha}$	Average heat transfer coefficient
CCL	CFX command language
CEL	CFX expression language
CFD	Computational fluid dynamics
C_D	Drag coefficient
D, d	Diameter
EOS	Equations of state
Fr	Froude Number
g	Gravitational acceleration
IAPWS	International Association for the Properties of Water and Steam
L_c	Characteristic length
NIST	National Institute of Standard and Technology
NRC	Nuclear Regulatory Commission
ρ	Density
$\bar{q}$	Average heat flux density
Re	Reynold's Number
Re_p	Particle Reynold's Number
RMS	Root mean square
σ	Surface tension
TRACE	TRAC/RELAP Advanced Computational Engine
U, u	Velocity
μ	Dynamic viscosity
We	Weber Number
X	Steam Quality

THIS PAGE INTENTIONALLY LEFT BLANK

ACKNOWLEDGEMENTS

I want to extend my sincerest thanks to Dr. Walter Smith, Dr. Anthony Gannon, and Dr. Garth Hobson for all of their guidance with completing this research. Having minimal familiarization with ANSYS CFX prior to this project, their experience was instrumental and without their mentorship this project would not have been possible. I also want to thank Dr. Anthony Pollman for his insight with learning how to implement TRACE. Finally, thank you to my wife, Morgan, who held down the fort and supported me constantly while I worked on this research.

THIS PAGE INTENTIONALLY LEFT BLANK

I. INTRODUCTION

A. MOTIVATION

The U.S. Navy's nuclear propulsion-powered platforms, aircraft carriers and submarines, undergo significant and continuous research to ensure they operate at peak performance and maximize the lifetime of their reactor cores. Part of this research effort involves investigating potential design optimizations in relevant geometries and their relative configuration to improve efficiency and performance. The increased sophistication of software used in computational fluid dynamics (CFD) research allows modelling significantly more complex flows and flow phenomena. Particularly useful is the ability to model the behavior of multiphase flows, such as a saturated steam system.

Steam turbine propulsion plants are subject to myriad factors which could reduce their overall performance. Such factors include the type and number of turbine staging used, the efficiency of the condensers, and the efficiency of moisture removal from the steam via moisture separators and steam traps. Focusing on the latter, excessive moisture in a saturated steam system leads to several adverse effects. Excessive condensate built up in the steam piping could rapidly flash to vapor, resulting in a hydraulic effect known as water hammer which places significant stress on the piping. Liquid water droplets also cause increased erosion in the piping systems, and have the potential to impinge on the turbine blades resulting in erosion and damage over time. The efficiency of the system is also reduced, as energy is lost through the process of phase transformation from vapor to liquid water due to pressure or temperature transients. Therefore, having a tool to reasonably predict where liquid droplets will concentrate within the piping, and how effects such as pressure transients and piping superheat affect liquid droplet formation and evaporation, could lead to design changes to improve the removal of moisture. These design changes could include redesigning or relocating steam traps. Use of CFD will also allow for modeling the effects of wall superheat on concentrated liquid, and determining under which conditions, if any, the wall superheat is sufficient to flash liquid back to vapor. Transient simulations can be used to analyze condensation and subsequent evaporation for pressure transients in the piping, such as during changes in propulsion or electrical power.

Current designs for steam piping systems are predicated on conservative deterministic design approaches to prevent the admission of moisture, sometimes resulting in excess conservatism and inefficient components. During normal steady-state operations, the steam system operates with high quality dry saturated steam and moisture admission is not a concern. However, implementing design features for possible transient conditions can lead to components whose potential may never be fully utilized, adding inefficiencies.

B. OBJECTIVE

This research aimed to develop a steady-state model of two-phase saturated steam flow in a piping system using a commercially available CFD software. Key to successfully modeling this system is the ability to model the physical properties of saturated steam, two-phase flow, mass transfer, momentum transfer, void fraction, turbulence, droplet entrainment and de-entrainment, and particle effects such as lift, drag and gravity. This effort included choosing an appropriate CFD software, implementing a representative geometry for a steam pipe system, and determining which model sets to implement to reliably run simulations for a range of inlet qualities and droplet sizes. This research focused on fluid phases with constant properties, however the ability to use correlations such as the International Association for the Properties of Water and Steam (IAPWS) thermodynamic property formulations was of importance for future increases in model complexity.

Implementation of the Nuclear Regulatory Commission (NRC) thermal-hydraulic system analysis code TRAC/RELAP Advanced Computational Engine (TRACE) is also investigated for steady-state modeling of the saturated steam system. Specifically, a one-dimensional model of the steam pipe was built to serve as the base for future investigations into the ability of TRACE to predicting outlet conditions similar to those produced by CFD analysis. TRACE allows rapid analysis of a system's response to a transient event and aids in understanding and implementing design constraints.

This thesis is the first step in a broader research effort to model transient conditions in a saturated steam system. The overarching goal of the broader effort is to use the models developed through this research to analyze the response of a saturated steam system to a

pressure transient representative of changing turbine power. Steam turbines are designed to accommodate some amount of moisture. These transient simulations will analyze what magnitude change in pressure would result in excessive moisture content at the steam turbine inlet, and if factors such as piping superheat or piping configuration can mitigate the formation of liquid in the saturated steam system.

C. THESIS OVERVIEW

This research effort developed an Ansys CFX model to evaluate the steady-state behavior of saturated steam in a piping system. The effects of changing inlet quality, liquid droplet diameter, and liquid turbulence model are examined. Additionally, steam traps were added to two sections of the pipe to analyze under which conditions liquid would collect in the traps, and whether the amount of liquid in the traps varied with changes in quality, droplet diameter and turbulence. Chapter II discusses theory of two-phase flows in piping systems. Chapter III discusses the implementation of CFX for modelling a wet steam flow. Chapter IV provides a case study used to test the implementation of the CFX model set. Chapter V describes the steam system modeled and the results of the steady-state analysis. Chapter VI describes the model built to implement TRACE for system analysis. Chapter VII summarizes and concludes the research conducted and details future work.

THIS PAGE INTENTIONALLY LEFT BLANK

II. LITERATURE REVIEW

Research on the behavior of two-phase flows in piping systems has resulted in the development of empirical models for predicting the disposition of different phases at piping junctions and the deposition of particles or dispersed phases. However, little experimental data exists involving the behavior of wet saturated steam in a piping system in the absence of non-condensable gas constituents. In order to adequately evaluate the effectiveness of the CFD model set produced by this research, a review of available literature was performed to understand various aspects of the flow physics individually and therefore determine qualitatively the viability of the model developed.

Multiphase flow is the simultaneous flow of fluids with multiple thermodynamic phases. The model used in this research uses a two-phase flow of high-quality wet saturated steam, with the liquid phase being modeled as dispersed constant diameter droplets. An important aspect of the relevant geometry is flow through and around T-Junctions, particularly oriented in the vertical direction. Azzopardi conducted an experiment on flow separation at a T-junction for annular two-phase air-water flow [1]. A vertical junction is shown in Figure 1. Azzopardi found that as the diameter of the branch increases, the fraction of gas and liquid removed from the main pipe also increases, but the quality, X, of the flow in the branch was highly dependent on the behavior of the flow before the branch [1]. For annular flows with a well-defined liquid wall film, the liquid diverted into the branch comes from the liquid film layer and not entrained droplets due to the relatively low momentum, whereas the high momentum of entrained droplets makes them more difficult to divert into the branch [1].

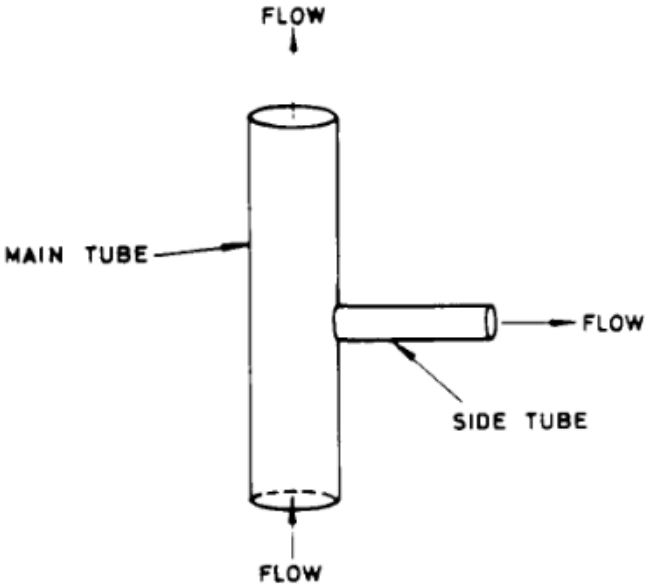

Figure 1. Schematic of vertical T-junction. Source: [2].

A separate study conducted by Azzopardi and Whalley found that for annular and churn flows, primarily liquid is deposited into the branch piping and that for bubbly flows the gas phase will enter the branch [2]. Figure 2 shows the results of various experiments measuring the fraction of liquid and gas removed in a piping branch. Seeger et. al. found that for branch piping oriented vertically downward perpendicular to the main piping that the quality of the flow in the branch is strongly dependent on the flow's behavior upstream of the branch, and an adequate model to predict the phase separation could not be developed [3]. A study of steam-water annular flow in a horizontal T-junction found that complete phase separation occurred when at least 30% of the total inlet flow was diverted to the branch piping [4]. The same study found that branch quality peaks between 20% and 30% flow split, and then lowers to the inlet quality when the mass flow rate through the branch reaches steady state [4].

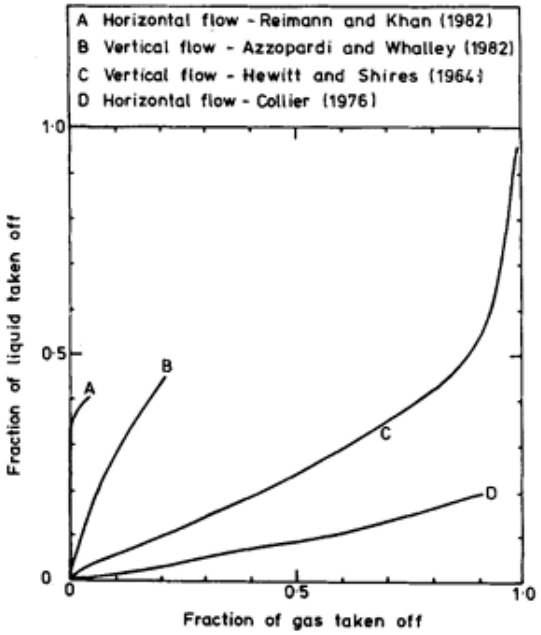

Figure 2. Example of gas and liquid fractions removed by a piping branch. Source: [1].

Pure saturated steam condensation in a horizontal tube, and the resulting heat transfer coefficient, was experimentally analyzed by Caruso et. al. [5]. The experiment used saturated steam from a mixing tank passed through a stainless-steel test section encased in a plexiglass enclosure with counterflow coolant. Caruso, et. al. found that for low velocity flows of pure steam, the heat transfer coefficient predicted using a Nusselt correlation was conservative and over-predicted the heat transfer coefficient when compared with experimental data for inclines less than 30° [5]. Furthermore, due to film thickness variations as the pipe was inclined, the research also observed variations in heat transfer coefficient for the same total steam mass flux as the pipe inclination was changed [5].

An understanding of droplet behavior within the vapor flow was important for analyzing the CFD flow results. An analysis of the Froude Number, which is a ratio of inertial to gravitational forces, was conducted. The Froude Number, Fr, is given by

$$\mathrm{Fr} = \frac{u}{\sqrt{gL_c}} \tag{1}$$

where u is the velocity, g is gravitational acceleration, and L_c is the characteristic length or diameter for spherical droplets [6]. For the research model's flow velocity of 40 m/s, Froude numbers of 4.04×10^5 and 1.28×10^5 were calculated for droplet diameters of 1 μm and 10 μm, respectively. These very high Froude numbers suggest that liquid droplets are likely to remain suspended in the flow since inertial effects will be highly dominant, and gravitational forces insignificant. Particle concentration or film formation in the pipe is not expected.

This research effort will develop a CFD model for examining the effect of inlet quality and droplet size on droplet distribution and overall flow characteristics for steam-water flow. An experiment conducted using steam-water flow with varying inlet quality from 20%-80% found that phase separation increases as inlet quality decreases for a horizontal branch of equal diameter to the main piping [7]. The same study also found that the quality of the branch piping tended to be greater than the inlet quality, so primarily vapor was diverted to the branch piping [7]. Peng et al. conducted a separate experiment examining the effect of branch piping oriented downward at zero, 45 and 90 degrees relative to a horizontal pipe with annular steam-water flow [8]. The experiment showed that, since film thickness tends to be greatest at the bottom of the pipe due to gravitational effects, more liquid was diverted into the branch piping as the inclination increased from zero to 90 degrees downward [8]. Also, the experiment showed that inlet quality has a significant effect on phase distribution, but the effect depends on the branch orientation. Increasing inlet quality results in a greater vapor velocity for the same total mass flow rate. The increased vapor velocity will then result in more uniform film thickness around the pipe circumference, which results in thinner film thickness at the bottom of the pipe. Therefore, the experiment showed that as inlet quality increases the quality of the flow in the branch also increased when the branch is oriented vertically downward, since there is less liquid in the film that can be extracted from the main pipe [8].

A study conducted of steam-water flow in a nozzle examined the critical Weber number for droplets in two-phase flows. The Weber number, We, is a ratio of aerodynamic to surface tension forces for a fluid droplet. The Weber number is calculated using Eq. (2)

$$\mathrm{We} = \frac{\rho_v \left(U_v - U_d\right)^2 D}{\sigma} \tag{2}$$

where ρ_v and U_v are the density and velocity of the vapor, U_d and D are the velocity and diameter of the droplets, and σ is the surface tension [9]. The Weber number at the onset of droplet breakup is the critical Weber number, typically determined empirically since its value is dependent on the fluid velocities and the droplet diameter, ranging between 6 and 14 for most gas-liquid flows but potentially as low as 1.9 for high quality steam [9]. If the flow characteristics, fluid properties, and a critical Weber number are known then a maximum stable droplet diameter can be determined for that flow.

Borishanskiy, et. al., conducted an experiment measuring the heat flux density and heat transfer coefficients for condensing steam in vertical pipes and coils [10]. Their experiment focused on low velocity steam from 0.79 MPa to 6.87 MPa in varying lengths of small diameter vertical pipes. The diameter of the pipes examined varied from 10 mm to 20 mm [10]. One of their experiments on a vertical pipe at 2.94 MPa was used as a case study in this research for developing a CFX model for flow of saturated steam.

THIS PAGE INTENTIONALLY LEFT BLANK

III. TWO FIELD MODELING OF WET STEAM

Effectively modeling a steady-state flow of wet steam in a piping system using CFD requires the chosen software to have several specific capabilities. For this research effort, the ability to model two-phase flow was required, as the wet steam would be modeled using a continuous vapor phase and dispersed liquid droplets. Mass and heat transfer between the phases must also be modeled, along with the ability to specify material properties individually for the continuous vapor and dispersed liquid droplets. Buoyancy effects, lift, and drag were also required to model droplet interactions with the continuous vapor phase. Availability of a turbulence model was also required. Finally, compatibility with IAPWS thermophysical property equations of state (EOS) was desired for comparison with the NRC system analysis code TRACE.

This research effort utilized Ansys CFX for CFD analysis of wet saturated steam in a piping system. Ansys CFX is a combined software suite that provides functionality for defining the flow properties and boundary conditions (pre-processing), a solver, and post-processing capability.

A. FLUID MATERIAL MODELS

Ansys CFX provides built-in wet steam material models for use in two-phase flow simulations. The fluid material models for wet steam are a combination of three individual material definitions: a liquid material, a gas material, and a homogeneous binary mixture of the liquid and gas materials. The purpose of the homogeneous binary mixture is to define the phase change between the liquid and gas substances. In CFX, the EOS governing the behavior of the wet steam homogeneous binary mixture models are IAPWS International Formulation 1997 (IF97) EOS [11]. Several variations of the wet steam material selections are available in CFX covering different ranges of saturation conditions, which can be user-modified to tailor the material definitions to a specific problem. Using the homogeneous binary mixture wet steam models in CFX precludes the user from defining a domain saturation temperature, since the saturation conditions are determined by the EOS associated with the CFX material definitions [12]. The second option available for a two-

phase model in CFX is using liquid and gas materials which are independently defined, not linked by a homogeneous binary mixture. When combined with the thermal phase change model, using independently defined fluids for each phase allows the user to defined the saturation temperature for the domain, which can be either a constant value or an CFX expression language (CEL) expression [12].

An additional benefit to implementing user-defined fluid materials is individual fluid properties, such as density, can be defined either as a constant value or as an expression. For a two-phase flow such as wet steam, this is advantageous since it allows selectively increasing the complexity of the model to maintain stability. This functionality also allows focusing the analysis on the behavior of a single property of interest while holding all others constant to reduce computational resources required.

For this research, user-defined materials for the liquid and vapor phase were created that were not constituents of a homogeneous binary mixture. One liquid-vapor pair was defined with constant thermal properties defined at the desired saturation point for the domain. The second pair were independent fluids whose properties were determined by IAPWS IF97 EOS. Like the constant property fluids, this allowed setting the domain saturation temperature rather than saturation conditions being determined by the material EOS through a homogeneous binary mixture. For fluids whose properties depend on EOS rather than constant values, temperature and pressure bounds must be set for property table generation along with a desired number of intervals. For steady-state solutions, a smaller temperature and pressure range will increase the fidelity of calculations performed by the chosen EOS. However, a large enough band must be set to account for the maximum expected range of temperature and pressure in the given system. Table values can be extrapolated, but the extrapolation will be limited to either the slope at the boundary of the lookup table or the value of the property at the table boundary which was violated [11]. In either case, deviation of the calculated properties from the expected properties may occur, so setting a slightly larger than expected range of temperatures and pressures is recommended. CFX command language (CCL) files, which can be imported into the CFX material database, showing how these custom fluid properties were defined for a wet steam condensation case study used in this research are provided in Appendix A.

For the steam condensation case study modeled in this research, the constant property liquid and vapor phases were used to obtain an initial solution. The constant property fluids are less computationally expensive and allowed the flow to develop more quickly. The results of the solution with constant property fluids were then used as the initial conditions for solver calculations using variable property fluids. Overall, the simplicity of using constant property fluids allowed additional focus on how the individual flow physics models, discussed in the next section, affected the solution.

B. FLOW PHYSICS SETUP

The wet steam model developed for this research utilized a continuous vapor phase and dispersed liquid phase with constant droplet diameter, known as an inhomogeneous model. For an inhomogeneous model, only the pressure field is common to both phases but all other fields are calculated on a phase specific basis and the phases interact based on the chosen interphase transfer model [12]. High quality wet steam flows were evaluated for this research, with liquid volume fractions on the order of 10^{-3} or lower and corresponding inlet qualities ranging from approximately 85% to 99%. This resulted in sparsely distributed liquid droplets at the inlet boundary.

A review of the available drag and lift models in CFX was performed, and two applicable drag models and one lift model were identified for use in this research. The liquid phase was modeled using a dispersed fluid morphology, which models the liquid as spherical droplets of a constant diameter. Therefore, the particle Reynold's number, Re_p, is important because that will determine whether the flow resides in the viscous regime, inertial regime, or in the transition region between them. The Re_p calculation implemented by CFX is given by

$$\mathrm{Re}_p = \frac{\rho_\alpha \left| U_\alpha - U_\beta \right| d_\beta}{\mu_\alpha} \tag{3}$$

where ρ_α and μ_α correspond to the vapor density and dynamic viscosity, d_β is the droplet diameter, and U_α and U_β are the velocities of the vapor and liquid phases respectively [13]. Low particle Reynold's numbers, much smaller than 1, make up the viscous regime

where the fluid viscosity is the dominant effect and the drag coefficient is determined by Stoke's Law

$$C_D = \frac{24}{\mathrm{Re}_p}, \quad \mathrm{Re}_p \ll 1 \tag{4}$$

where C_D is the drag coefficient [13]. The transition between the viscous and inertial regime consists of $\mathrm{Re_p}$ between 0.1 and 1000 for spherical particles, and is governed largely by empirical drag models.

The Schiller-Naumann model implemented in CFX is applicable to sparsely distributed spherical particles at low $\mathrm{Re_p}$ and in the transition region between the viscous and inertial regimes, where fluid droplets do not deform and behave similarly to solid particles. The model implements an empirical drag coefficient correlation for droplets in the transition region, with a maximum value for particles in the inertial regime of 0.44 [13]. The Ishii-Zuber model is suitable for both sparsely distributed droplets as well as more densely packed droplets providing additional flexibility for models where liquid droplets may become more densely packed. For sparsely distributed particles in the inertial regime, the Ishii-Zuber drag model automatically accounts for potential particle deformation into elliptical or spherical cap shapes [13]. For densely distributed spherical particles, the Ishii-Zuber model implements the same correlation as the Schiller-Naumann model using a mixture dynamic viscosity vice the continuous phase dynamic viscosity [13]. The Ishii-Zuber model also accounts for densely packed distorted particles using appropriate drag coefficient correlations. Of the available lift models in CFX, the Legendre and Magnaudet lift model was selected which is applicable for resolving the lift forces on small spherical fluid droplets. The Legendre-Magnaudet model differs from the other droplet model available in CFX, the Saffman-Mei model, by accounting for momentum transfer between the flow on the particle surface and internal recirculation [13].

CFX includes three domain heat transfer models, two of which were considered for use, the thermal energy and total energy model. This research utilized the thermal energy model, given by

$$\frac{\partial(\rho h)}{\partial t} + \nabla \bullet (\rho \bar{U} h) = \nabla \bullet (\lambda \nabla T) + \tau : \nabla \bar{U} + \bar{S}_E \quad (5)$$

where ρ is density, h is enthalpy, T is temperature, U is the velocity vector, λ is thermal conductivity, $\tau : \nabla \bar{U}$ is viscous dissipation, and $\bar{S}_E$ is an energy source. The thermal energy model will account for the transfer of enthalpy between phases and is suitable for low-Mach number flows of compressible gases [13]. Of note, the thermal energy equation implemented in CFX does not include a pressure gradient term, so variations in pressure alone do not result in a phase change. This is crucial for stability of a steady-state saturated steam model when using fluid materials not defined by constant thermodynamic properties. Slight variations in the solver calculated pressure from user-defined conditions at the boundaries can cause significant instability in the solver as the liquid phase flashes to vapor or vapor instantly condenses to liquid. The resultant near-instantaneous mass transfer from one phase to the next caused extremely high Mach numbers and solver failure. This is particularly evident when defining a saturated mixture at the inlet boundary, but was less significant for a liquid volume fraction of zero. For this reason, the total energy model was not used.

The ability to use user-defined expressions for the domain saturation temperature was also evaluated. Using the IAPWS IF97 equation of state for saturation temperature on the saturation line, a CEL expression was written that calculated the saturation temperature based on a user-defined expression "Press" which was set to a constant value [14]. Appendix B includes the CCL file for implementing the saturation temperature expression based on a user-defined pressure. The "Press" expression was also used as the input for the static pressure boundary condition. This allowed use of the liquid and vapor phases defined by IAPWS IF97 EOS without using a homogeneous binary mixture. This increased solver stability using variable property fluid materials by rigidly fixing the inlet boundary at the desired saturation condition, preventing rapid phase change from occurring due to slight variations in solver calculated pressure. If a user defined expression for pressure is not used as the input for the saturation temperature calculation, then the saturation temperature calculation must be a function of absolute pressure since CFX does not allow expressions that reference solver calculated values [12].

When establishing the fluid domain, a reference pressure of zero was chosen for this research. It is usually recommended to use a reference pressure representative of the system pressure that is being modeled to prevent round-off errors for small changes in dynamic pressure relative to the domain pressure [12]. Pressures defined in the boundary conditions are then specified relative to the reference pressure. However, for the model used in this research, the reference pressure of 0 MPa was chosen to test implementation of the user defined "Press" expression that controlled the saturation temperature.

Separate from the fluid specific heat transfer model discussed, a fluid pair heat transfer model must also be selected. The fluid pair heat transfer model determines how thermal energy is transferred between the phases, in this case liquid and vapor. The two resistance model was selected, with the liquid phase modeled using a zero resistance model and the vapor phase using the Ranz-Marshall correlation. The Ranz-Marshall model is applicable to convection around spherical particles in a Newtonian fluid and calculates a Sherwood number as a function of Re_p and Prandtl number [12]. The zero resistance model for the liquid phase is numerically equivalent to defining an infinite heat transfer coefficient, which results in the interfacial temperature being equal to the liquid phase temperature [12].

For cases that require modeling conjugate heat transfer from the pipe walls for a steady-state solution, using pseudo-transient boundary conditions is recommended. Using a CEL expression, the wall heat flux boundary condition for can be modeled as an if-statement that ramps down to the final experimental value of the wall heat flux starting from zero. This allowed a controlled extraction of heat for a set number of iterations to improve model stability. Once the final heat flux condition was reached, the computation would continue for the specified number of total iterations. An example of this expression is provided in Appendix B. A case study of steam condensing in a vertical pipe was used to test the implementation of this expression and is discussed in Chapter IV.

C. USE OF EXPRESSIONS AND USER VARIABLES

Several monitor points and expressions were used to qualitatively and quantitively analyze the results while the solver was running. These points provided early indication of

whether the flow was developing as expected while the solver was running, rather than waiting to post-process the results. Examples of monitor points used include the average vapor mass fraction at the inlet and outlet boundaries. Bulk mass flow and individual phase velocity at the inlet and outlet were also monitored as an indication of whether flow continuity was reached. An example of the monitor points and expressions implemented for modeling condensing steam in a vertical pipe are provided in Appendix B.

In addition to expressions used for monitoring the development of the flow, a user defined variable for monitoring the total liquid mass accumulated in the pipe was implemented. A user variable "Mass Total" was added to the CFX additional variable library, then implemented for the liquid and vapor phase. The Mass Total was the product of the volume of finite volumes, the phase density and the phase volume fraction calculated on a per cell basis. Then, an expression was added which calculated the sum of the liquid phase Mass Total for each cell. The sum was then input as a monitor point for "Liquid Mass" and displayed in the solver interface. This monitor point provided a real-time plot of the liquid mass and was used as an additional tool to determine whether mass continuity was reached within the domain. The implementation of this variable for a two-component flow is provided as a CCL in Appendix C which shows how the variable is defined and implemented for each phase.

THIS PAGE INTENTIONALLY LEFT BLANK

IV. CONDENSATION CASE STUDY

A. CASE STUDY DESCRIPTION

Experimental data from condensation of steam in a straight vertical pipe was used to develop a wet steam model in CFX. The experiment calculated the heat flux density on the inner pipe wall and the average heat transfer coefficient for vertical straight pipes containing condensing steam [10]. The test apparatus passed boiler steam through a superheater and then supplied the steam to the top of a vertical pipe, which was housed within an evaporator housing. The pipe walls were maintained at a constant temperature for each experiment [10].

Numerous data points were collected from the experiment for various pipe lengths, pipe diameters, and system pressures. The calculated heat transfer coefficient and heat flux density data for a three meter long, 20 mm inner diameter vertical pipe at 2.94 MPa was chosen since the pressure is similar to the model pressure for the saturated steam system analyzed in this research. Fluid properties for the steam were obtained from the National Institute of Standard and Technology (NIST) thermophysical properties of fluid systems [15]. The steam properties for the experiment are listed in Table 1.

Table 1. Thermophysical properties of saturated steam at 2.94 MPa. Adapted from [15].

Property	Liquid	Vapor
Saturation Temperature, T_{sat} (K)	505.89	505.89
Density, ρ (kg/m^3)	823.42	14.70
Specific Enthalpy, h (J/kg)	1003100	2803100
Specific Entropy, s (J/kg•K)	2635.3	6193.5
Specific Heat Capacity (Constant Pressure), C_p (J/kg•K)	4709.4	3587.3
Viscosity, μ (Pa•s)	1.1475E-04	1.6802E-05
Thermal Conductivity, k (W/m•K)	0.63412	0.045639
Surface Tension, σ (N/m)	0.030097	-

The experimentally derived heat transfer coefficient and heat flux density are provided in Table 2. Using that data, quantities necessary to model the experiment in CFX were calculated, including the total heat extracted from the steam in the pipe (Q), the average inner wall temperature ($\bar{T}_{wall}^{in}$), and the mass flow rate ($\dot{m}$). The inner wall temperature was derived from the experimental determination of the average heat transfer coefficient, $\bar{\alpha}$, given by

$$\bar{\alpha} = \frac{\bar{q}}{T_{sat} - \bar{T}_{wall}^{in}} \tag{6}$$

where T_{sat} is saturation temperature and $\bar{q}$ is the average heat flux density on the inner wall [10]. Calculated parameters are provided in Table 3.

Table 2. Validation experiment heat transfer data. Adapted from [10].

Case Number	Heat Flux Density on Condensing Surface (W/m^2)	Heat Transfer Coefficient ($W/m^2 \cdot K$)
1	30900	9670
2	32200	8060
3	41500	9030
4	48100	6870
5	67500	7270
6	78800	6280
7	19550	9310
8	34900	8120
9	43250	8320
10	60100	8140
11	67500	6510
12	83800	6400
13	88600	5940
14	995000	5990
15	114500	5680
16	116700	5990
17	133700	6150
18	145400	5450
19	145400	6620
20	151200	6175
21	161500	5850
22	174500	5660
23	175500	5980
24	190700	6040
25	20800	6000
26	227500	6050
27	287000	5600

Table 3. Calculated flow parameters from experiment heat transfer data

Case Number	Total Heat (W)	$T_{Wall, in}$ (K)	Mass Flow Rate (kg/s)	Steam Velocity (m/s)	Liquid Velocity (m/s)
1	5.82E+03	502.69	3.236E-03	0.70	1.25E-02
2	6.07E+03	501.89	3.372E-03	0.73	1.30E-02
3	7.82E+03	501.29	4.346E-03	0.94	1.68E-02
4	9.07E+03	498.89	5.037E-03	1.09	1.95E-02
5	1.27E+04	496.61	7.069E-03	1.53	2.73E-02
6	1.49E+04	493.34	8.252E-03	1.79	3.19E-02
7	3.69E+03	503.79	2.047E-03	0.44	7.91E-03
8	6.58E+03	501.59	3.655E-03	0.79	1.41E-02
9	8.15E+03	500.69	4.529E-03	0.98	1.75E-02
10	1.13E+04	498.51	6.294E-03	1.36	2.43E-02
11	1.27E+04	495.52	7.069E-03	1.53	2.73E-02
12	1.58E+04	492.80	8.776E-03	1.90	3.39E-02
13	1.67E+04	490.97	9.278E-03	2.01	3.59E-02
14	1.88E+05	339.78	1.042E-01	22.56	4.03E-01
15	2.16E+04	485.73	1.199E-02	2.60	4.64E-02
16	2.20E+04	486.41	1.222E-02	2.65	4.72E-02
17	2.52E+04	484.15	1.400E-02	3.03	5.41E-02
18	2.74E+04	479.21	1.523E-02	3.30	5.89E-02
19	2.74E+04	483.93	1.523E-02	3.30	5.89E-02
20	2.85E+04	481.40	1.583E-02	3.43	6.12E-02
21	3.04E+04	478.28	1.691E-02	3.66	6.54E-02
22	3.29E+04	475.06	1.827E-02	3.96	7.06E-02
23	3.31E+04	476.54	1.838E-02	3.98	7.10E-02
24	3.59E+04	474.32	1.997E-02	4.32	7.72E-02
25	3.92E+03	502.42	2.178E-03	0.47	8.42E-03
26	4.29E+04	468.29	2.382E-02	5.16	9.21E-02
27	5.41E+04	454.64	3.005E-02	6.51	1.16E-01

From the extracted data, the Reynold's number for the vapor, Froude number, and Weber number were calculated for each case using Eqs. (7), (1), and (8) respectively and provided in Table 4. For the Reynold's number calculation

$$\mathrm{Re} = \frac{\rho u L_c}{\mu} \tag{7}$$

μ is the dynamic viscosity and L_c is the pipe diameter [6]. For the Weber number calculation

$$\mathrm{We} = \frac{\rho u^2 L_c}{\sigma} \tag{8}$$

L_c is the droplet diameter and σ is surface tension [6]. Calculations of Weber number and Froude number assumed a droplet diameter to 100 μm. This droplet diameter was chosen since it is a similar order of magnitude to other condensing experiments with water droplet growth on the wall in slow flows [16]. Comparison of these dimensionless parameters resulted in the selection of five individual cases from the experiment to use as case studies.

Table 4. Steam flow Re, Fr, and We numbers

Case Number	$\mathrm{Re}_{\mathrm{vapor}}$	Fr	We
1	1.23E+04	1.58E+00	2.40E-02
2	1.28E+04	1.65E+00	2.60E-02
3	1.65E+04	2.12E+00	4.33E-02
4	1.91E+04	2.46E+00	5.81E-02
5	2.68E+04	3.46E+00	1.14E-01
6	3.13E+04	4.03E+00	1.56E-01
7	7.76E+03	1.00E+00	9.60E-03
8	1.38E+04	1.79E+00	3.06E-02
9	1.72E+04	2.21E+00	4.70E-02
10	2.38E+04	3.08E+00	9.07E-02
11	2.68E+04	3.46E+00	1.14E-01
12	3.33E+04	4.29E+00	1.76E-01
13	3.52E+04	4.54E+00	1.97E-01
14	3.95E+05	5.09E+01	2.49E+01
15	4.54E+04	5.86E+00	3.29E-01
16	4.63E+04	5.97E+00	3.42E-01
17	5.30E+04	6.84E+00	4.49E-01
18	5.77E+04	7.44E+00	5.31E-01
19	5.77E+04	7.44E+00	5.31E-01
20	6.00E+04	7.74E+00	5.74E-01
21	6.41E+04	8.27E+00	6.55E-01
22	6.92E+04	8.93E+00	7.65E-01
23	6.96E+04	8.98E+00	7.74E-01
24	7.57E+04	9.76E+00	9.14E-01
25	8.25E+03	1.06E+00	1.09E-02
26	9.03E+04	1.16E+01	1.30E+00
27	1.14E+05	1.47E+01	2.07E+00

Case number 1, 5, 14, 25 and 27 were chosen to model in CFX. Case 1 and 5 had similar orders of magnitude heat flux density and Froude number, but the Weber number for Case 5 is one order of magnitude greater. Case 14 was chosen since it had the highest heat flux density recorded. Case 25 was chosen since it had nearly identical inner wall temperature and similar Froude and Weber number compared to Case 1. However, Case 25 had the second lowest total heat flux density and a heat transfer coefficient approximately two third of that for Case 1. Finally, Case 27 was chosen due to having the same order of magnitude Reynold's number and Froude number as Case 14, but with a Weber number one order of magnitude less. Overall, this selected group of cases from the experiment provided a broad range of conditions to model in CFX, covering the bounds of the provided data. A condensed collection of the relevant data for these cases is provided in Table 5.

Table 5. Data for the five condensation cases selected to model in CFX

Case Number	Heat Flux Density on Condensing Surface (W/m^2)	Heat Transfer Coefficient ($W/m^2 \cdot K$)	Re_{vapor}	Fr	We
1	30900	9670	1.23E+04	1.58E+00	2.40E-02
5	67500	7270	2.68E+04	3.46E+00	1.14E-01
14	995000	5990	3.95E+05	5.09E+01	2.49E+01
25	20800	6000	8.25E+03	1.06E+00	1.09E-02
27	287000	5600	1.14E+05	1.47E+01	2.07E+00

B. BUILDING THE MODEL IN CFX

Using Solidworks, the fluid domain was generated as a solid cylinder 3 m in length and 20 mm in diameter, vertically oriented as in the experiment. The top of the cylinder was the inlet and the bottom the outlet for flow in the negative y-direction.

1. Model Mesh

The model mesh was generated using the built in Ansys CFX mesh program native to Ansys Workbench. The bulk mesh used one millimeter element size and growth rate

factor of 1.2. Ten inflation layers were added at the wall of the pipe using the same 1.2 growth rate factor with a resulting first element thickness of 0.15 mm. The average aspect ratio for the domain of 4.13 and average vapor Y+, the non-dimensional distance from the wall based on friction velocity, of 6.8 at the wall which was sufficiently low since resolution of the laminar sub-layer was not required for this model. The resulting mesh consisted of approximately 5.9 million elements. An image of the mesh viewed from the pipe inlet is provided in Figure 3. All models built for this case study used the same mesh.

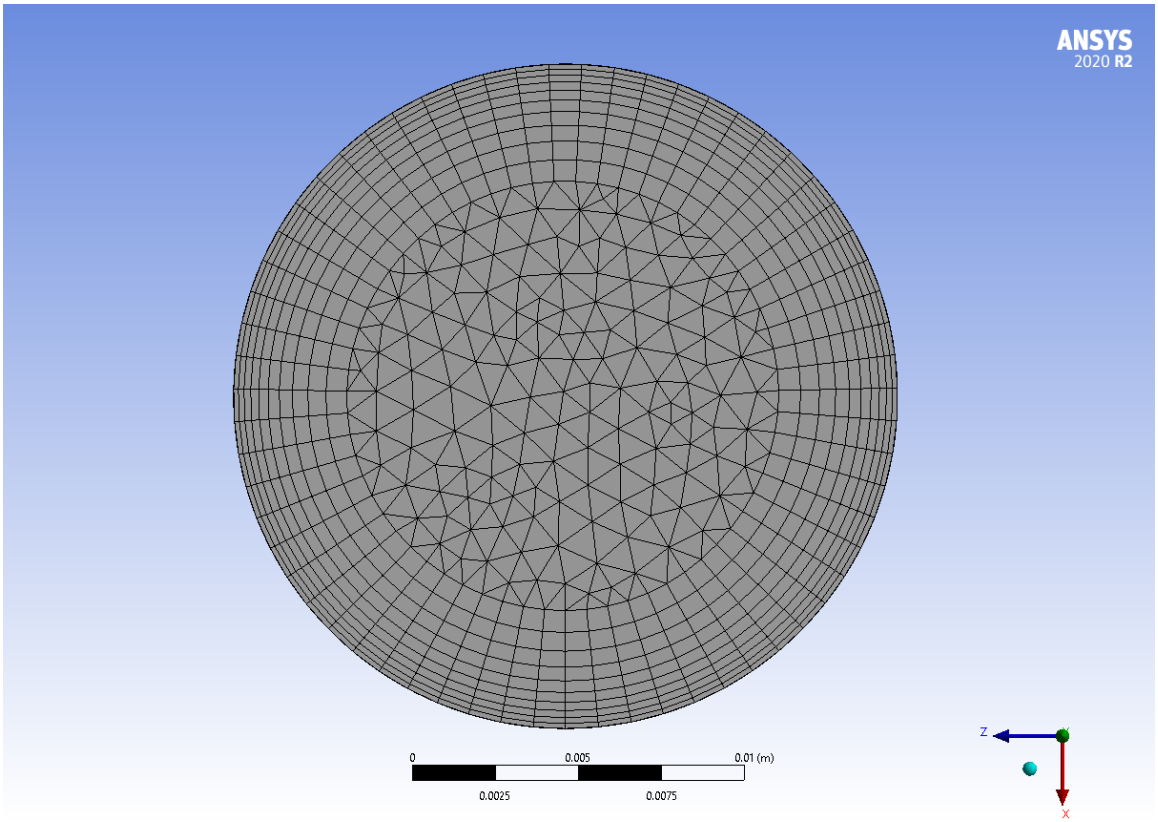

Figure 3. The final mesh for the vertical condensing pipe

2. Model Physics

User-defined constant property liquid and vapor phase materials were built in CFX using the thermodynamic properties listed in Table 1, which are referenced to the system saturation pressure of 2.94 MPa. In addition to the constant property material definitions for the liquid and gas phase, liquid and gas materials were user-defined whose properties

were defined by the IAPWS IF97 EOS. Since the saturation temperature corresponding to 2.94 MPa is 505.89 K, the table generation values were set to a temperature range of 300 K to 600 K and corresponding saturation pressure range of 3.5368 kPa to 12.345 MPa [15]. This range was sufficiently large to account for potential supercooling of the liquid phase at the wall boundary.

When defining the domain physics models, the vapor was modeled as a continuous fluid and the liquid as a dispersed fluid with a constant droplet diameter of 100 μm. Gravitational acceleration was defined downward along the vertical axis, and buoyancy effects were modeled for the liquid droplets. The selected heat transfer model for both the liquid and gas phase was thermal energy, with thermal phase change selected as the mass transfer model for the fluid pair. The Ranz-Marshall correlation was selected for the vapor phase heat transfer and zero resistance for the liquid phase. Additional models activated were the k-epsilon turbulence model for the gas phase and laminar model for the dispersed liquid droplets. Specific boundary conditions for each case are discussed individually in further detail.

C. MODEL DEVELOPMENT

Several different versions of boundary conditions and physics models were used to model the conditions of Case 1. Since Case 1 had relatively low heat flux density and a median Re number compared to the other four cases chosen to mode, Case 1 was used to test implementation of constant and variable property fluids as well as the selected drag and lift models. Case 1 was also used to compare the effects of different boundary conditions on the solution to inform the decision of which boundary conditions to use for the steam pipe described in Chapter V.

1. Boundary Condition Comparison

Two main categories of boundary conditions were evaluated for use. The first utilized static temperature and static pressure at the inlet, either velocity or bulk mass flow rate at the outlet, and heat flux for the wall of the pipe. The second combination used defined velocity and static temperature at the inlet, static pressure at the outlet, and heat flux for the wall. A no-slip wall boundary condition and ramped wall heat flux expression

to step down the heat removal were used. A summary of boundary conditions used for the various models generated for Case 1 are specified in Table 6.

Table 6. Initial conditions for Case 1

Solution	Domain Models	Domain Basic Settings	Inlet Boundary Conditions	Outlet Boundary Conditions	Wall Boundary Conditions
1	Constant property fluids, drag, buoyancy	P_{ref} : 2.94 MPa T_{sat} : 505.89 K	T_{static} : 505.89 K P_{static} (Rel): 0 MPa VF_{vapor} : 0.999	Normal Speed: 0.021509 m/s	Heat Flux: -30900 W/m^2
2	Constant property fluids, drag, lift, buoyancy	P_{ref} : 2.94 MPa T_{sat} : 505.89 K	T_{static} : 505.89 K P_{static} (Rel): 0 MPa VF_{vapor} : 0.999	Normal Speed: 0.021509 m/s	Heat Flux: -30900 W/m^2
3	Variable property fluids, drag, lift, buoyancy	P_{ref} : 2.94 MPa T_{sat} : 505.89 K	T_{static} : 505.89 K P_{static} (Rel): 0 MPa VF_{vapor} : 0.999	Normal Speed: 0.021509 m/s	Heat Flux: -30900 W/m^2
4	Constant property fluids, drag, lift, buoyancy	P_{ref} : 2.94 MPa T_{sat} : 505.89 K	T_{static} : 505.89 K P_{static} (Rel): 0 MPa VF_{vapor} : 0.999	Bulk Mass Flow Rate: 0.003236 kg/s	Heat Flux: -30900 W/m^2
5	Variable property fluids, drag, lift, buoyancy	P_{ref} : 0 MPa T_{sat} : 505.89 K	T_{static} : 505.89 K P_{static} (Rel): 2.94 MPa VF_{vapor} : 0.9999	Bulk Mass Flow Rate: 0.00324 kg/s	Heat Flux: -30900 W/m^2
6	Constant property fluids, drag, lift, buoyancy	P_{ref} : 0 MPa T_{sat} : 505.89 K	T_{static} : 505.89 K Normal Speed: 0.69 m/s VF_{vapor} : 0.9999	P_{static} (Rel): 2.94 MPa	Heat Flux: -30900 W/m^2
7	Variable property fluids, drag, lift, buoyancy	P_{ref} : 0 MPa T_{sat} : 505.89 K	T_{static} : 505.89 K Normal Speed: 0.69 m/s VF_{vapor} : 0.9999	P_{static} (Rel): 2.94 MPa	Heat Flux: -30900 W/m^2

2. Results of Boundary Condition Comparison

a. Comparison of solution without and with lift model selected

The first calculation used constant property liquid and vapor phases. The inlet vapor volume fraction corresponded to an inlet quality of 94.7%. The wall heat flux was stepped down from zero to -30900 W/m^2 over the first 250 iterations, lowering 123.6 W/m^2 each iteration, and then maintained at -30900 W/m^2 for an additional 250 iterations for 500 iterations total. The calculation was run using 30 partitions in parallel for approximately 200000 elements per partition. The solver wall clock time to complete 500 iterations was 4 hrs 2 min 27.5 sec using 16.44 GB of memory. Figure 4 is a plot of the bulk mass flow rate at the inlet and outlet. At 250 iterations, the point where the maximum value of the heat being removed from the pipe wall was reached, a notable change in the inlet mass flow rate occurs. The inlet mass flow rate does not reach the expected value of 0.003236 kg/s from Table 3, but steadies at a value of 0.002934 kg/s which is 9.3% lower due to this combination of boundary conditions not achieving a reasonable level of stability. Of note, CFX displays outlet mass flow rate as negative by convention. After 500 iterations a representative plot of outlet quality, calculated as the average vapor mass fraction at the inlet and the outlet, had rapidly approached a value of approximately 0.56% at the outlet plane and the expected value of 94.7% at the inlet. The plot of average vapor mass fraction is provided in Figure 5. The monitor point was used as an indication of stability being reached at the outlet plane rather than a quantitative evaluation of outlet quality. Actual quality at the outlet plane, X_{outlet}, was calculated in CFX Post using a CEL expression modeled after Eq. (9)

$$X_{outlet} = \frac{\dot{m}_{vapor,out}}{\dot{m}_{vapor,out} + \dot{m}_{liquid,out}} \tag{9}$$

where $\dot{m}_{vapor,out}$ and $\dot{m}_{liquid,out}$ are the solver calculated values for the vapor and liquid phase mass flow rates at the outlet, respectively. Solutions where a wall boundary was placed at the inlet or outlet by the solver resulted in greater deviation of the average vapor mass fraction from the actual flow quality.

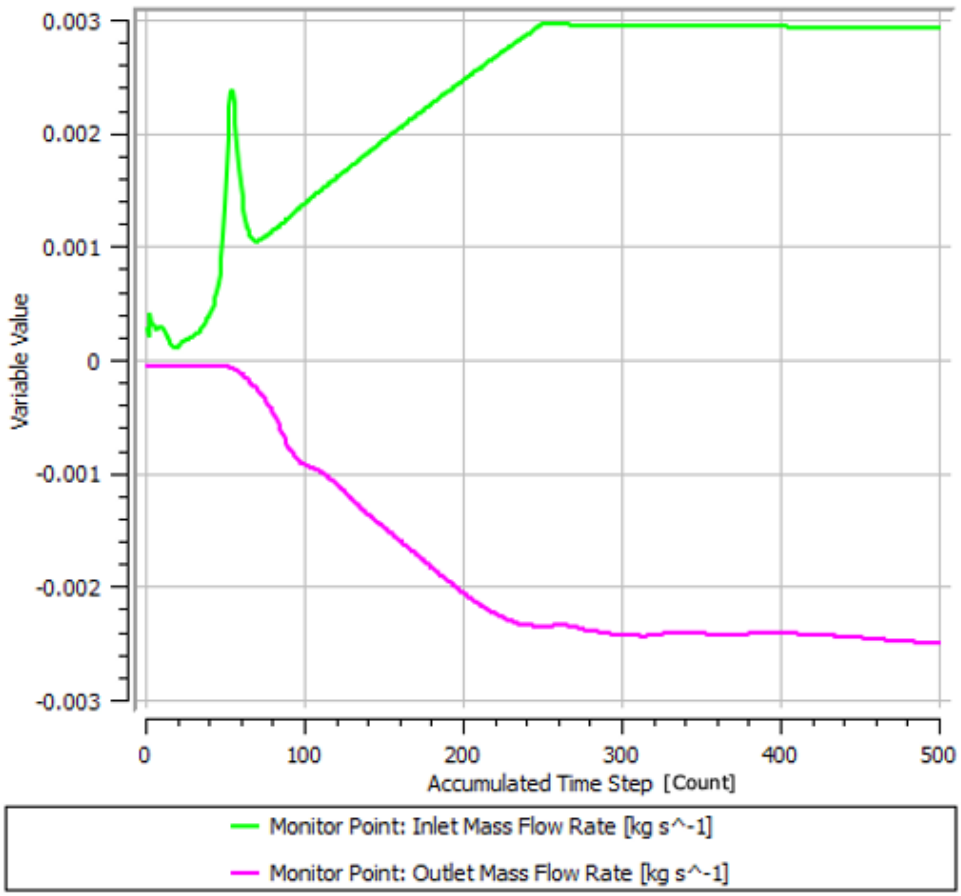

Figure 4. Plot of inlet and outlet mass flow rate for Case 1 initial calculation

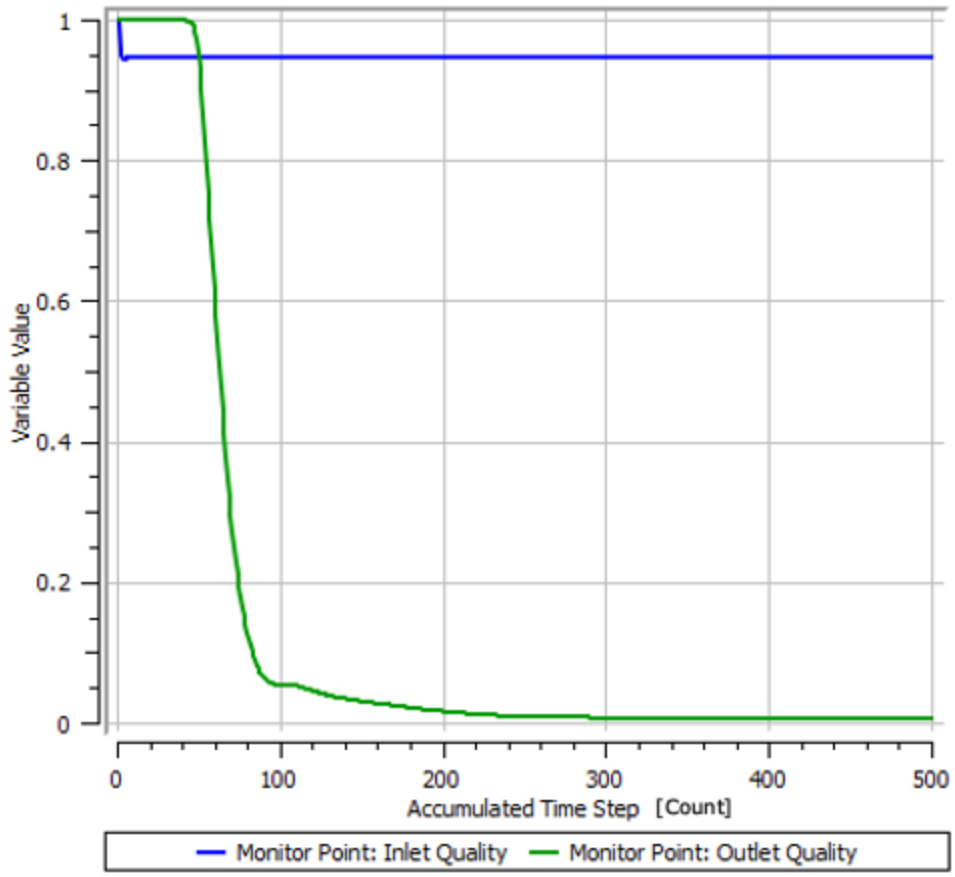

Figure 5. Plot of inlet and outlet average vapor mass fraction, denoted "Quality" on the plot, for the first run of Case 1

A second calculation was then conducted using the same settings as the first, but with the Legendre Magnaudet lift activated. The first run was used as the initial conditions for the second calculation. An additional 500 iterations were run, totaling 1000 outer loop iterations, using the same solver setting of 30 parallel partitions. The activation of the lift model did not appreciably affect computational time or power, requiring 4 hrs 6 min 3.5 sec and 16.44 GB of memory to complete 500 iterations. A plot of the inlet and outlet bulk mass flow rate is provided in Figure 6, and a plot of the average inlet and outlet vapor mass fraction is provided in Figure 7. With the Legendre Magnaudet lift model activated, a distinct increase in the inlet mass flow rate occurs with a corresponding jump down in the outlet mass flow rate. The solver determined inlet mass flow rate was 0.003023 kg/s, within 6.5% of the expected vale, an improvement over the first solution. The average

vapor mass fraction measured at the outlet lowered slightly to approximately 0.41%. Closer examination of the plot showed that the average outlet quality was continuing to trend downward. Figure 8 is a rescaled plot showing the trend in outlet quality over the last 100 iterations.

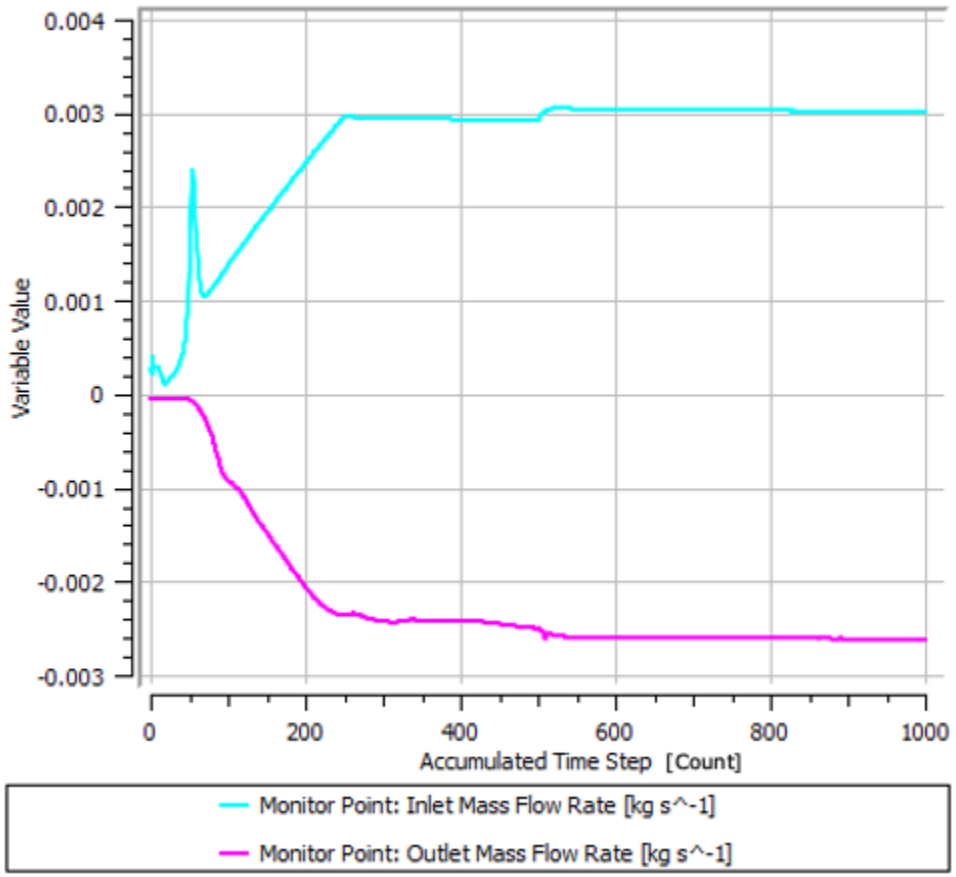

Figure 6. Plot of inlet and outlet mass flow rate for Case 1 calculation with the lift model activated

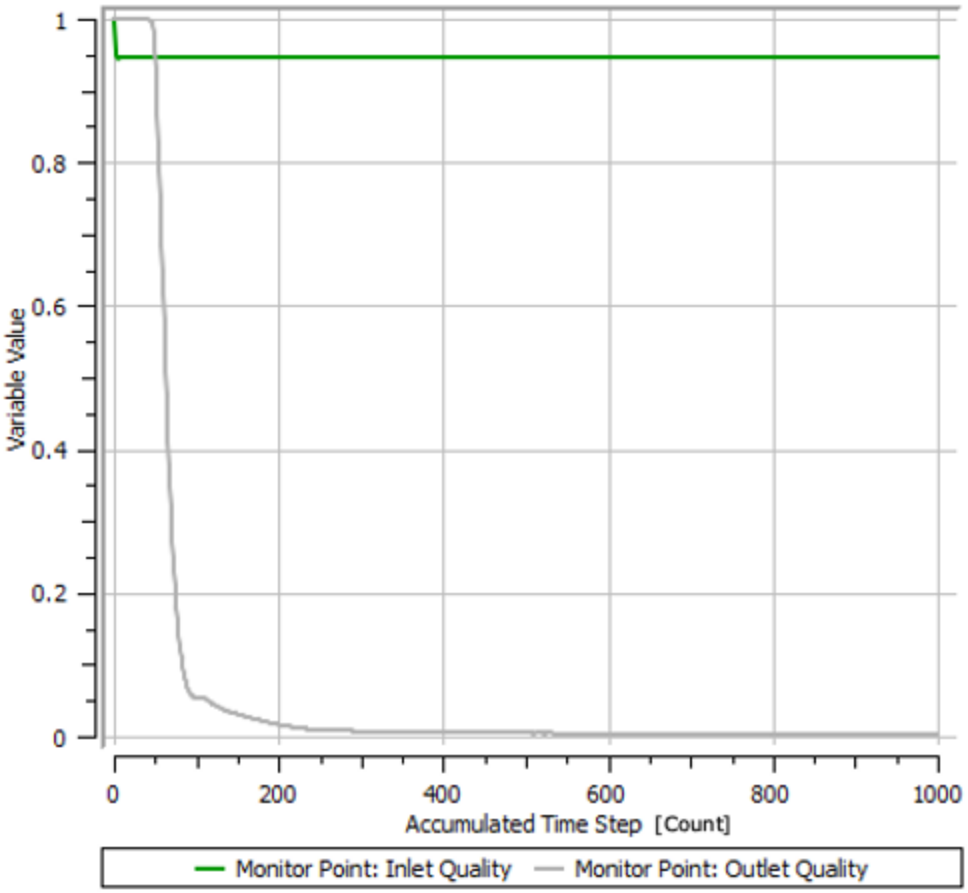

Figure 7. Plot of inlet and outlet average vapor mass fraction for Case 1, denoted "Quality," with the lift model activated

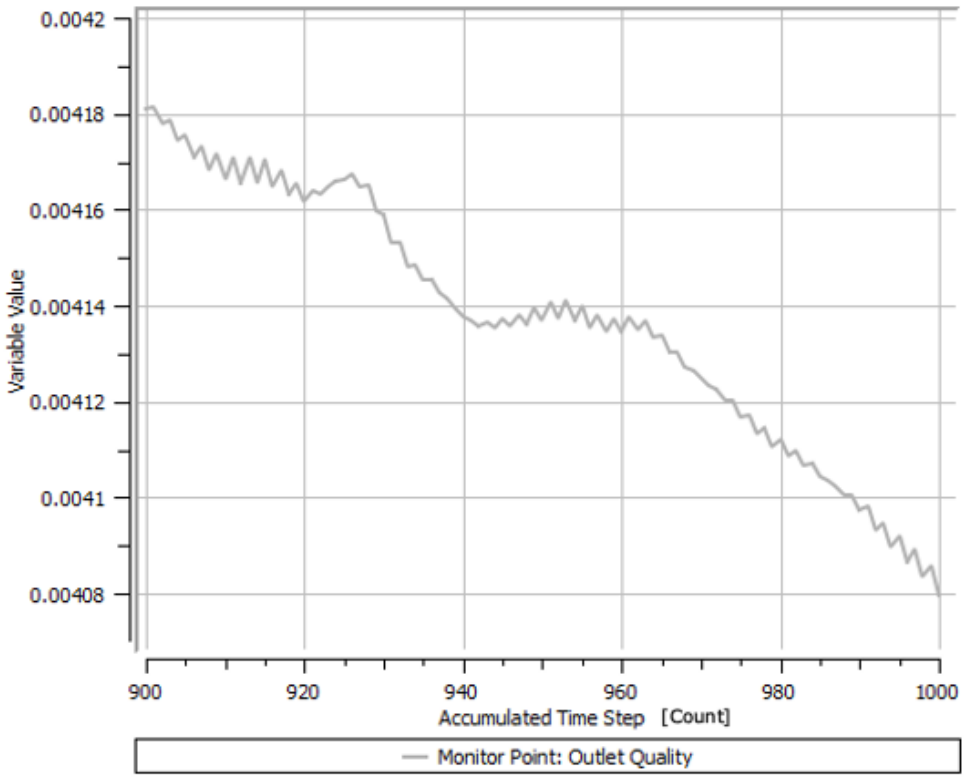

Figure 8. Rescaled plot of the outlet quality for Case 1 with the lift model activated

In both cases, the outlet velocity boundary condition was defined assuming the vapor fully condensed to liquid. Since the outlet area and density of the liquid are constant, defining the outlet boundary condition using the calculated liquid velocity is equivalent to setting a fluid-dependent mass flow outlet condition with the vapor mass flow defined as 0 kg/s. Therefore, the solver calculating an outlet quality of less than 1% is expected since the solver is forced to meet the outlet velocity boundary condition.

Post processing the results was completed using ParaView. The results for the first two runs for Case 1 are presented side by side in Figure 9, which shows a vapor mass fraction contour on the wall. The vertical scale has been adjusted to one tenth of the pipe's length. With the lift model activated, liquid begins accumulating on the wall nearer to the inlet plane. This is likely due to the introduction of the lift model resulting in liquid droplets being removed from the wall and replaced by vapor. The vapor then subsequently condenses and the droplets are again removed from the wall, resulting in a greater

concentration of liquid in the bulk flow vice in the regions near the wall. Inserting a cut plane along the pipe centerline and plotting the same vapor mass fraction contour revealed significant differences in the behavior of the two flows. Figure 10 is a side-by-side comparison of a vapor mass fraction contour for the two solutions along the pipe centerline. Without the lift model activated, a thin film does form on the wall, but the majority of the bulk flow mass consists of the vapor phase. With the lift model, the liquid film forms and is removed from the wall sooner, resulting in greater liquid mass in the bulk flow towards the pipe outlet.

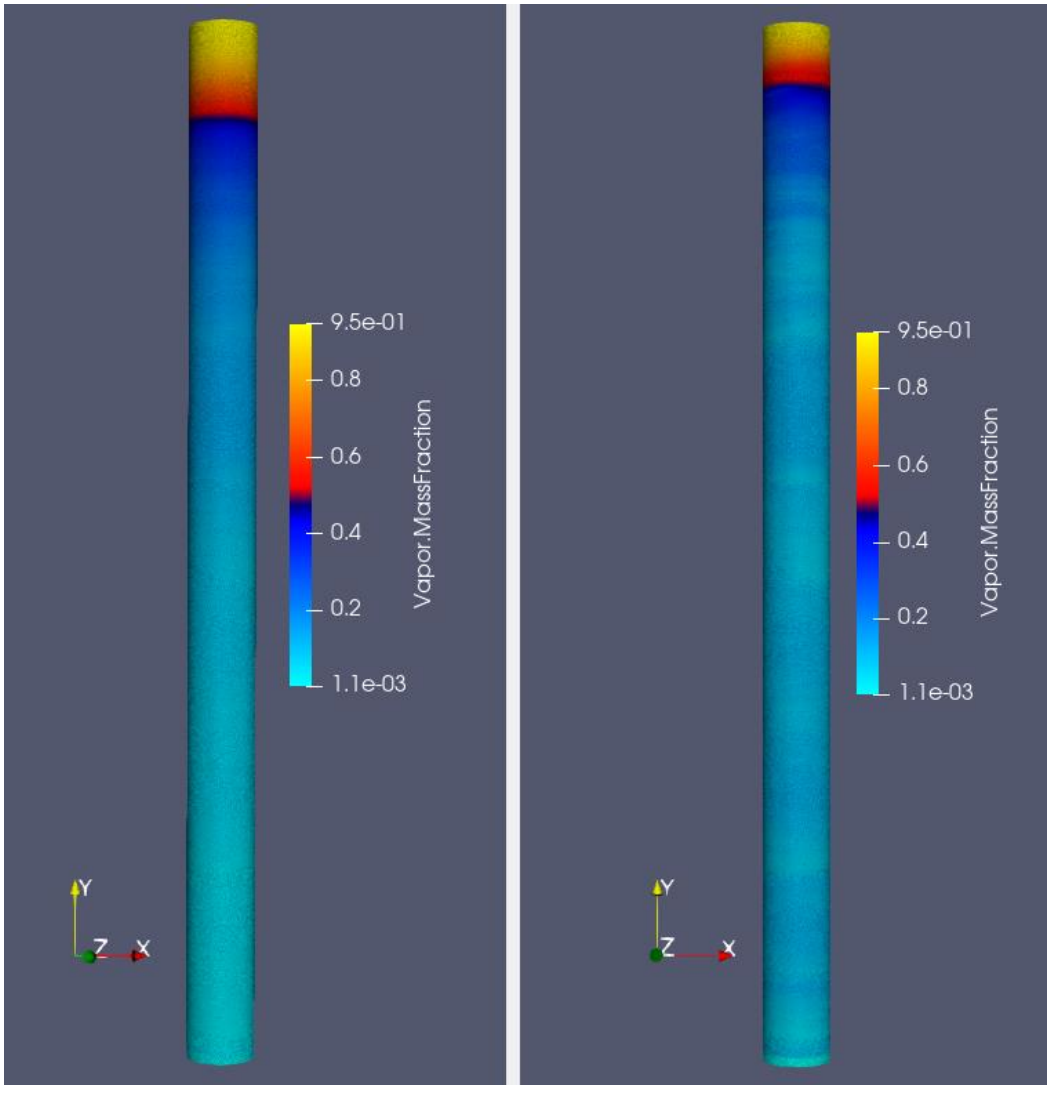

Figure 9. Side by side comparison of the vapor mass fraction contour without the lift model activated (left) and with lift activated (right)

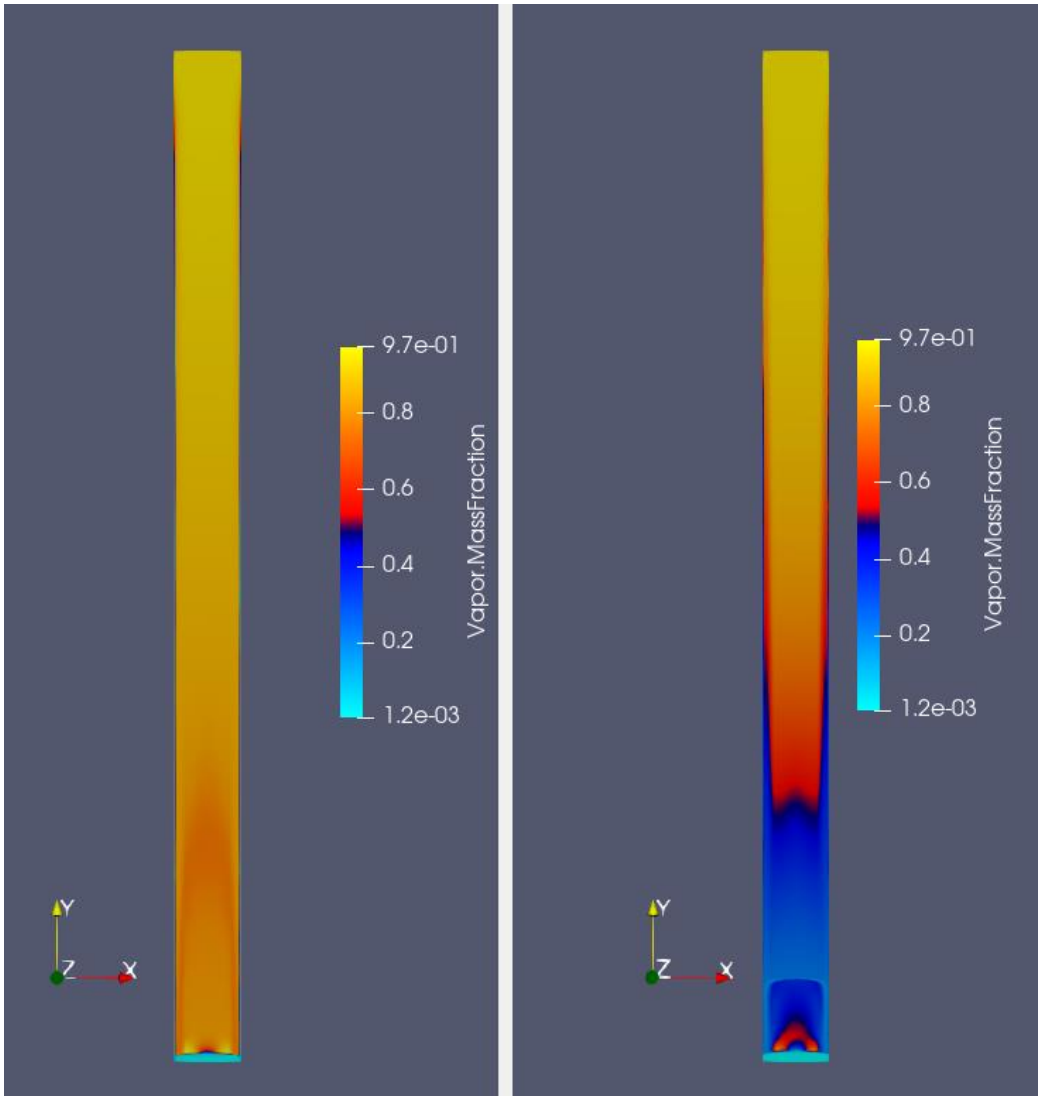

Figure 10. Comparison of the vapor mass fraction along the pipe centerline without (left) and with (right) the lift model activated

Some similarities in the flow behavior at the outlet are apparent between the two solutions. In each case, a dome of liquid exists at the outlet that is approximately 0.025 m thick, 25% larger than one pipe diameter measured from the outlet. Figure 11 shows the similarity in size of the liquid dome for the two solutions. Figure 12 shows the vapor and liquid velocity vectors at the outlet of the pipe. This concentration of liquid mass at the outlet is attributed to the chosen outlet boundary condition. The behavior of the film growth when a lift model is used in addition to drag and buoyancy led to all subsequent models incorporating the Legendre-Magnaudet lift force.

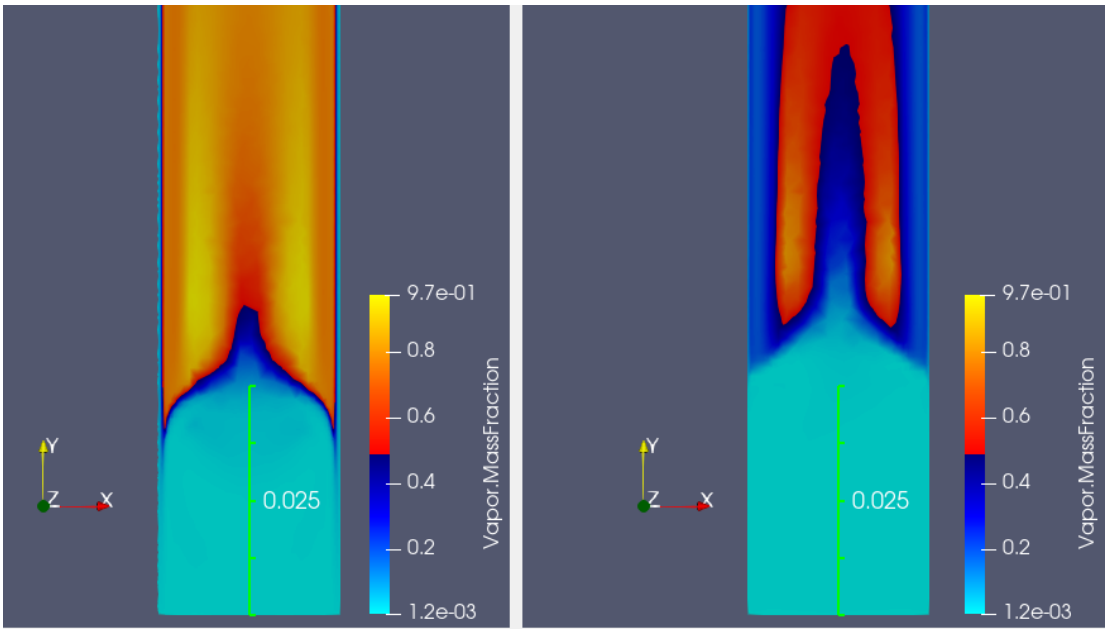

Figure 11. Comparison of the liquid dome present at the outlet without (left) and with (right) the lift model activated

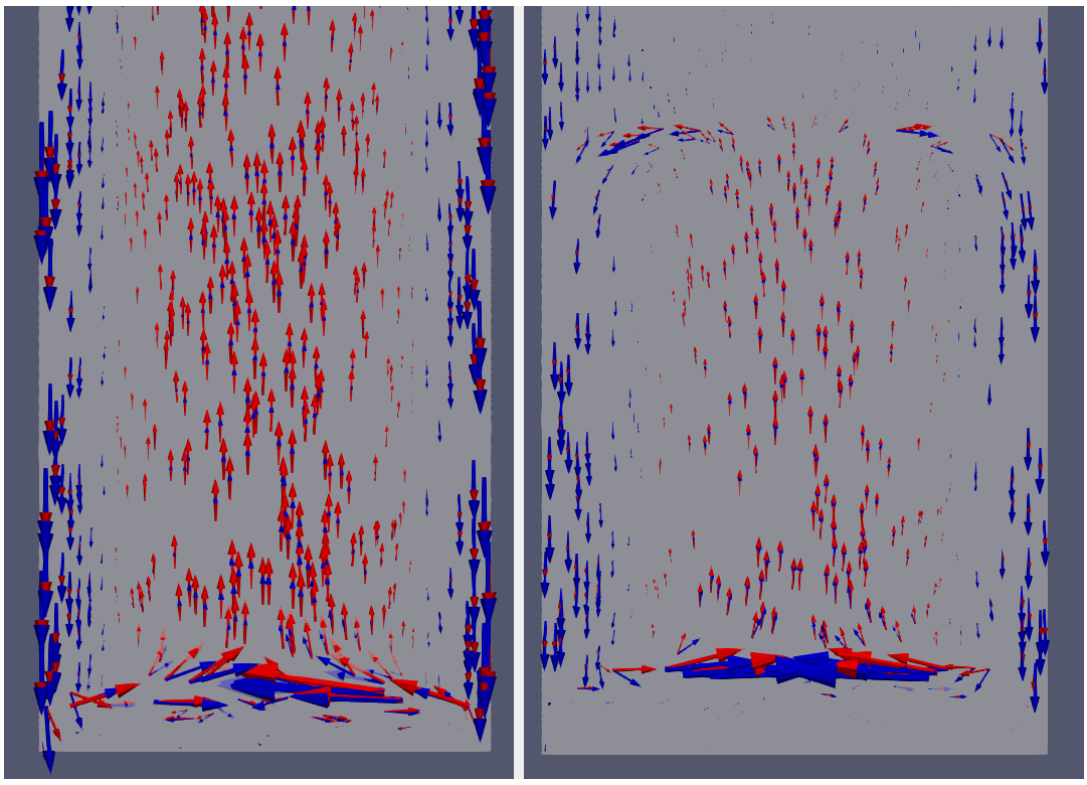

Figure 12. Comparison of liquid (blue) and vapor (red) velocity vectors

The behavior of the liquid film at the wall boundary was also examined. In both cases, a liquid film builds due to the heat flux at the wall which is greater than one element in thickness. When no lift model is used, the transition from the liquid film to the bulk flow is abrupt since the majority of the bulk flow remains vapor. With the Legendre-Magnaudet lift model activated, the liquid droplets are swept from the wall and a growth in film thickness is seen moving from inlet to outlet.

b. Comparison of solution using constant property and variable property fluids

The third solution used the same boundary conditions as the first solution, with no lift model activated, but changed the material definitions to the variable property liquid and vapor phases. The behavior was similar to that of the constant property fluid solution, with the same liquid film growth and bulk flow behavior. This result confirmed that a stable solution could be reached using variable property fluids not bound by a homogeneous binary mixture and governed by IAPWS IF97 equations of state. A comparison of the vapor mass fraction contours for these two solutions is provided in Figure 13. Figure 14 is a plot of the inlet and outlet average vapor mass fraction generated by solver monitor points showing similar behavior to solution 2 with constant property fluids.

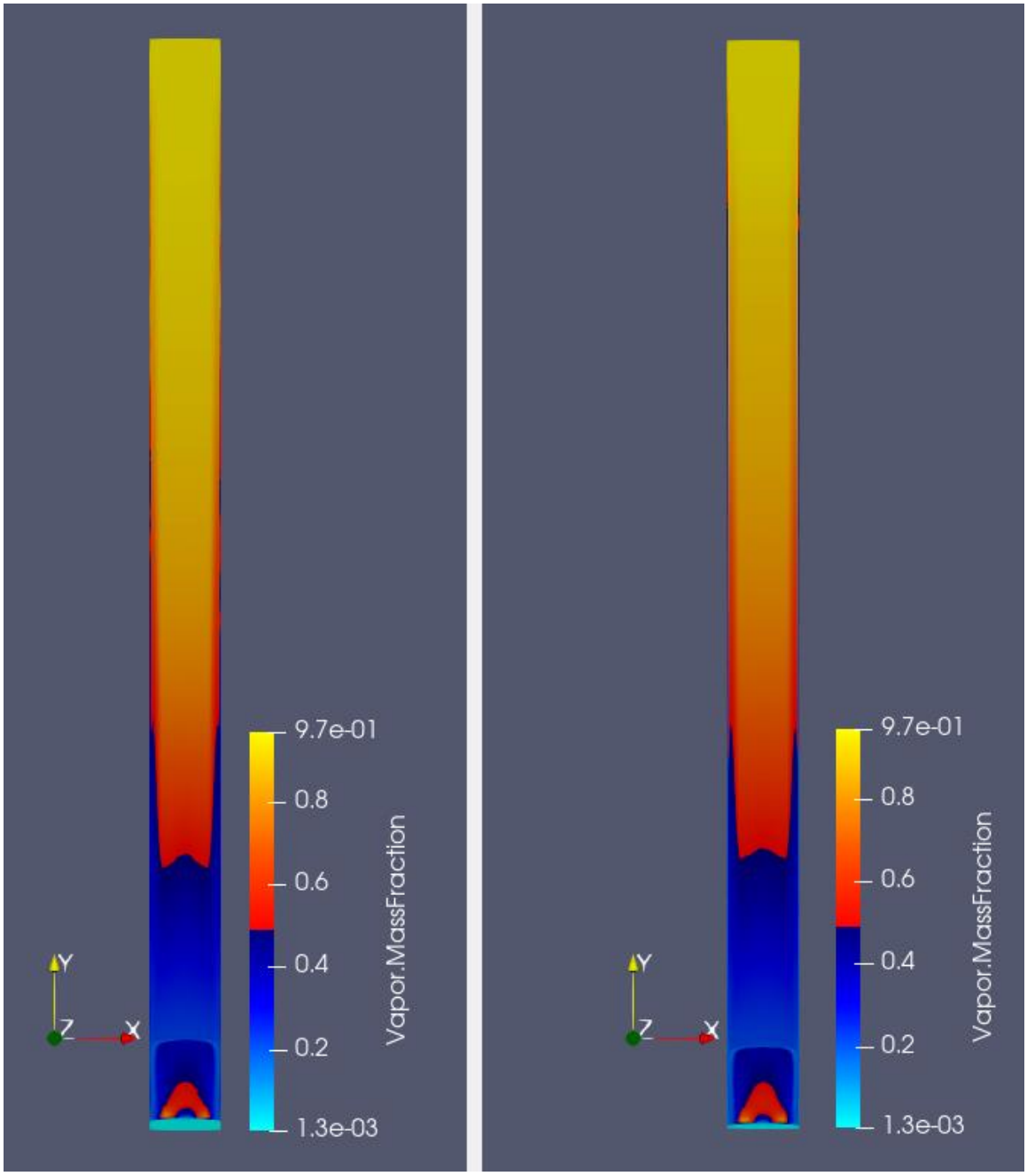

Figure 13. Comparison of models using constant property (left) and variable property (right) fluid definitions

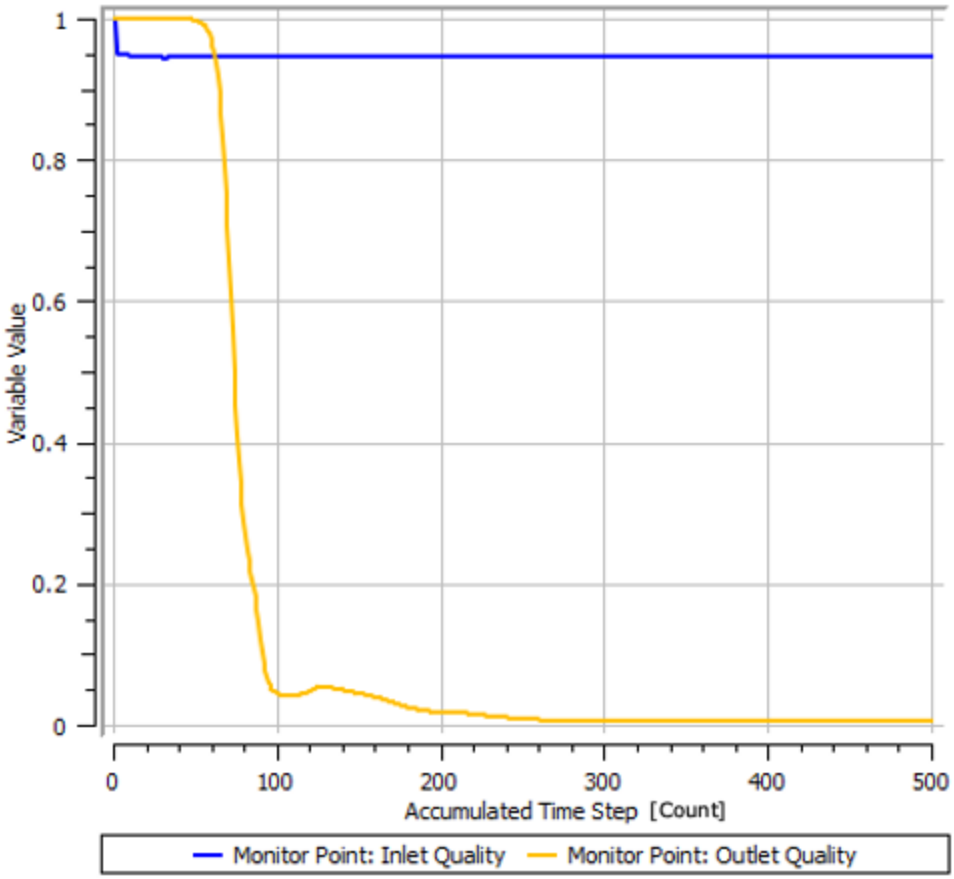

Figure 14. Inlet and outlet quality monitor points for solution 3 using variable property fluids

c. Comparison of normal speed and bulk mass flow rate outlet boundary condition

The next comparison was between solution two, using the previously defined liquid velocity outlet boundary condition, and a new solution defined using a bulk mass flow rate outlet boundary condition. Both models used the constant property fluids for the gas and vapor phases, as well as the same buoyancy, drag and lift models. The wall boundary condition was also the same ramped heat flux boundary condition. The bulk mass flow rate was set to the calculated value from Table 3 for Case 1, which was 0.003236 kg/s. The solution run using a bulk mass flow rate outlet boundary condition resulted in a distinct change in the behavior of the flow at the outlet. Rather than having a pool of liquid coalesced at the outlet, the mass flow rate outlet boundary condition resulted in a

recirculation region of vapor at the center of the pipe with liquid exiting near the walls. Figure 15 shows a comparison between the vapor mass fraction contour for the two solutions. The recirculation of vapor at the outlet resulted in a much higher quality at the outlet for the bulk mass flow rate solution, with an average vapor mass fraction of 0.276 after 1500 iterations. An examination of the vapor mass fraction contour at the outlet plane showed that a liquid film was still present at the wall boundary as with the previous solution. However, the mass flow rate condition was met by distributing the vapor and liquid proportionately at the outlet with much higher velocities, vice pooling condensed liquid as was seen for the normal speed outlet boundary condition. Figure 16 shows the distribution of the liquid and vapor phases at the outlet plane. A significant difference in the velocity profile of the liquid was also apparent between the two solutions. For the normal speed boundary condition, the average liquid phase outlet velocity was 0.037 m/s, nearly three times the specified normal speed boundary condition. The solution using a bulk mass flow rate outlet boundary resulting in an average liquid outlet velocity of 0.324 m/s, an order of magnitude higher. Figure 17 is a comparison of the liquid velocity profiles for these two solutions shown 0.2 m from the outlet. The liquid y-velocity component is shown as a contour with liquid velocity magnitude vectors overlayed. The bulk mass flow rate outlet boundary condition resulted in some recirculation but had an overall more uniform liquid velocity distribution.

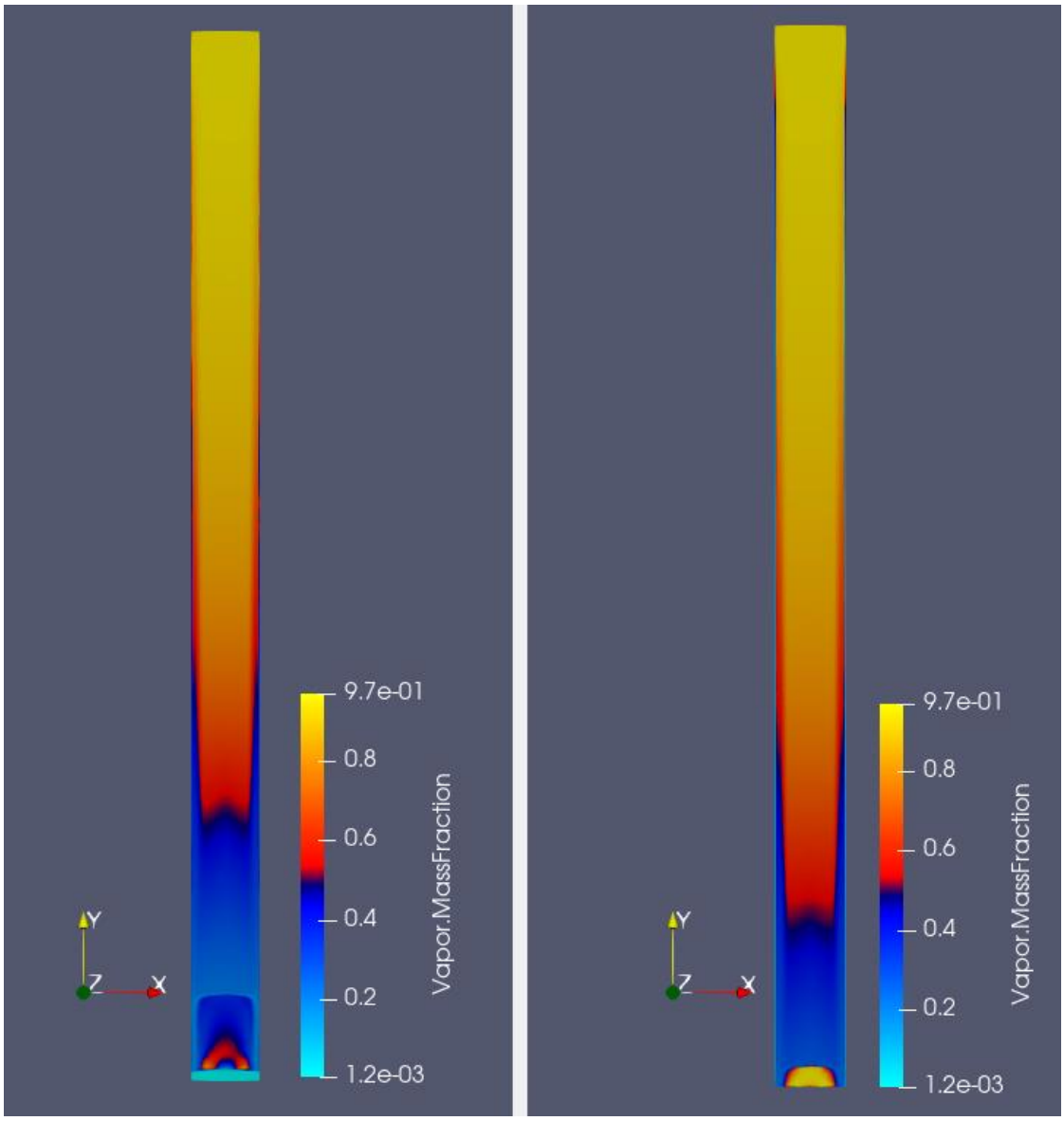

Figure 15. Comparison of vapor mass fraction contours for a normal speed outlet boundary condition (left) with a bulk mass flow rate boundary condition (right)

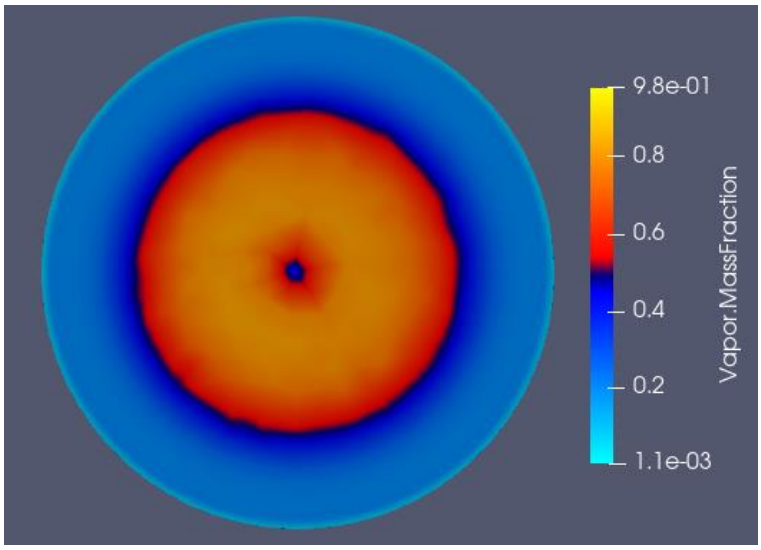

Figure 16. Vapor mass fraction contour at the outlet for a bulk mass flow rate outlet condition

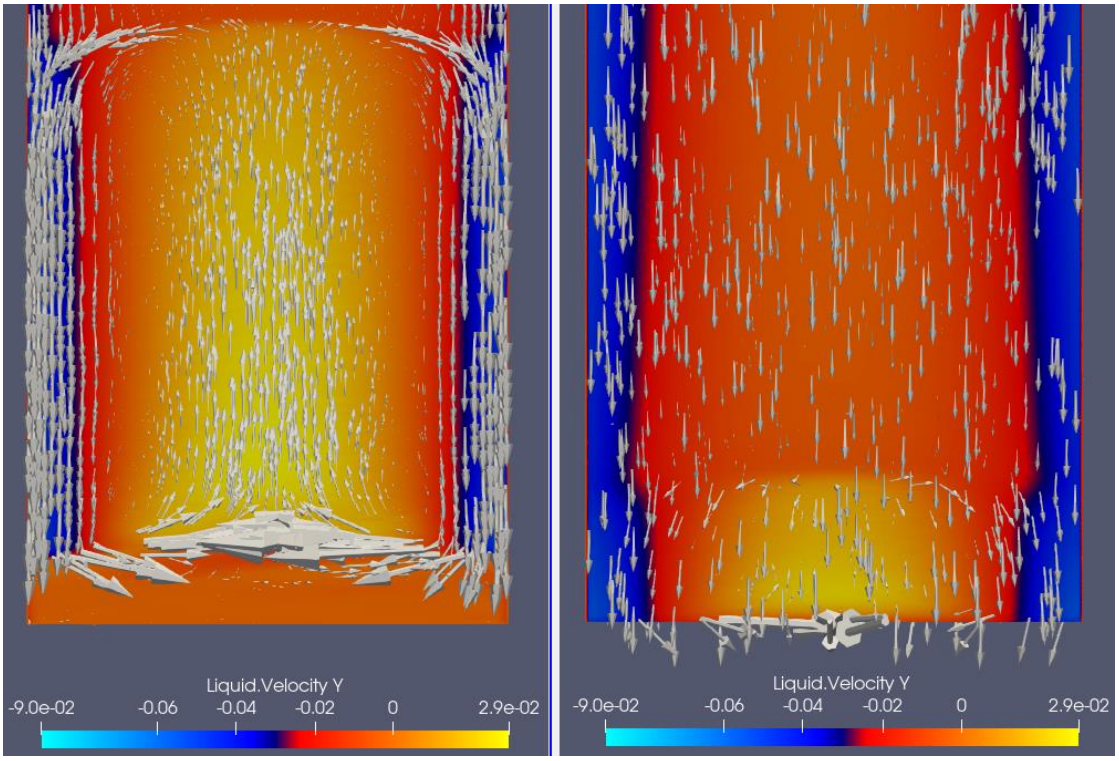

Figure 17. Contours of liquid y-velocity with overlayed liquid velocity vectors for a normal speed (left) and bulk mass flow rate (right) boundary condition

A fifth model was built, which also used a bulk mass flow rate outlet boundary condition but variable property fluids for the liquid and vapor phases. The outlet mass flow rate was 0.00324 kg/s, and the fluids were defined based on IAPWS IF97 EOS. The inlet vapor volume fraction was also changed from 0.999 to 0.9999, resulting in an inlet quality of 99.44%, approximately 5% higher than the previous solution. This model resulted in complete condensation of the vapor in the pipe. However, this model also resulted in the solver placing walls at the inlet and outlet boundaries, which prevented the mass flow rate from reaching continuity between inlet and outlet. The inlet mass flow rate was reduced to 4.9×10^{-4} kg/s, an order of magnitude less than the defined outlet boundary condition. A wall was placed at 15.5% of the inlet area to prevent the backflow of vapor through the inlet boundary. Figure 18 is a contour showing the vapor mass fraction for the solution using constant property and variable property fluids.

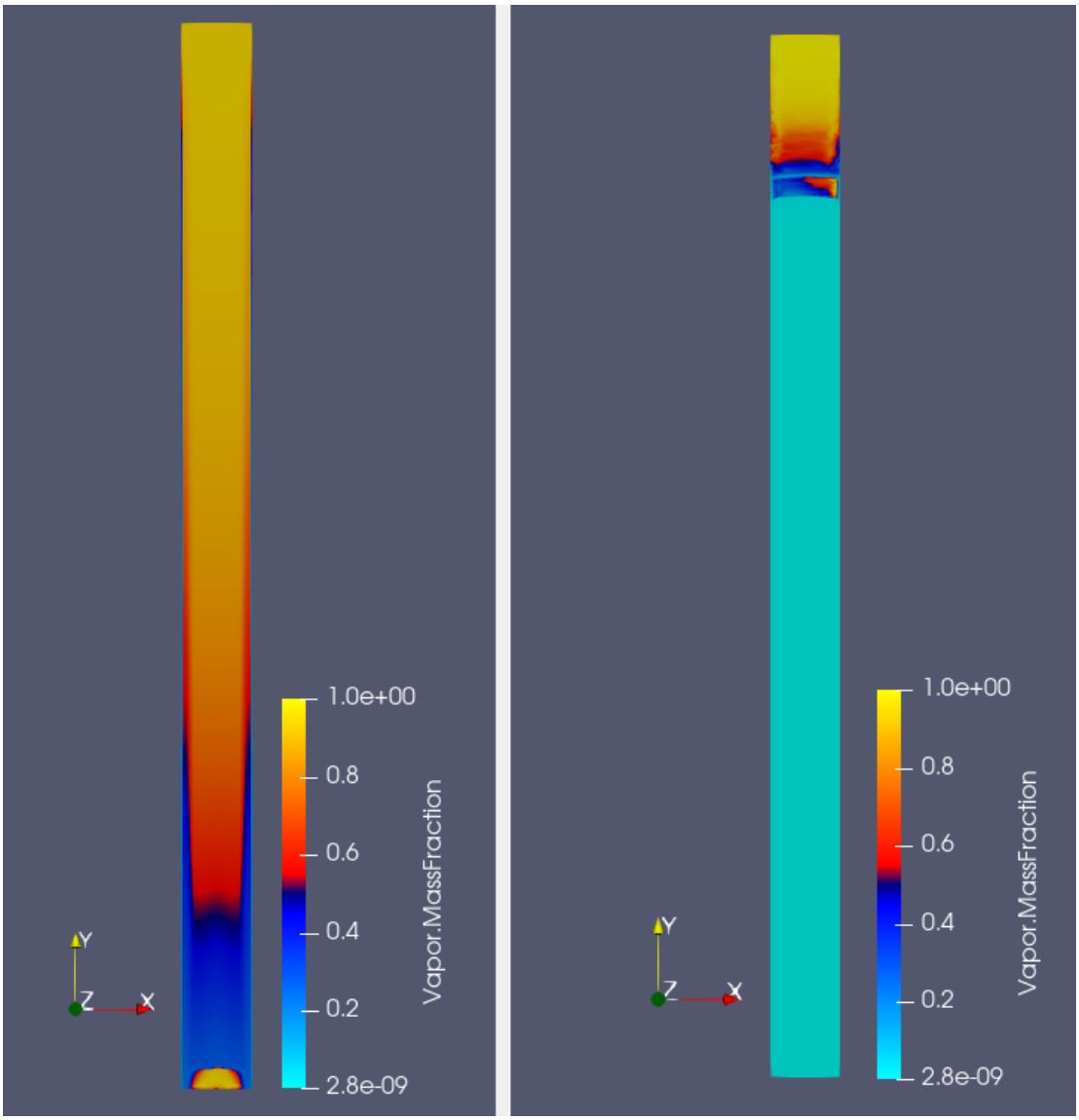

Figure 18. Vapor mass fraction contour for a bulk mass flow rate outlet boundary condition using constant property fluids (left) and variable property fluids (right)

d. Result of defining velocity and temperature as inlet boundary conditions

The final variation of the boundary conditions that was done was to define the inlet boundary conditions using normal speed and static temperature and the outlet boundary using average static pressure. The first model, solution number six in Table 6, was run using constant property fluids. The inlet velocity was determined to be 0.69 m/s using the mass flow rate of 0.003236 kg/s and a mixture density of 14.85 kg/m^3 at 99% quality. The

vapor mass fraction at the inlet was also changed to 0.9999, corresponding to an inlet quality of 99.44%, approximately 5% higher than solutions one through four. A second model, solution number seven in Table 6, using the same boundary conditions but variable property fluids based on IAPWS IF97 EOS was also run.

The results for solution six and seven were very similar to the results obtained using a mass flow rate outlet boundary condition and constant property fluids, solution four in Table 6. A dome of recirculating vapor formed near the outlet with an annular-type flow at the outlet plane. However, a wall was placed at 42.5% of the outlet area of solution six and approximately 47% of the outlet area for solution seven which resulted in a recirculation region of vapor at the outlet. Solution six reached an average vapor mass fraction of 0.356 after 1500 iterations, whereas solution seven had an average of 0.3587 after 1500 iterations. Each had also nearly reached continuity between the inlet and outlet. Solution six had a mass flow rate of 0.0031987 at the inlet and 0.0031978 kg/s at the outlet, both of which are within 1.2% of the expected mass flow rate from Table 3. Similarly, solution seven using variable property fluids had an inlet mass flow rate of 0.0031978 kg/s and outlet mass flow rate of 0.0031984 kg/s. The similarity of the results when using constant property and variable property fluids suggests this is a very stable set of boundary conditions. Figure 19 shows the vapor mass fraction contour along the pipe centerline for both solutions. Figure 20 shows the vapor mass fraction contour at the outlet plane for each solution.

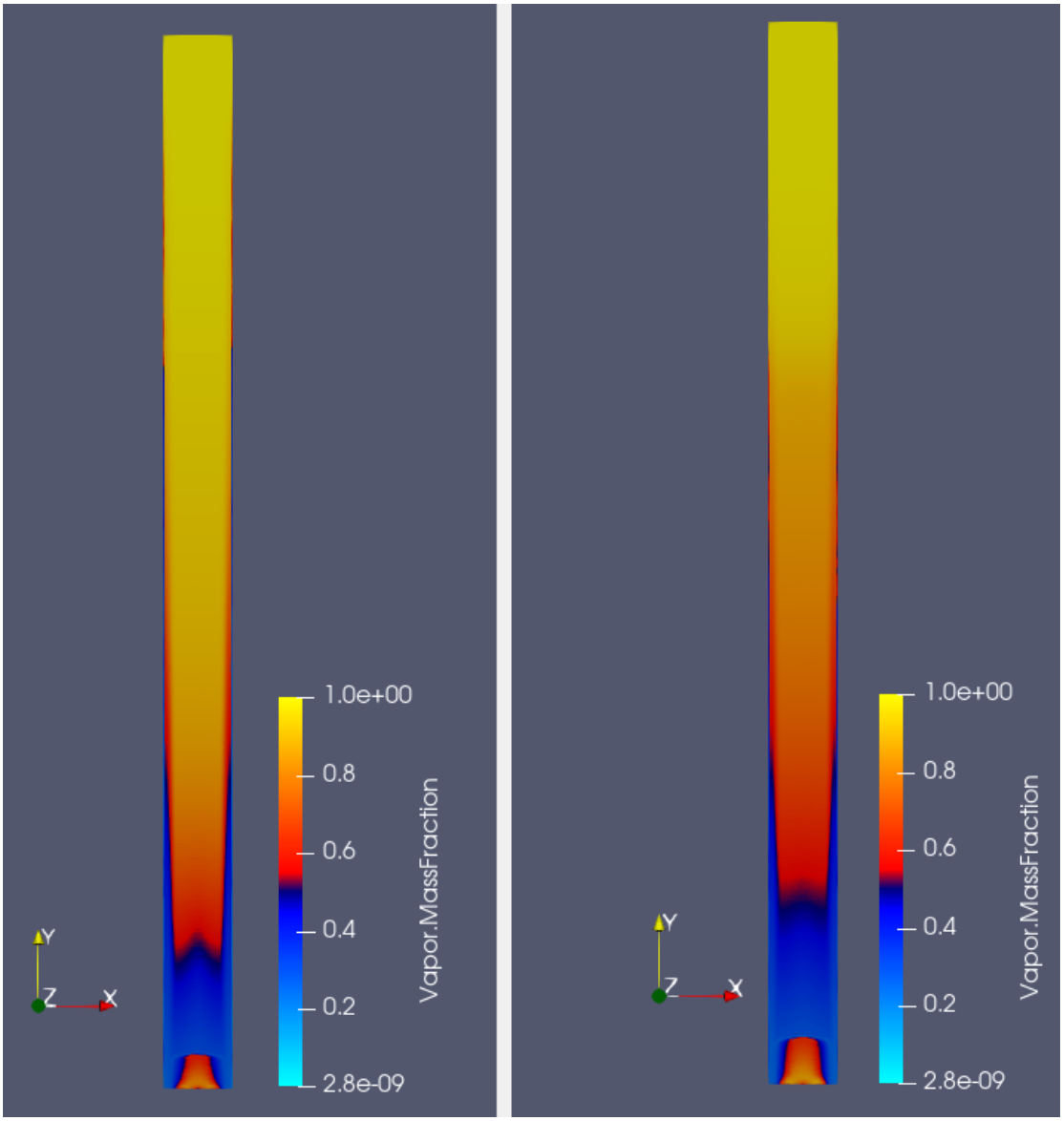

Figure 19. Comparison of vapor mass fraction contour for solutions six and seven

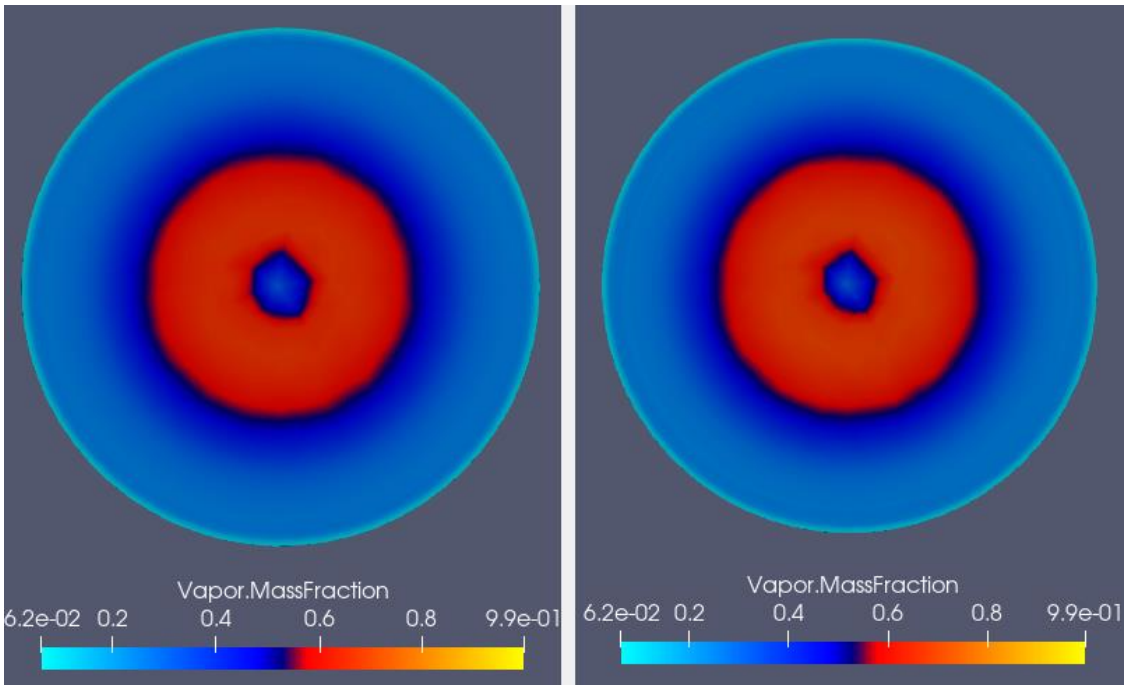

Figure 20. Comparison of the vapor mass fraction contour at the outlet plane for solutions six (left) and seven (right)

A review of the different characteristics of the seven solutions generated to test various boundary conditions and model configurations resulted in choosing the bulk mass flow rate outlet boundary condition with variable property fluids to test the remaining cases. The combination of bulk mass flow rate outlet boundary condition and variable property fluids resulted in the most complete condensation of the vapor within the pipe. The solution also did not have the non-physical liquid pool or vapor dome at near the outlet of the pipe, conditions which were forced by the solver attempting to meet the assigned boundary conditions. However, artificial walls were placed at the outlet in both cases to meet the assigned boundary conditions. In the case of the bulk mass flow rate outlet boundary condition, the artificial walls placed at the inlet and outlet boundaries prevented the flow from reaching continuity between inlet and outlet and introduced some instability. When implementing the normal speed inlet boundary condition, an artificial wall was only placed at the outlet boundary, allowing the solution to reach continuity of mass flow with a vapor recirculation region at the outlet.

This test of various combinations of boundary conditions also informed decisions for the boundary conditions used in modeling the steam pipe. The stability and consistency of the combination of normal speed and static temperature at the inlet boundary without forcing a non-physical outlet condition was preferred for initial development of the steam pipe model discussed in Chapter V. The similarity of the results using constant property and variable property fluids suggested that constant property fluids should be used to quickly obtain a solution to use as the initial conditions for a more complex model with variable property fluids without severely affecting the model stability.

D. MODEL IMPLEMENTATION

Following comparison of the effects of different boundary conditions, the model built for Case 1 was then implemented for the remaining four cases. Each of the four remaining cases was modeled using two sets of boundary conditions. First, each case was modeled using static temperature and normal speed at the inlet with variable property fluids. Next, each was modeled using a bulk mass flow rate outlet boundary condition with variable property fluids. All four cases used the same inlet vapor volume fraction of 0.9999, corresponding to an inlet quality of 99.44%.

1. Case 5 Results

Using the data from Table 3, two models for Case 5 were set up in CFX. The first model was set up using variable property fluids and a normal speed defined at the inlet boundary. As with solutions six and seven for Case 1, the normal speed was calculated using the mixture density at 99% quality and the mass flow rate from Table 3. Also as before, the saturation temperature and static temperature were set to the user expression T_{sat} which calculated a saturation temperature using IAPWS IF97 equation of state based on the user expression Press, which was set to 2.94 MPa and used as the input for the outlet static pressure boundary condition. The calculated T_{sat} was 505.89 K. The wall heat flux boundary condition was ramped down from zero over 250 iterations, then held constant to increase model stability. The second solution used a bulk mass flow rate outlet boundary condition set to the corresponding value from Table 3. The inlet boundary conditions for that solution were static temperature and static pressure, set to the user expression for T_{sat}

and Press respectively. Table 7 is a consolidated listing of the boundary conditions and their values for Case 5.

Table 7. Domain settings and boundary conditions for Case 5

Solution	Domain Models	Domain Basic Settings	Inlet Boundary Conditions	Outlet Boundary Conditions	Wall Boundary Conditions
1	Variable property fluids, drag, lift, buoyancy	P_{ref} : 0 MPa T_{sat} : 505.89 K	T_{static} : 505.89 K Normal Speed: 1.52 m/s VF_{vapor} : 0.9999	P_{static} (Rel): 2.94 MPa	Heat Flux: -67500 W/m^2
2	Variable property fluids, drag, lift, buoyancy	P_{ref} : 0 MPa T_{sat} : 505.89 K	T_{static} : 505.89 K P_{static} (Rel): 2.94 MPa VF_{vapor} : 0.9999	Bulk Mass Flow Rate: 0.00707 kg/s	Heat Flux: -67500 W/m^2

a. Solution 1 Results

The first solution for Case 5 was run for 1500 iterations and reached continuity between the inlet and outlet mass flow rates. The calculated mass flow rate was 0.0070446 kg/s at the inlet plane and 0.0070449 kg/s at the outlet plane, a difference of 0.004%. Both the inlet and outlet solver calculated mass flow rates were within 0.4% of the expected mass flow rate of 0.00707 kg/s from Table 3. The resulting average vapor mass fraction at the outlet plane was 0.3707. This resulted in a calculated outlet quality of 19.7%, compared to 99.44% at the inlet.

Unlike Case 1, the use of normal speed and static temperature boundary conditions did not result in a recirculating vapor dome at the pipe outlet. An artificial wall was placed at 13.4% of the outlet area by the solver, approximately one third of the wall placed at the outlet for Case 1 using the same boundary condition. This difference in the restriction of the outlet flow resulted in no recirculation of vapor at the outlet. The flow developed a more distinct annulus as well, with the highest concentration of liquid at the wall boundary. Figure 21 shows the vapor mass fraction contour along the center plane of the pipe. A

distinct liquid film began forming within the first inflation layer approximately 10 mm, half the pipe radius, downstream of the inlet, shown in Figure 22. By the pipe midpoint, the liquid film at the wall had grown to 0.3 mm in thickness, approximately two cells thick, as shown in Figure 23. The film formation is more apparent in an examination of the vapor mass fraction at the pipe outlet plane and the middle of the pipe, shown in Figure 24. An annular flow is present at the middle of the pipe. This annular flow continues to the outlet where it becomes more uniform as vapor continued to condense.

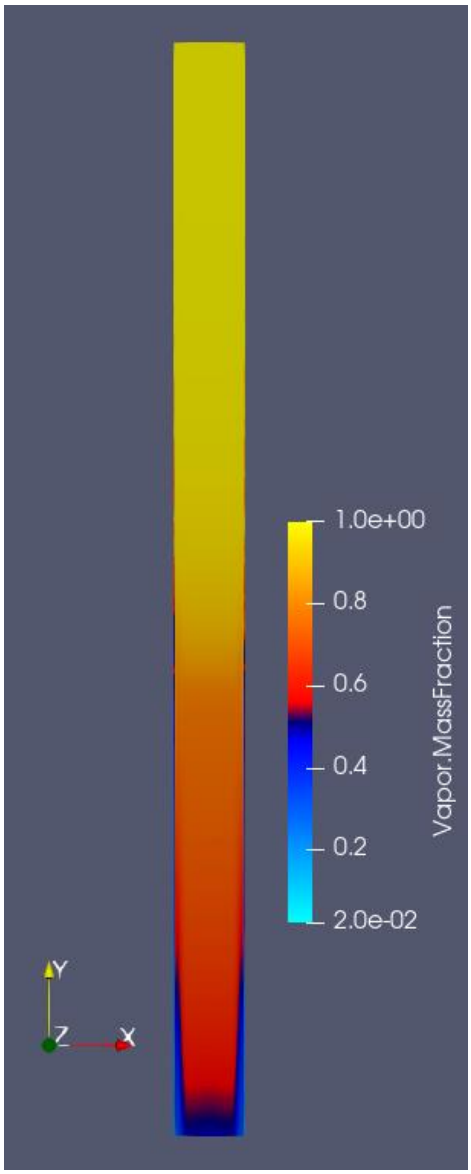

Figure 21. Vapor mass fraction contour at the pipe central plane for Case 5 solution 1

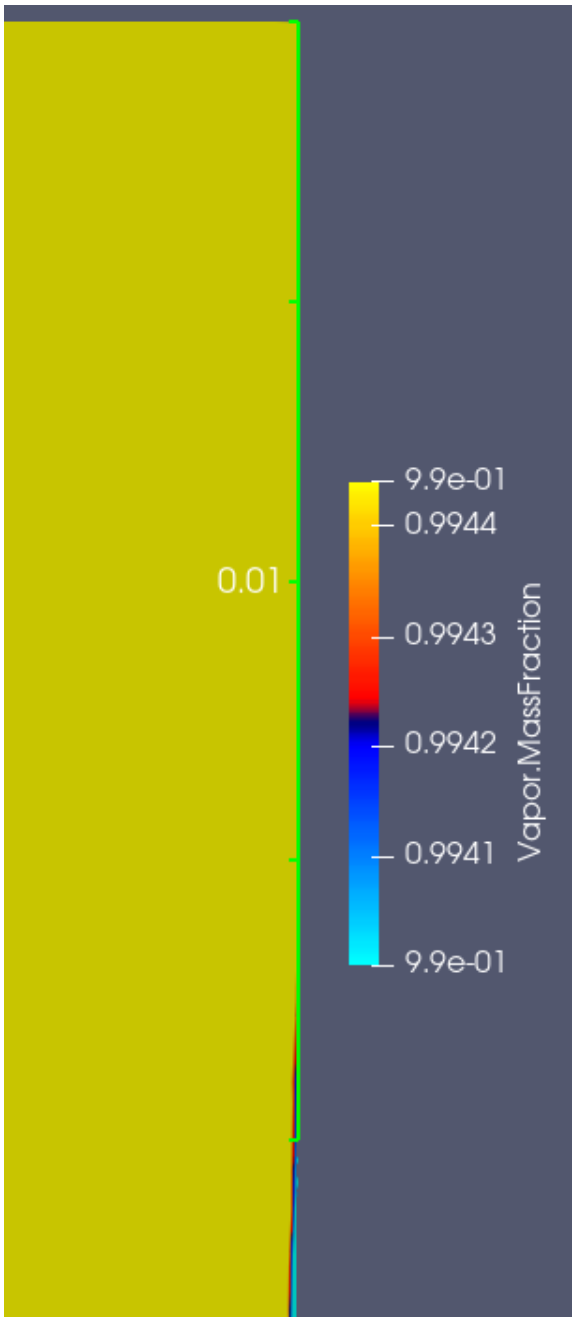

Figure 22. Vapor mass fraction contour at the wall downstream of the inlet

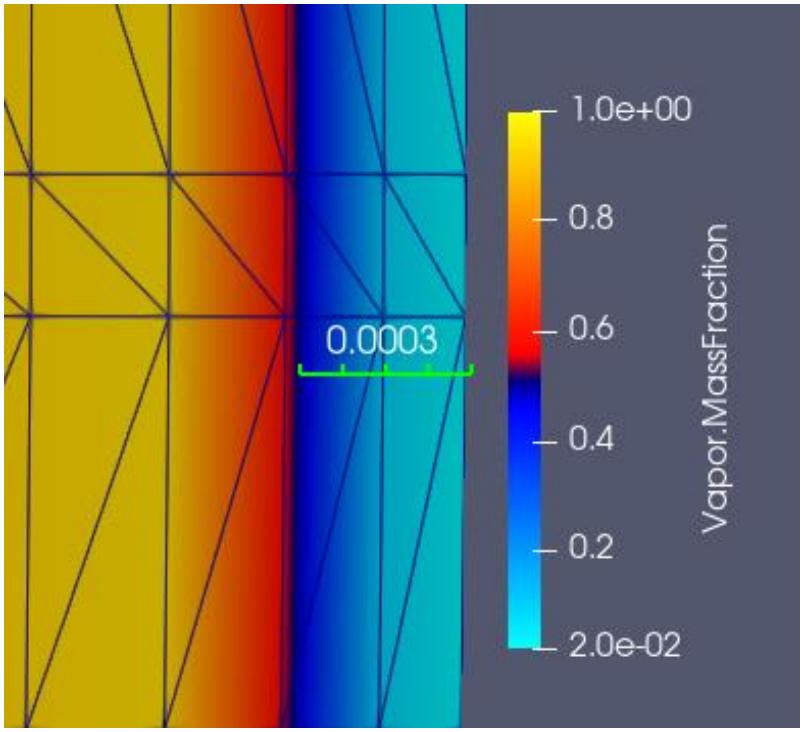

Figure 23. Liquid film shown at the pipe midpoint

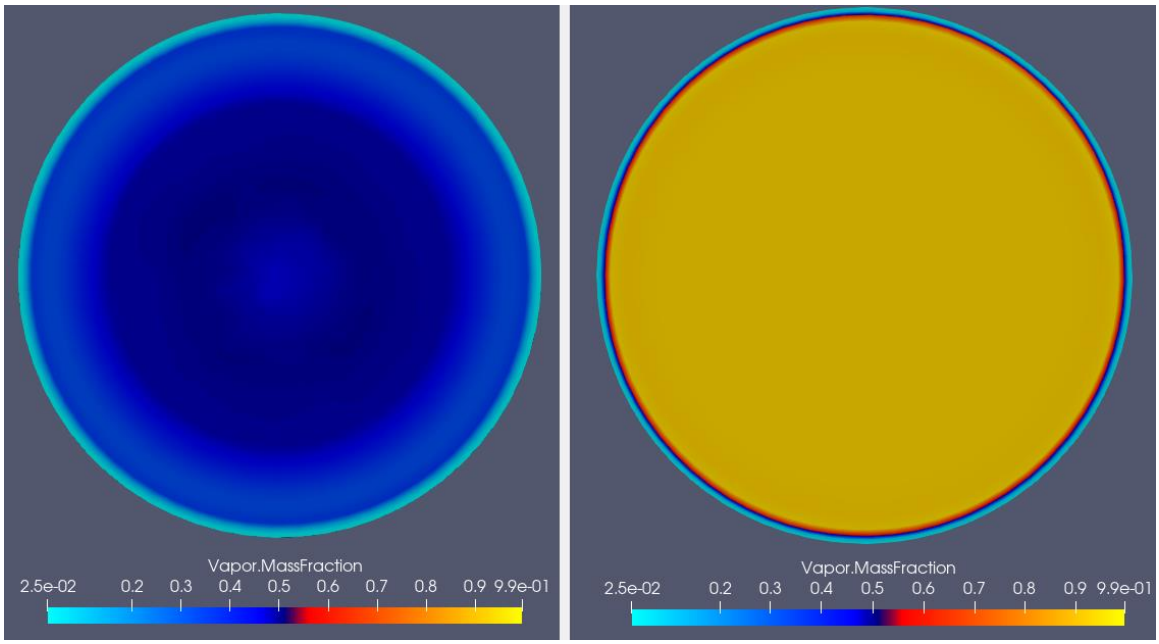

Figure 24. Comparison of vapor mass fraction at the pipe outlet plane (left) and middle (right)

b. Solution 2 Results

The second model for Case 5 used the bulk mass flow rate outlet boundary condition. Like with the results for Case 1, the bulk mass flow rate outlet boundary condition resulted in an outlet quality of 2.86×10^{-5}%, effectively completely liquid, when calculated using Eq. (9). However, the solver placed artificial wall boundaries at the inlet to prevent vapor backflow and at the outlet to prevent liquid and vapor backflow. The artificial wall at the inlet lowered the calculated inlet quality to 98.9% compared to the specified value of 99.44%. Continuity was also not reached, with the wall at the inlet resulting in a reduction of the inlet mass flow rate by an order of magnitude to 0.000785 kg/s. Outlet mass flow rate was slightly lower than the specified boundary condition due to instability, preventing the solution from reaching continuity and resulting in an outlet mass flow rate of 0.007068 kg/s. A vapor mass fraction contour is provided in Figure 25.

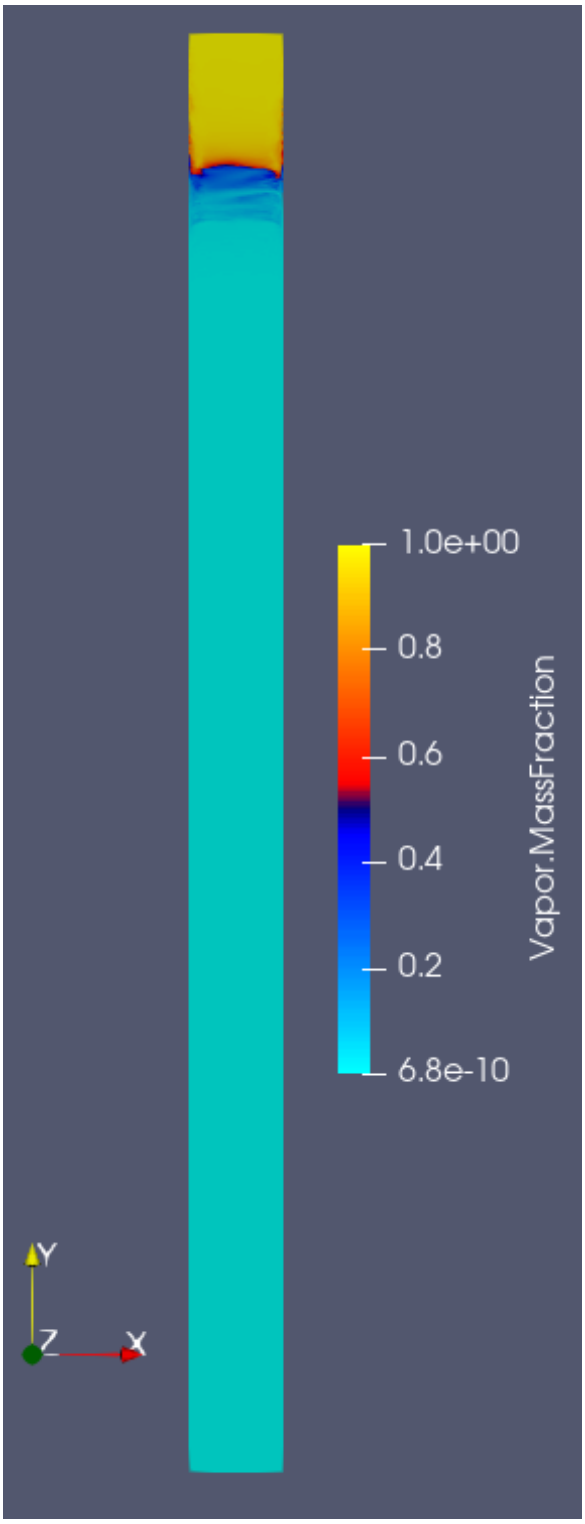

Figure 25. Vapor mass fraction contour for Case 5 solution 2

Overall, the results for Case 5 were similar to those for Case 1, which was expected since the Reynold's number and Froude number for both were of the same order of magnitude respectively. As with Case 1 solution 8, the normal speed inlet boundary condition for Case 5 was more stable and produced expected flow characteristics, including the formation of a liquid film at the wall and subsequent annular flow. The normal speed inlet boundary condition also resulted in the solver reaching continuity between the inlet and outlet. While the vapor in the pipe did not completely condense as with the bulk mass flow rate outlet boundary condition, the characteristics of the flow were sufficient to show that the boundary conditions chosen were suitable for modeling phase change of saturated steam.

2. Case 14 Results

Neither set of boundary conditions used to model Case 14 was successful, likely due to significantly greater wall heat flux and corresponding higher rate of condensation. Table 8 summarizes the settings used for the two attempts at modeling Case 14. The wall heat flux was ramped down starting from zero over 500 iterations for the first two models, then 1000 iterations for the third. For the first two solutions, the solver failed after reaching the maximum wall heat flux boundary condition. The first solution became unstable at approximately 400 iterations, with significant fluctuations in the measured outlet mass flow rate beginning after 470 iterations. The second solution showed signs of increasing instability after 375 iterations, with significant fluctuations in inlet mass flow rate, since the outlet mass flow rate was the defined boundary condition, beginning after 400 iterations. For the third model, where the heat flux was stepped down over 1000 iterations, the solver failed at 760 iterations, where the wall heat flux boundary condition had only reached -756000 W/m^2.

Table 8. Domain settings and boundary conditions for Case 14

Solution	Domain Models	Domain Basic Settings	Inlet Boundary Conditions	Outlet Boundary Conditions	Wall Boundary Conditions
1	Variable property fluids, drag, lift, buoyancy	P_{ref} : 0 MPa T_{sat} : 505.89 K	T_{static} : 505.89 K Normal Speed: 22.3 m/s VF_{vapor} : 0.9999	P_{static} (Rel): 2.94 MPa	Heat Flux: -995000 W/m^2
2	Variable property fluids, drag, lift, buoyancy	P_{ref} : 0 MPa T_{sat} : 505.89 K	T_{static} : 505.89 K P_{static} (Rel): 2.94 MPa VF_{vapor} : 0.9999	Bulk Mass Flow Rate: 0.104 kg/s	Heat Flux: -995000 W/m^2
3	Variable property fluids, drag, lift, buoyancy	P_{ref} : 0 MPa T_{sat} : 505.89 K	T_{static} : 505.89 K P_{static} (Rel): 2.94 MPa VF_{vapor} : 0.9999	Bulk Mass Flow Rate: 0.104 kg/s	Heat Flux: -995000 W/m^2

a. Solution 1 Results

Post-processing of a backup file saved at 510 iterations revealed that near the pipe outlet regions of very high liquid velocity and correspondingly high Courant numbers was present. The highest liquid velocity along the center of the pipe was 810 m/s, and the highest Courant number was 50304. Figure 26 shows a contour of where the courant number exceeded 100 in the pipe and the liquid velocity magnitude along the center of the pipe. The majority of the domain had a Courant number below 50. Also of interest was the fact that the majority of the pipe contained vapor, with what liquid had condensed concentrated near the outlet. Figure 27, a monitor plot of the inlet and outlet bulk mass flow rate, shows how the outlet mass flow rate increased significantly before the solver failed.

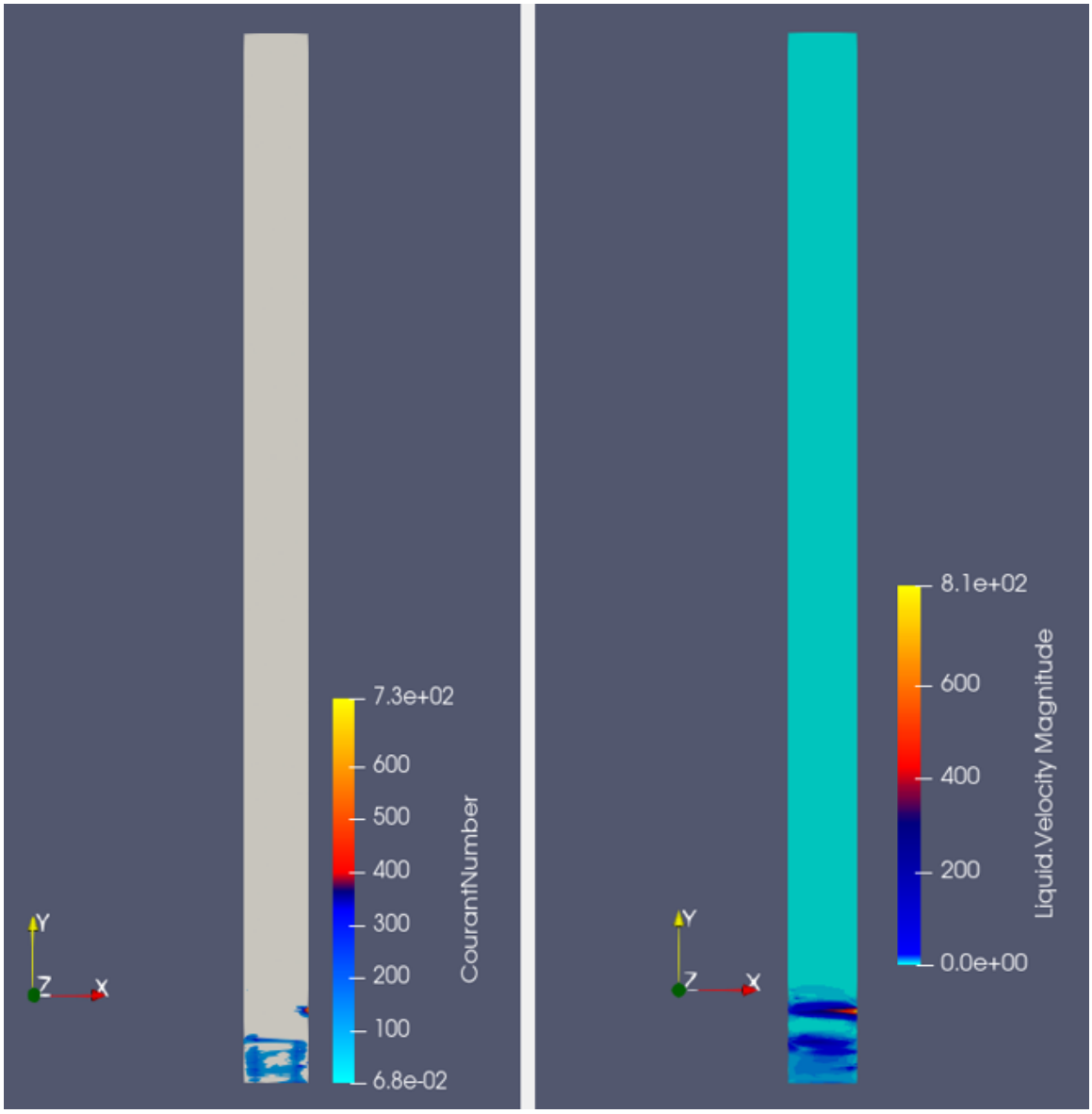

Figure 26. Contours of the Courant number near the outlet and liquid velocity

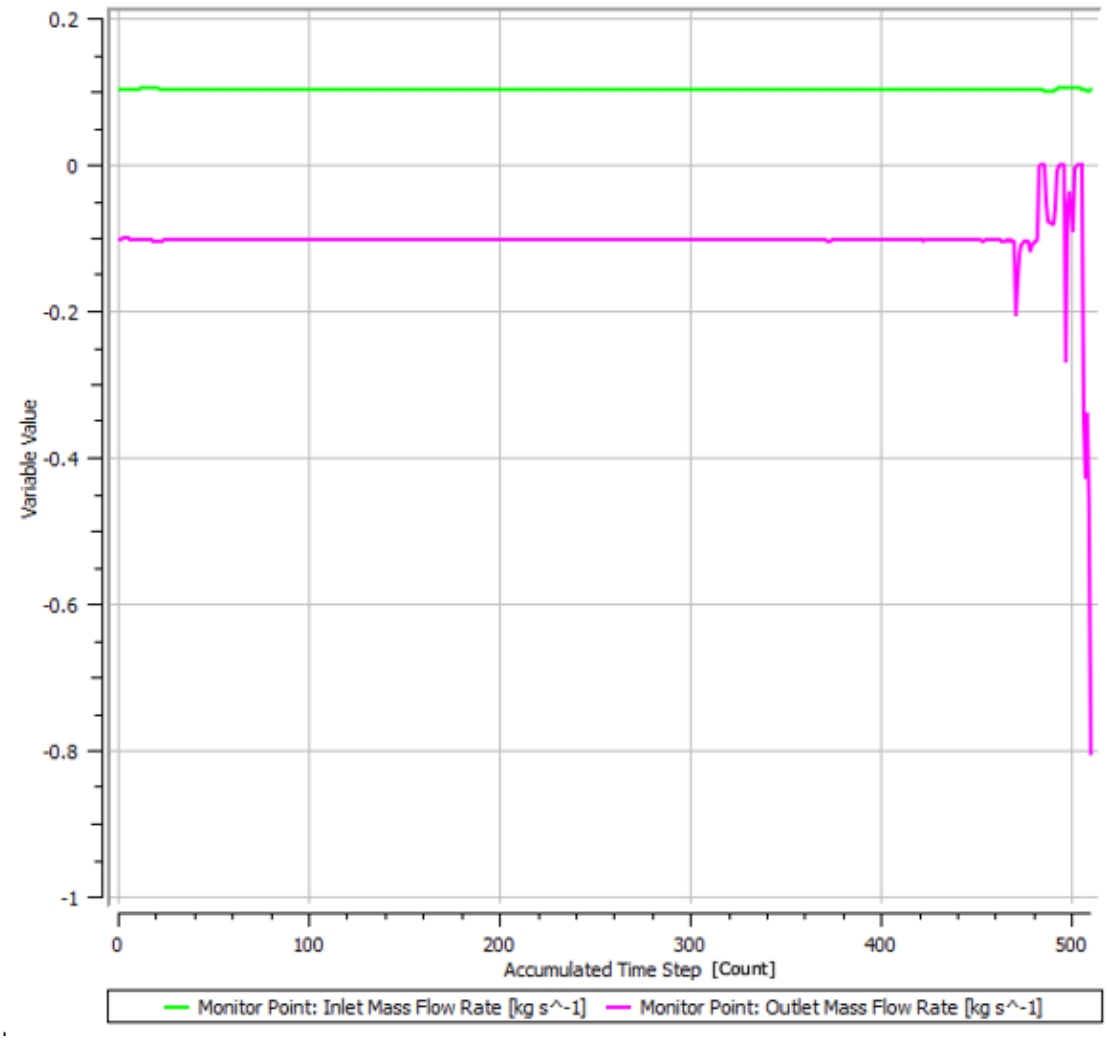

Figure 27. Plot of the inlet and outlet mass flow rate for Case 14 solution 1

b. Solution 2 Results

Examination of the CFX out file for the bulk mass flow rate outlet boundary condition revealed significant differences between this case and the previous cases. Unlike Case 1 and Case 5, no artificial wall was placed at the inlet or outlet boundaries by the solver until 525 iterations when the inlet mass flow rate was 0.201 kg/s, almost double the outlet mass flow rate as shown in Figure 28. At 525 iterations, a wall was placed at 1% of the outlet area to prevent vapor backflow and 0.2% of the outlet area to prevent liquid backflow. Multiple variables also violated their upper table bounds, including both liquid and vapor density, thermal conductivity, dynamic viscosity, temperature, and local speed

of sound. A maximum Mach number warning for a maximum Mach number of 3.96 appeared at 513 iterations and persisted at various Mach numbers until the solver failed at 528 iterations due to fatal overflow in the solver. The maximum Mach number just prior to failure was 1.819×10^{6}. An analysis of the vapor temperature at the wall showed that significant regions of vapor at the wall boundary was at a temperature well below 273 K, shown in Figure 29. This non-physical saturated vapor temperature is likely the result of the large heat flux at the wall.

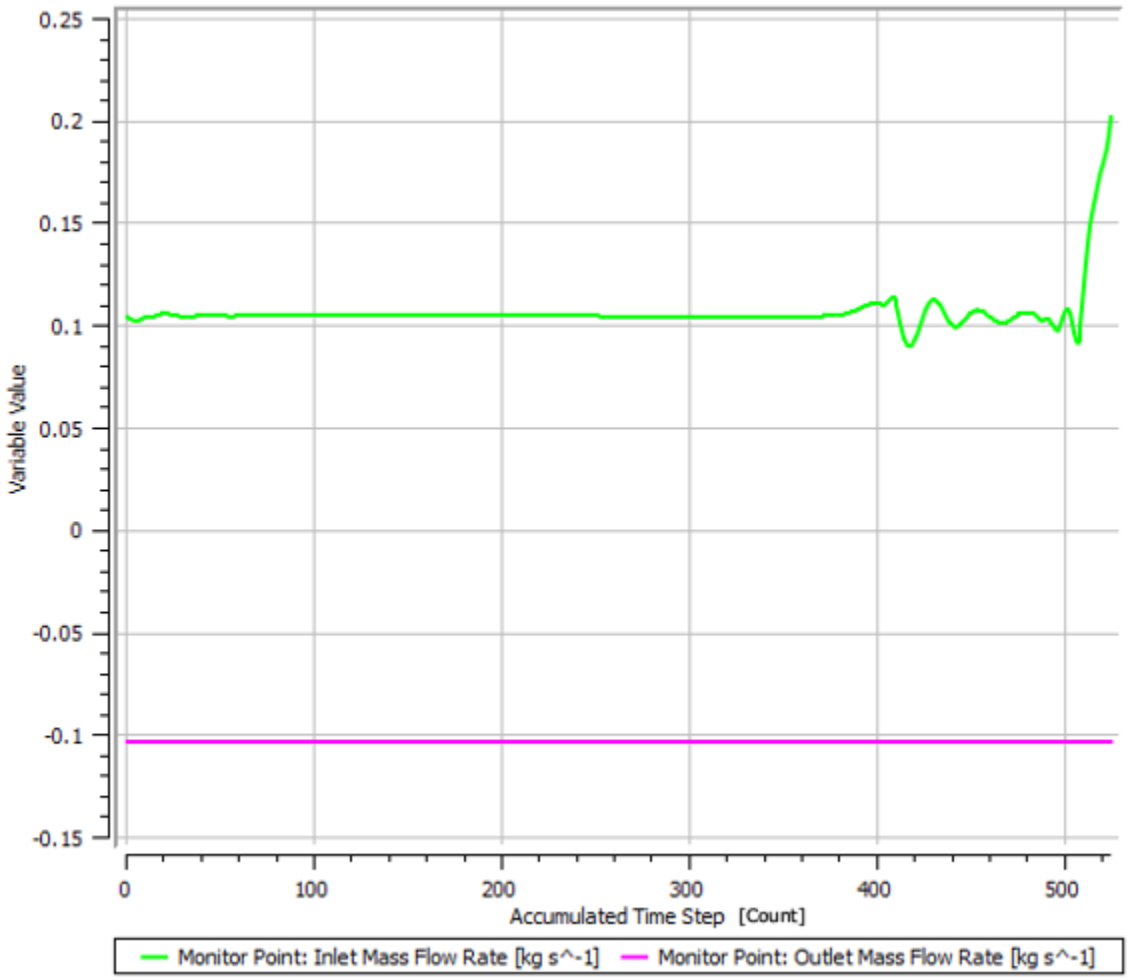

Figure 28. Plot of the inlet and outlet mass flow rate for Case 14 solution 2

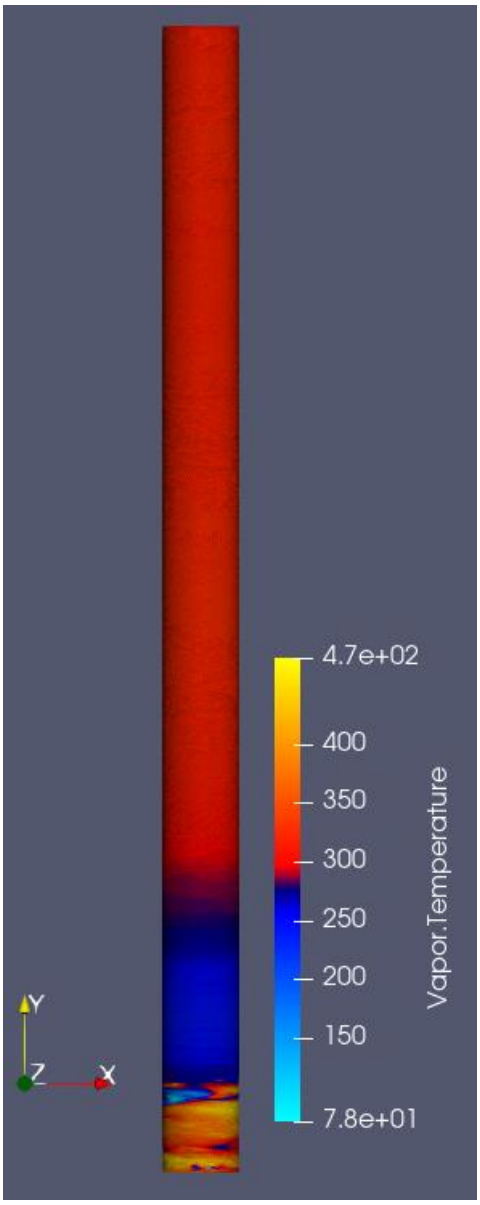

Figure 29. Vapor temperature contour for Case 14 solution 2

c. Solution 3 Results

A third attempt at modeling Case 14 used the same bulk mass flow rate outlet boundary condition but ramped the wall heat flux boundary condition over 1000 iterations vice 500. The solver failed at 760 iterations due to a divide by zero condition in the solver. Prior to the solver failing, vapor static entropy violated its lower table bound at 756 iterations and the value was extrapolated. An analysis was conducted of a backup file saved

at 755 iterations which showed that the vapor temperature at the wall was well below 273 K, similar to the results for solution 2.

Overall, the CFX solver was unable to model the condensation of saturated vapor at such a high wall heat flux boundary condition using the models discussed. Neither an inlet normal speed or outlet bulk mass flow rate boundary condition resulted in the solution converging or maintaining stability, and in two cases resulted in non-physical results for vapor temperature.

3. Case 25 Results

Case 25 had the lowest wall heat flux of the five cases selected to model. Solution one, using a normal speed boundary condition at the inlet, was unsuccessful with the solver failing before the maximum value of the wall heat flux was reached. Solution two, using a bulk mass flow rate boundary condition, was mostly successful with some non-physical characteristics similar to both Case 1 and Case 5. Table 9 is a summary of the boundary conditions.

Table 9. Domain settings and boundary conditions for Case 25

Solution	Domain Models	Domain Basic Settings	Inlet Boundary Conditions	Outlet Boundary Conditions	Wall Boundary Conditions
1	Variable property fluids, drag, lift, buoyancy	P_{ref} : 0 MPa T_{sat} : 505.89 K	T_{static} : 505.89 K Normal Speed: 0.467 m/s VF_{vapor} : 0.9999	P_{static} (Rel): 2.94 MPa	Heat Flux: -20800 W/m^2
2	Variable property fluids, drag, lift, buoyancy	P_{ref} : 0 MPa T_{sat} : 505.89 K	T_{static} : 505.89 K P_{static} (Rel): 2.94 MPa VF_{vapor} : 0.9999	Bulk Mass Flow Rate: 0.00218 kg/s	Heat Flux: -20800 W/m^2

a. Solution 1 Results

The wall heat flux boundary condition was setup to ramp down to its maximum value of 20800 W/m^2 over 250 iterations. The solver failed at 232 iterations due to overflow, with an artificial wall boundary placed at 100% of the outlet area by the solver at 230 iterations. When the solver failed, a wall boundary was still present at 98.6% of the outlet area to prevent vapor and liquid backflow. A review of the monitor plot for liquid velocity showed that at 230 iterations, the average liquid velocity at the outlet jumped dramatically from 0.136 m/s to 387 m/s while the outlet mass flow rate was 0 kg/s. The artificial wall placed at the outlet by the solver ultimately cause the solver to crash. A backup file saved at 230 iterations was used for analysis.

A wall was placed at the outlet boundary beginning at 176 iterations at 0.3% of the outlet area to prevent vapor backflow, which grew rapidly to 100% of the area by 230 iterations. This restriction of vapor flow at the outlet, coupled with the very low velocity, caused the vapor to swirl randomly about the long axis of the pipe, with most of the liquid mass suspended near the middle of the pipe. Figure 30 is a vapor mass fraction contour showing the distribution of liquid mass near the middle of the pipe. A plot of the velocity vectors near the pipe outlet shows how the flow was swirling around the y-axis at a very low velocity due to the wall boundary condition at the outlet. Figure 31 shows the velocity vectors overlayed with an axial cross-section of the pipe at the outlet.

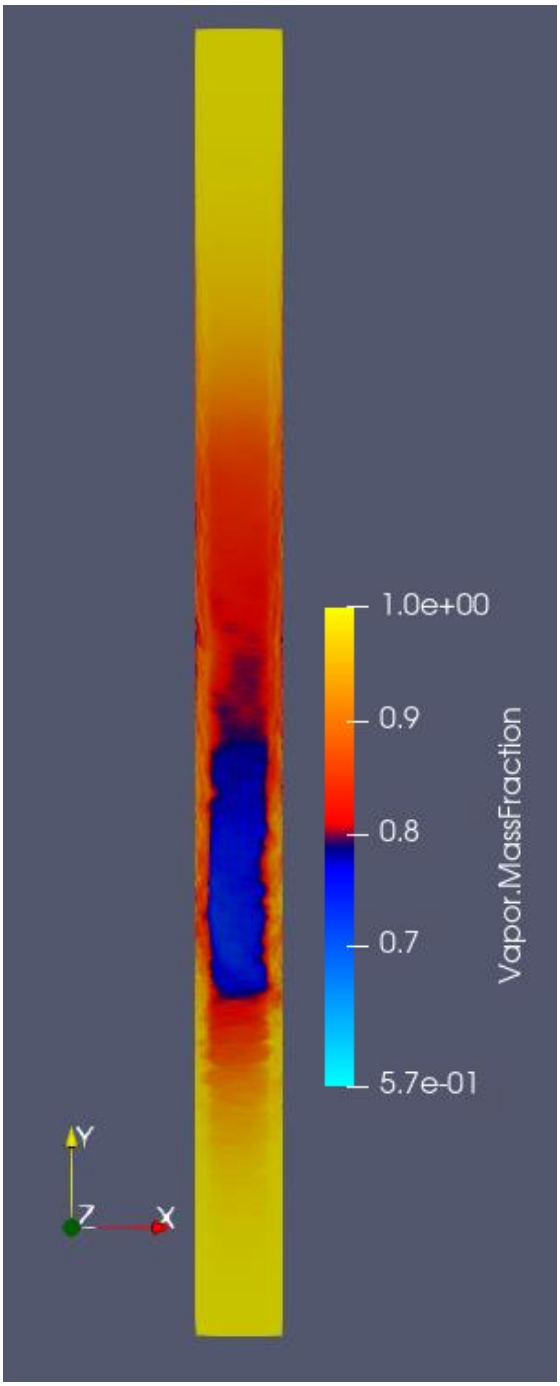

Figure 30. Vapor mass fraction contour along the pipe center for Case 25 solution 1

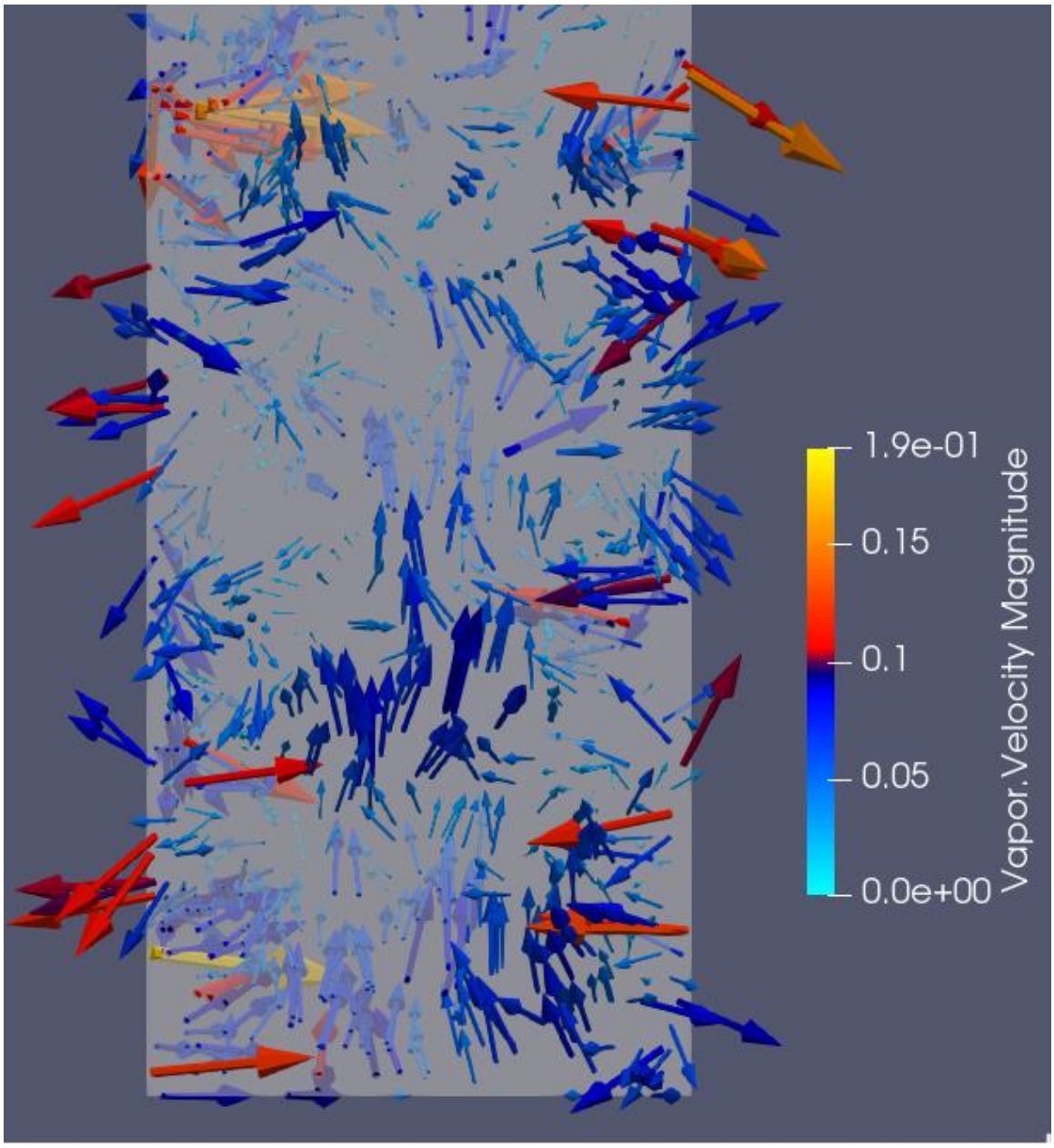

Figure 31. Plot of vapor velocity magnitude vectors near the pipe outlet for Case 25 Solution 1

b. Solution 2 Results

Use of the bulk mass flow rate outlet boundary condition resulted in significant condensation of the vapor within the pipe. As with previous models, a liquid film forms and grows moving towards the outlet where the liquid begins to coalesce. Continuity was

nearly reached between the inlet and outlet after 1500 iterations, with the inlet mass flow rate calculated as 0.002182 kg/s and trending down. Figure 32 shows the vapor mass fraction at the center of the pipe. However, an artificial wall boundary was again placed at the outlet covering 41% of the area to prevent vapor backflow. Another irregularity with the solution was a significant portion of the vapor at the wall was below 273 K, which is non-physical for a saturated steam system. This is likely due to the low vapor velocity and lack of wall film model, which results in heat being transferred between phases and between each phase and the wall. Figure 33 shows the vapor temperature at the pipe wall, where large regions of vapor below 273 K are present.

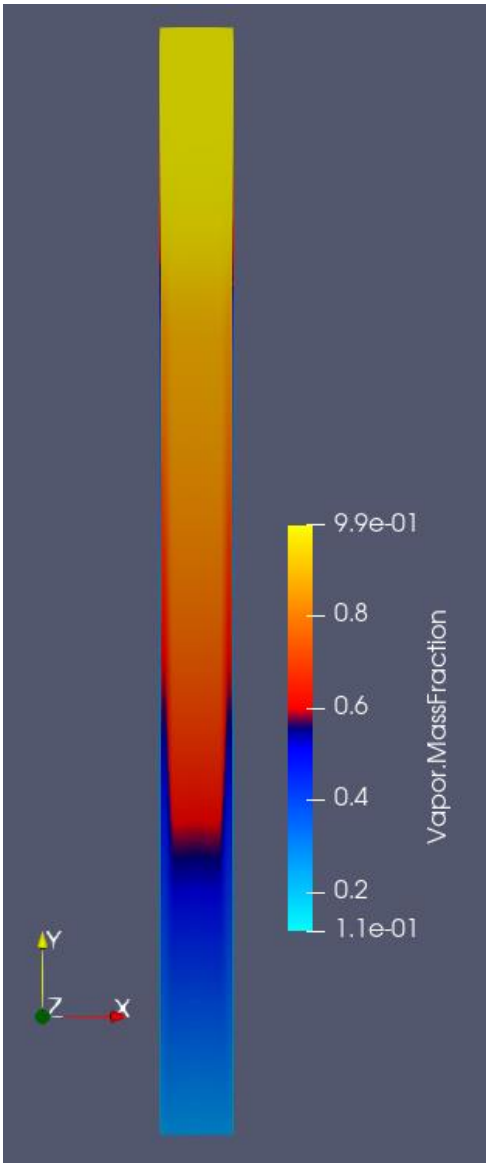

Figure 32. Vapor mass fraction contour at pipe center for Case 25 solution 2

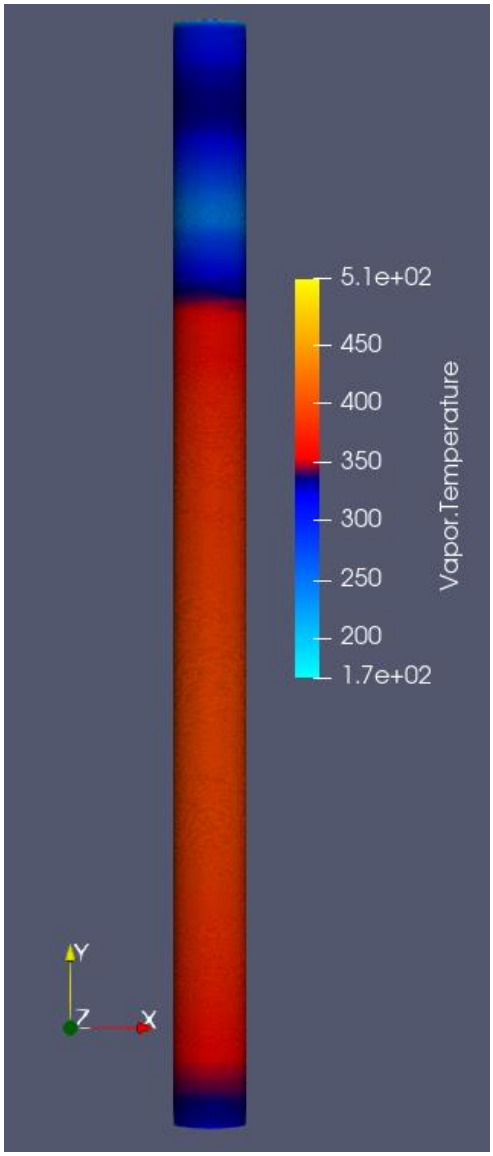

Figure 33. Vapor temperature contour for Case 25 solution 2

4. Case 27 Results

The model for Case 27 did not reach convergence using either set of boundary conditions examined. Compared to Case 14, Case 27 had the same order of magnitude total wall heat flux and vapor Re number, but one order of magnitude lower vapor velocity. For both the normal speed inlet boundary condition and bulk mass flow rate outlet boundary condition the wall heat flux was ramped down over 500 iterations. A summary of the boundary conditions for the two solutions is provided in Table 10.

Table 10. Domain settings and boundary conditions for Case 27

Solution	Domain Models	Domain Basic Settings	Inlet Boundary Conditions	Outlet Boundary Conditions	Wall Boundary Conditions
1	Variable property fluids, drag, lift, buoyancy	P_{ref} : 0 MPa T_{sat} : 505.89 K	T_{static} : 505.89 K Normal Speed: 0.467 m/s VF_{vapor} : 0.9999	P_{static} (Rel): 2.94 MPa	Heat Flux: -20800 W/m^2
2	Variable property fluids, drag, lift, buoyancy	P_{ref} : 0 MPa T_{sat} : 505.89 K	T_{static} : 505.89 K P_{static} (Rel): 2.94 MPa VF_{vapor} : 0.9999	Bulk Mass Flow Rate: 0.00218 kg/s	Heat Flux: -20800 W/m^2

a. Solution 1 Results

Solution 1 failed before reaching the maximum wall heat flux boundary condition, failing at 467 iterations due to a divide by zero floating point error in the solver. The error was most likely cause by vapor static entropy, which violated its lower bound the previous iteration. The suspected cause was regions where the vapor temperature was below 273 K, which an analysis of a backup file at 465 iterations confirmed. Vapor static entropy first violated its lower bound at 386 iterations, and the value was extrapolated by the solver. At the same time, the outlet mass flow rate and outlet average vapor mass fraction began decreasing. Overlaying vapor velocity vectors with a vapor mass fraction contour just before solver failure showed that a strong vapor recirculation region formed upstream of the outlet with vapor velocities approximately five times higher than the specified inlet boundary condition, shown in Figure 34. The same location also corresponded to a region of higher pressure and low vapor temperature, resulting in the vapor being subcooled. Figure 35 shows the local pressure contour where the vapor has accelerated to 30 m/s. These conditions caused significant instability in the solver and resulted in the failed model.

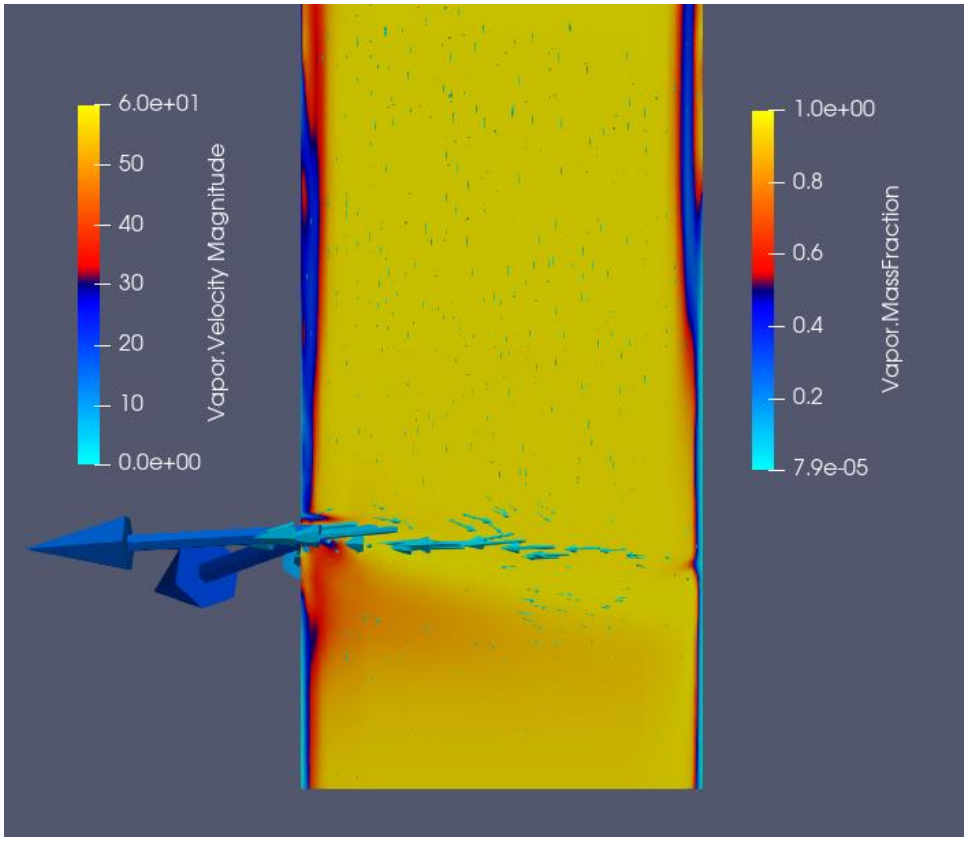

Figure 34. Vapor velocity vectors overlayed with a vapor mass fraction contour

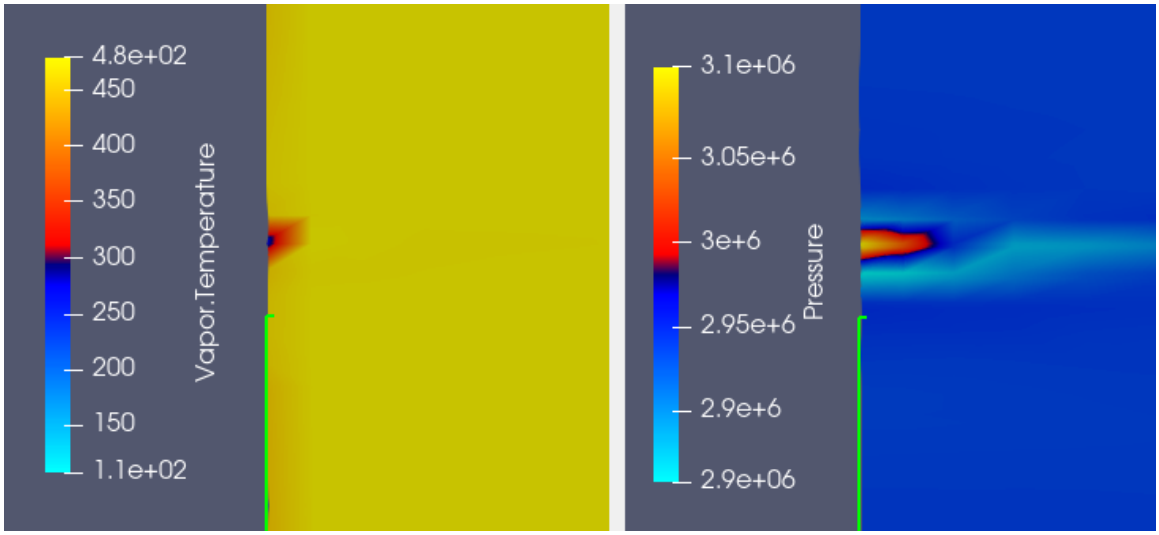

Figure 35. Local pressure and temperature contour at location of high vapor velocity

b. Solution 2 Results

The initial attempt at implementing a bulk mass flow rate outlet boundary condition failed at 407 iterations, before reaching the maximum wall heat flux boundary condition. Similar to Cases 14 and 25, failure occurred shortly after vapor static entropy violating its lower table bound, which occurred at 401 iterations. Analysis of a backup file saved at 400 iterations showed that a liquid film had formed and was being removed from the wall near the pipe outlet. Figure 36 shows the region near the outlet where the liquid mass was being entrained and removed from the wall film.

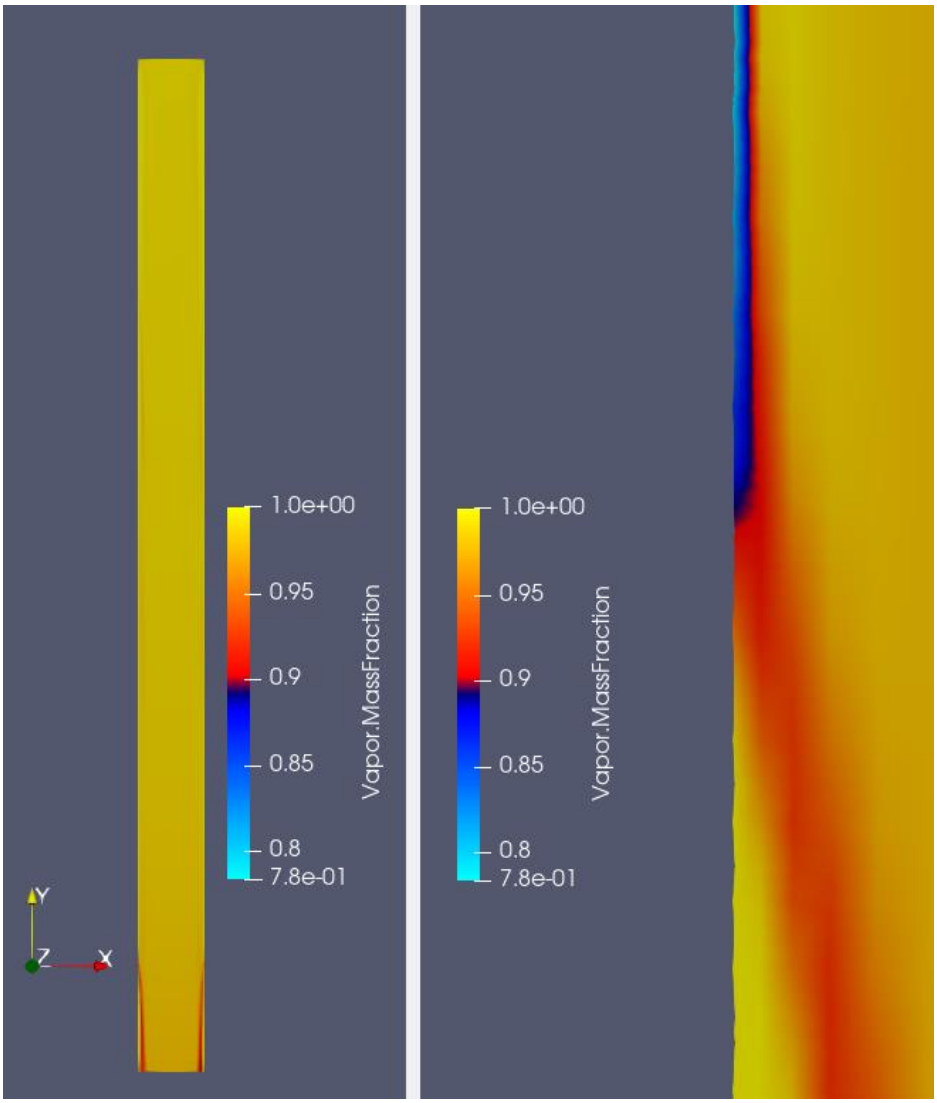

Figure 36. Vapor mass fraction contour showing the liquid entrainment

A second attempt at obtaining a solution was made by restarting the solver from the backup file at 400 iterations because the cause of the solver failing was unclear. At 437 cumulative iterations, a wall boundary was placed at 3.4% of the outlet area to prevent vapor backflow and 0.6% of the area to prevent liquid backflow. The artificial wall area fluctuated sporadically, including disappearing all together, until the wall heat flux reached its specified value at 500 iterations. This caused significant instability in the inlet mass flow rate as the solver attempted to reach continuity. Figure 37 is a plot of the inlet mass flow rate through 500 cumulative iterations.

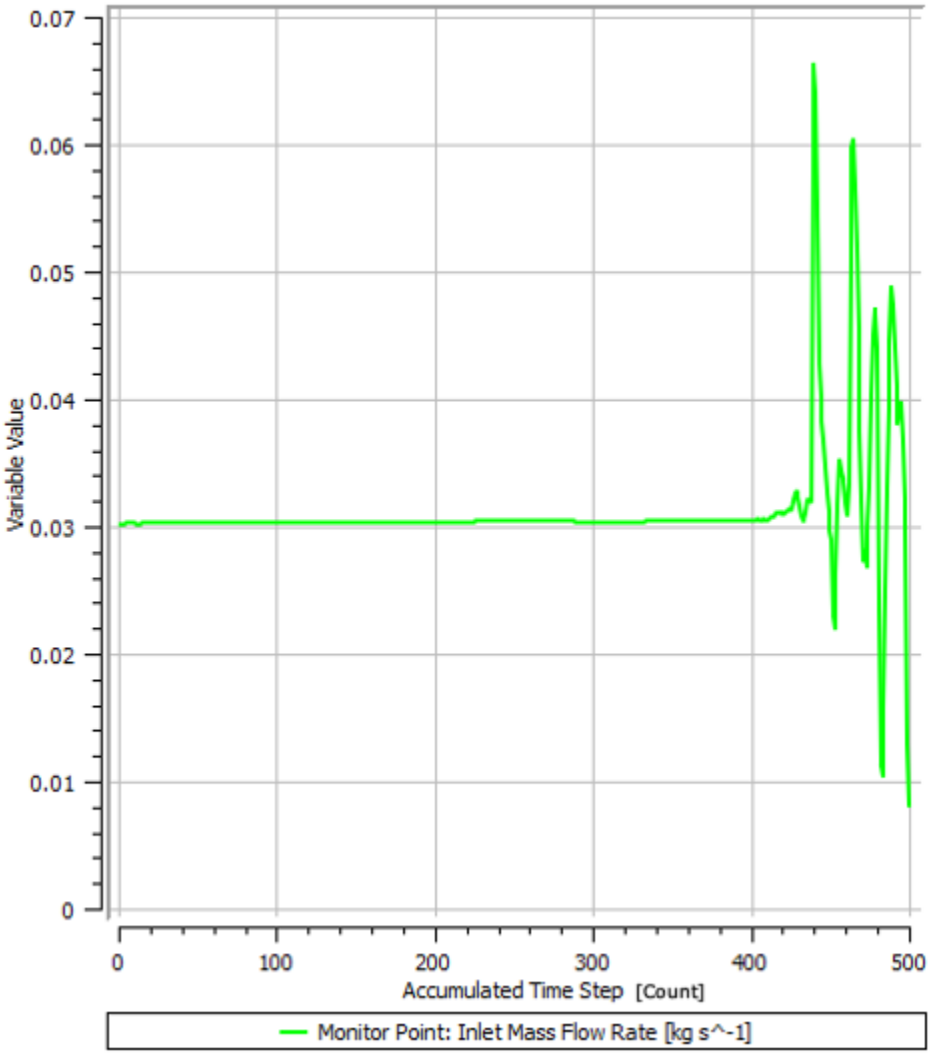

Figure 37. Plot of inlet mass flow rate for Case 27 solution 2

The solver failed at 561 iterations after a warning appeared for a high Mach number at 560 iterations. The maximum Mach number was over 649, which resulted in numerous parameters violating their upper bounds in partitions near the outlet. The properties included vapor temperature, density, thermal conductivity, specific heat capacity with respect to constant volume and pressure, dynamic viscosity, and static entropy. The corresponding liquid phase properties also violated their table limits. A significant amount of the vapor at the wall boundary was below 273 K, the same non-physical result obtained in other cases. Figure 38 shows the vapor temperature distribution at the wall. Also of note, the vapor wall heat flux was orders of magnitude greater than the liquid wall heat flux. This additional heat extraction from primarily the vapor phase resulted in the non-physical cooling of the vapor below 273 K. The vapor experiences greater wall heat flux due to the liquid being modeled as discreet dispersed droplets, which may not be present at the wall in significant concentrations. The vapor, a continuous liquid and modeled as a continuum, has contact with the pipe wall anywhere a discreet liquid droplet is not present. A comparison of the heat flux distribution for each phase is provided in Figure 39. Overall, the solution was very unstable and no convergence was reached.

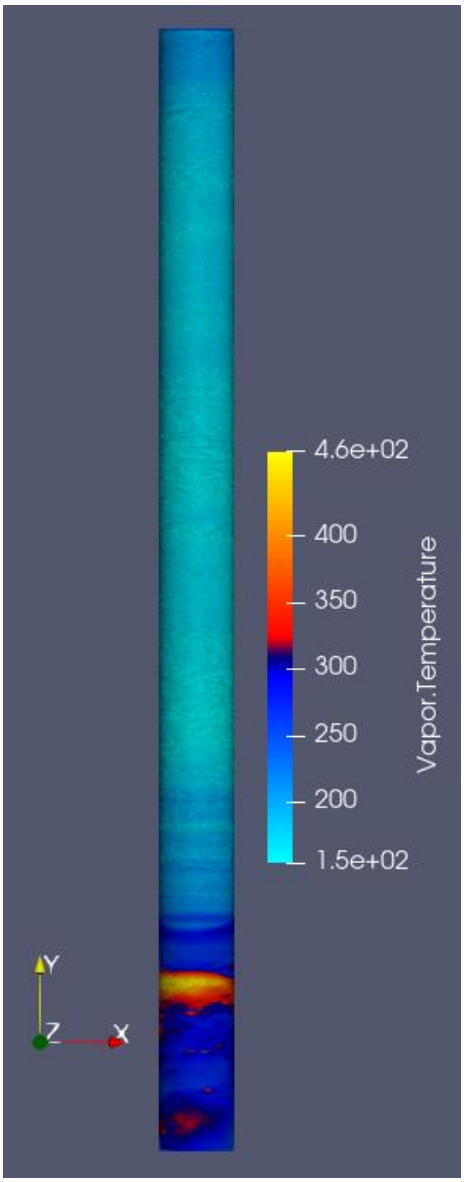

Figure 38. Vapor temperature near the pipe wall

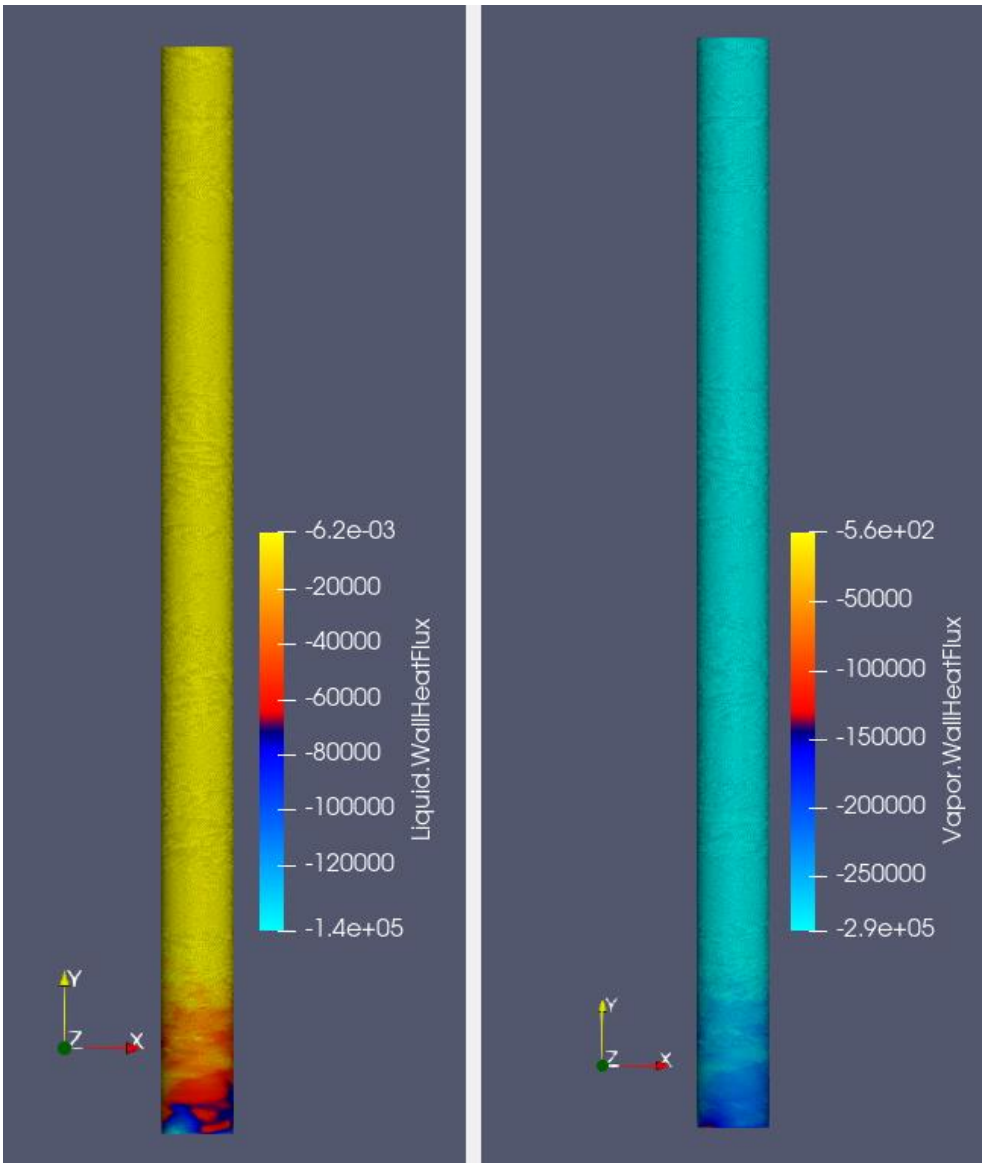

Figure 39. Contour of the liquid (left) and vapor (right) wall heat flux

E. CASE STUDY CONCLUSION

Important limitations on the ability to model phase change and two-phase saturated steam flow with heat transfer in CFX were found by modeling the five chosen cases. First, the choice of boundary conditions can greatly affect the solver results, including the development of non-physical flow conditions. Examples from this research include the pooling liquid using a normal speed outlet boundary condition, and a large region of vapor recirculation at the outlet when using a normal speed inlet boundary. The chosen phase

morphology also plays a significant role because a dispersed fluid phase interacts differently with the wall boundary than a continuous phase. When modeling a wall heat flux boundary condition, the continuous phase will undergo more heat transfer with the boundary, resulting in non-physical phase temperatures below 273 K at regions of the wall. The use of constant property fluids instead of variable property fluids dependent on EOS increases solver stability by preventing solver clipping or extrapolation of fluid properties. Finally, the use of a normal speed boundary condition at the inlet seemed to produce the most stable results, but did not result in the same degree of phase change as a mass flow rate outlet boundary condition. Overall, CFX is capable of modeling conjugate heat transfer in a saturated steam system, but careful consideration of the fluid properties and boundary conditions is required to obtain accurate results.

V. STEAM PIPING SYSTEM

A. MODEL GEOMETRY

The steam pipe geometry for this research was arranged to strike a balance between modeling the effect of complex geometry on wet steam flow and maintaining a relatively small domain to minimize computation resources required to develop the model. Two separate model geometries were generated which included features such as 90° bends, changes in pipe slope, and the addition branches that represent inlets to steam traps.

The geometry is 25 cm in diameter and is 23 m in total length. The pipe inlet is a 2 m long horizontal leg of piping followed by a 90° bend downward to a 2 m vertical leg. Another 90° bend leads to the mid-section of the pipe, which has an overall six degrees downward slope towards the outlet leg. A 6 m section is connected by a 90° bend to a 3 m section, which is again connected to an 8 m section by a 90° bend. Finally, the end of the 8 m leg of the piping turns to a vertically oriented upward outlet leg 2 m in length. All bends have a bend radius equal to the pipe diameter of 25 cm. In total, there are five bends in the piping, with two vertical sections, one horizontal section, and three sections sloped six degrees downward. The total elevation change measured from the centerline of the inlet to the outlet plane is 1.777 m. The total elevation change measured from the centerline of the inlet to the center of the fifth bend, the pipe's low point, is 3.748 m. Figure 40 is a profile view of the geometry. Figure 41 is a front view of the geometry showing the measured elevation changes.

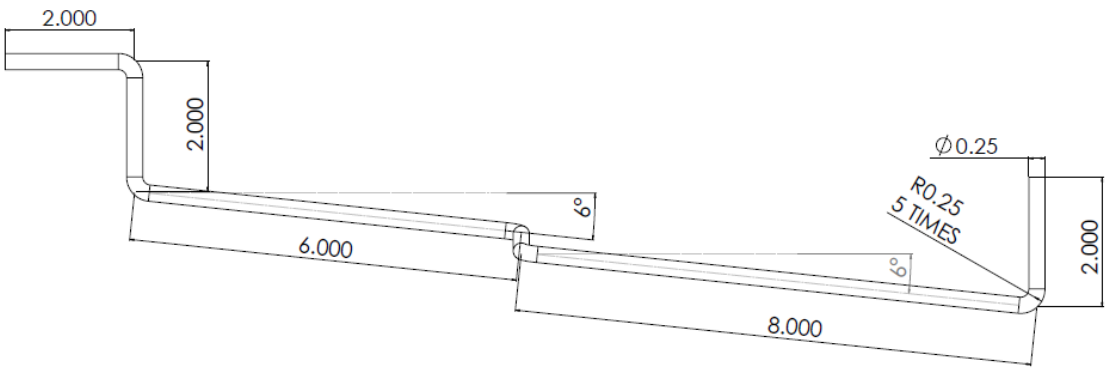

Figure 40. Profile view of the pipe geometry without steam trap branches and all measurements in meters.

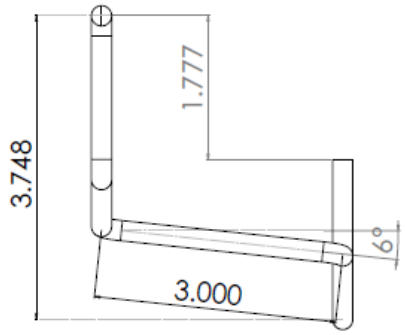

Figure 41. Front view of pipe geometry showing changes in elevation with all measurements in meters.

The second geometry modeled maintained the same features as the first, but included two branches oriented vertically downward. Each branch was full-diameter piping, and extended two pipe diameters in length from the main pipe wall measured at the branch centerline, for a length of 0.5 m. When measured from the main pipe centerline, the distance to the outlet plane of the branch was 0.75 m. The first branch was positioned two pipe diameters, 0.5 m, downstream of the second bend. The second branch was positioned two pipe diameters upstream of the fifth bend at the pipe low point. The elevation change from the centerline of the inlet to the outlet plane is the same as the pipe without the branches. However, the elevation change from the inlet centerline to the low point at the outlet of the second branch is 4.445 m. Figure 42 is a profile view of the steam pipe with

branches. Figure 43 is a front view of the pipe showing elevation changes from the inlet to the second branch outlet.

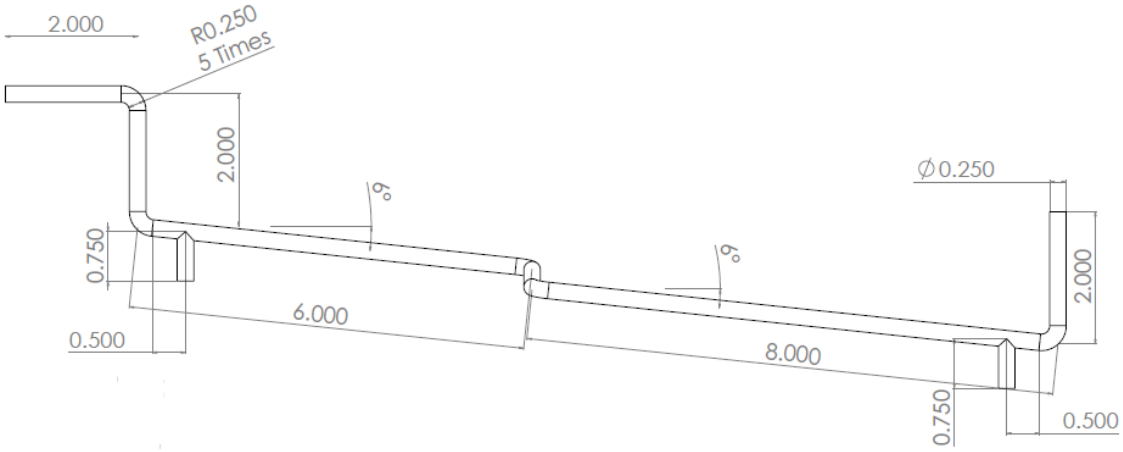

Figure 42. Profile view of steam pipe geometry with steam trap branches with all measurements in meters.

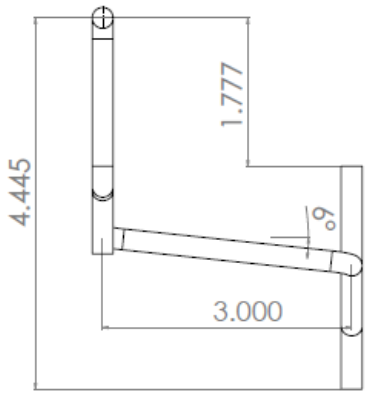

Figure 43. Front view of geometry with steam trap branches showing changes in elevation with all measurements in meters.

B. MODEL MESH

The size of the fluid domain for both steam pipe models drove the decision to use a relatively coarse mesh, reducing the computational resources required for a steady-state solution. This allowed more rapid implementation and evaluation of different flow and boundary conditions to inform future research efforts. The same mesh parameters were implemented for the steam pipe with and without the steam trap outlet piping. However, the geometry of the added steam trap piping resulted in different mesh structures. A fine mesh was implemented for the steam pipe without branches to evaluate the effect on the solution and computational resources required.

1. Steam Pipe without Branches

The steam pipe model without the steam trap branches used an element size of 15 mm with a maximum size of 30 mm. Three inflation layers were added at the pipe walls a growth rate of 1.2 and the CFX default 0.77 transition ratio. The inflation layers were added by using the inlet face as the scope and the inlet perimeter edge as the boundary. The result was a mesh constructed predominately of hexahedra with relatively few wedges. Details of the mesh statistics are provided in Table 11. Reviewing the mesh structure, the higher aspect ratios occur in the cells on the outside of each bend radius. Rather than pinching the cells in the inner radius, the outer cells were stretched around the outside of the bend. However, the element sizing chosen also meant that inflation layers were not pinched or cut off at the inside edge of the pipe bends. These characteristics of the mesh were the result of the large element size and the inflation layer scoping method, which extruded the mesh from the inlet plane over the length of the pipe. Figure 44 shows the mesh at the inlet plane of the pipe. A section plane of the mesh along the centerline of the first bend in the pipe is provided in Figure 45 which shows the stretching of the outer cells. The CCL file for the 0.9999 inlet vapor volume fraction model is provided in Appendix F.

Table 11. Mesh statistics for steam pipe without branches

Element Type and Number	Total Elements	Minimum Aspect Ratio	Maximum Aspect Ratio	Average Aspect Ratio
Hexahedra: 939840 Wedges: 17088	956928	1.612	11.46	2.506

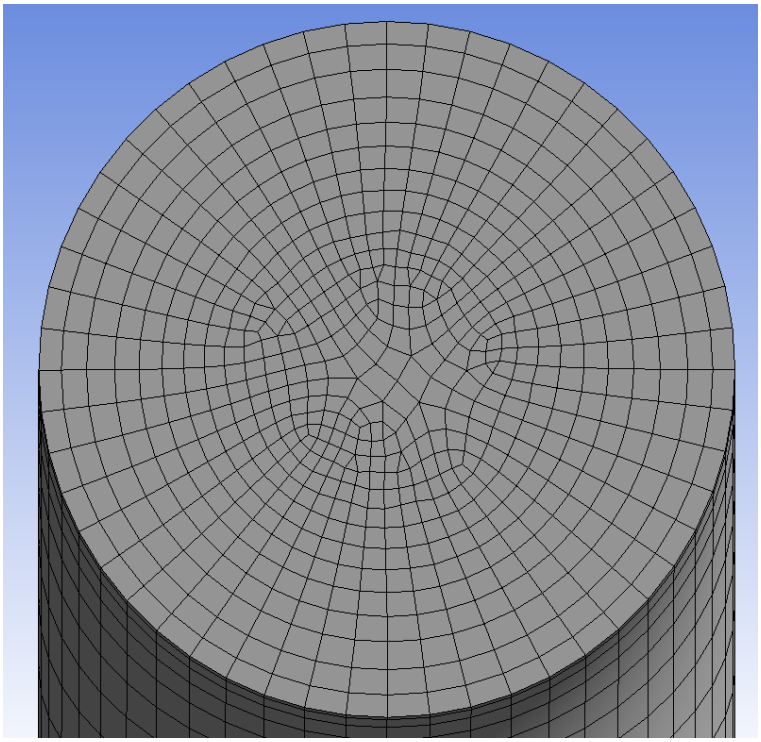

Figure 44. Mesh at the inlet of the steam pipe without branches

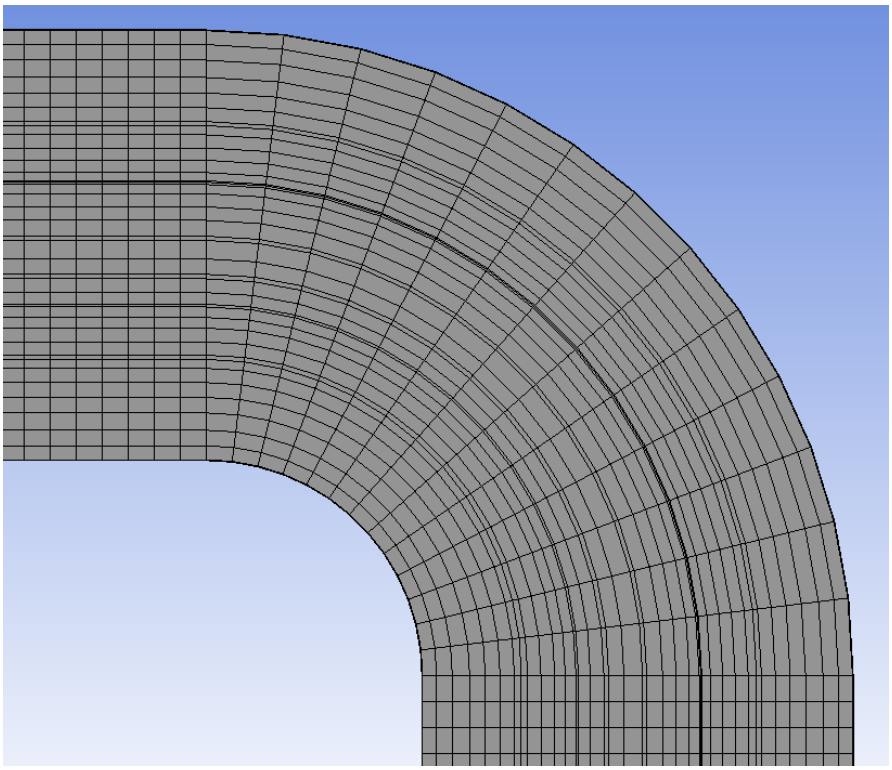

Figure 45. Centerline section plane of the first bend

A finer mesh was also implemented which was sized based on a mesh calculation provided in Appendix D. The element size was lowered to 5 mm with 20 inflation layers added at the wall. The mesh calculation performed assumed a first layer thickness of 0.0001 m and tetrahedral elements, predicting a total of 3.06×10^{8} elements. When the desired element size and number of inflation layers was implemented in the CFX using the default growth rate of 1.2 and transition ratio of 0.77. The resulting mesh contained over 2.72×10^{7} elements with a first layer thickness of 0.00012 m and average aspect ratio of 8.3 over the entire domain. The order of magnitude less elements compared to the prediction is due to the mesh generated by CFX containing predominately hexahedral elements vice tetrahedrons, and stretching of the cells on the outside of the pipe bends. Table 12 contains the mesh statistics for the fine mesh implemented for the steam pipe without branches. Figure 46 and Figure 47 show the mesh at the pipe inlet and the first bend, respectively, for the reduced element size.

Table 12. Mesh statistics for steam pipe without branches and fine mesh

Element Type and Number	Total Elements	Minimum Aspect Ratio	Maximum Aspect Ratio	Average Aspect Ratio
Hexahedra: 27217994 Wedges: 81491	27299485	1.089	135.7	8.301

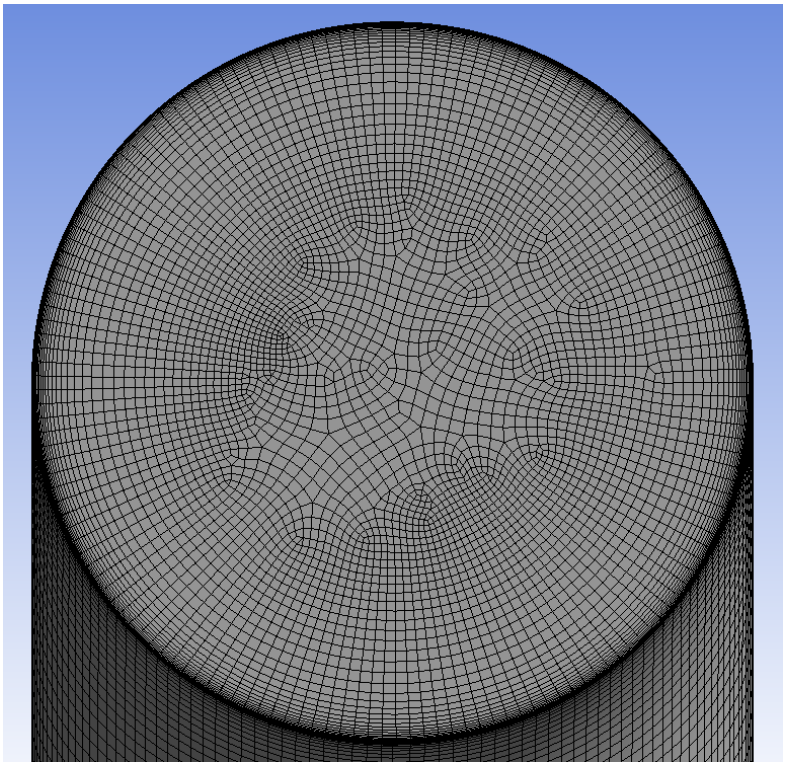

Figure 46. Mesh at pipe inlet for 5 mm element size

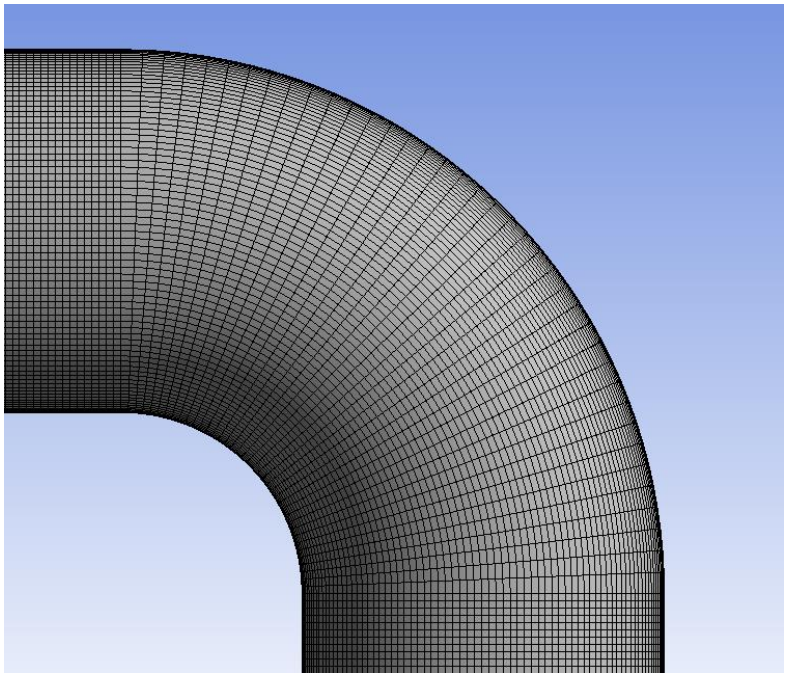

Figure 47. Mesh at first bend for 5 mm element size

2. Steam Pipe with Branches

The steam pipe model with the steam trap branch piping also used an element size of 15 mm with a maximum size of 30 mm. Three inflation layers were added at the pipe walls a growth rate of 1.2 and the CFX default 0.77 transition ratio. The inflation scoping method for used the domain as the scope and the wall of the pipe as the boundary. The result was a mesh constructed tetrahedra and wedges. Details of the mesh statistics are provided in Table 13. The average element aspect ratio was similar to the pipe without branches, with a slightly lower maximum aspect ratio. The difference in the mesh structure resulted in minimal stretching of cells in the inflation layer at the outside of the bend radii. Inflation layers were also preserved at the inside corner of pipe bends. Higher aspect ratio tetrahedra were present throughout the bulk mesh. High aspect cells were also present at the junction between the steam pipe branch wall and the pipe wall. Figure 48 shows the mesh at the inlet plane of the pipe. A section plane of the mesh along the centerline of the first bend in the pipe is provided in Figure 49. A centerline section plane at the first pipe branch is shown in Figure 50.

Table 13. Mesh statistics for steam pipe with branches

Element Type and Number	Total Elements	Minimum Aspect Ratio	Maximum Aspect Ratio	Average Aspect Ratio
Tetrahedra: 809855 Wedges: 594900	1404755	1.434	9.705	2.125

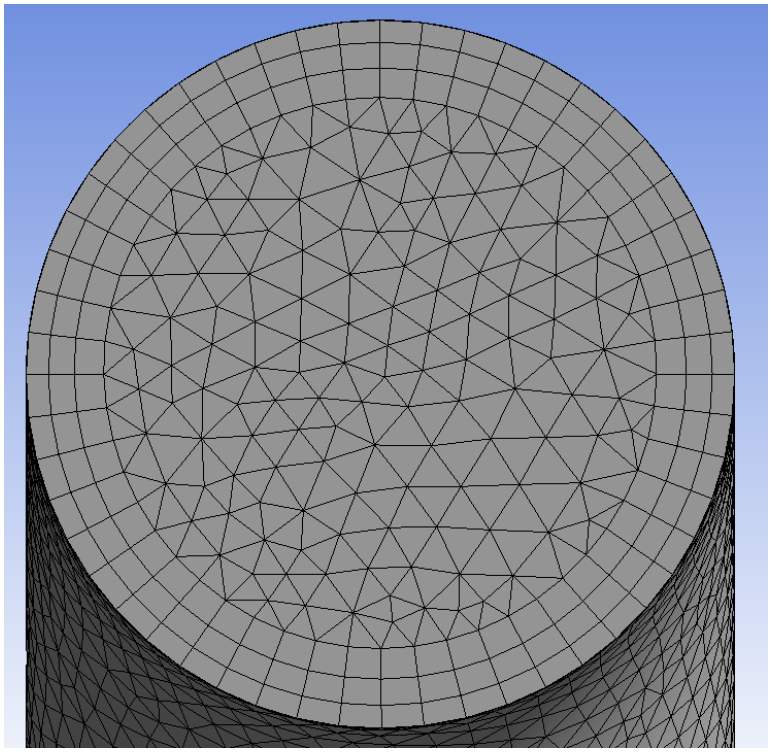

Figure 48. Mesh at the inlet of the steam pipe model with branches

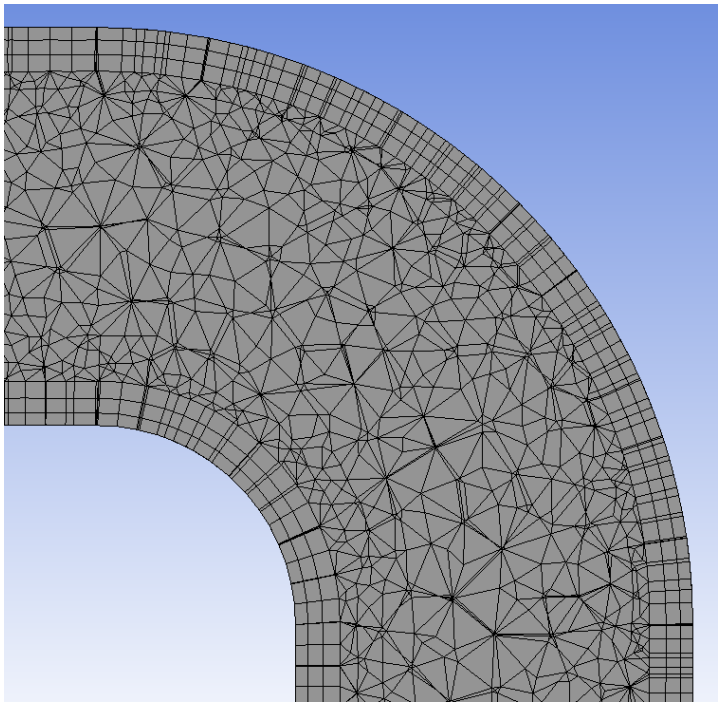

Figure 49. Centerline section plane of the first bend for the steam pipe with branches

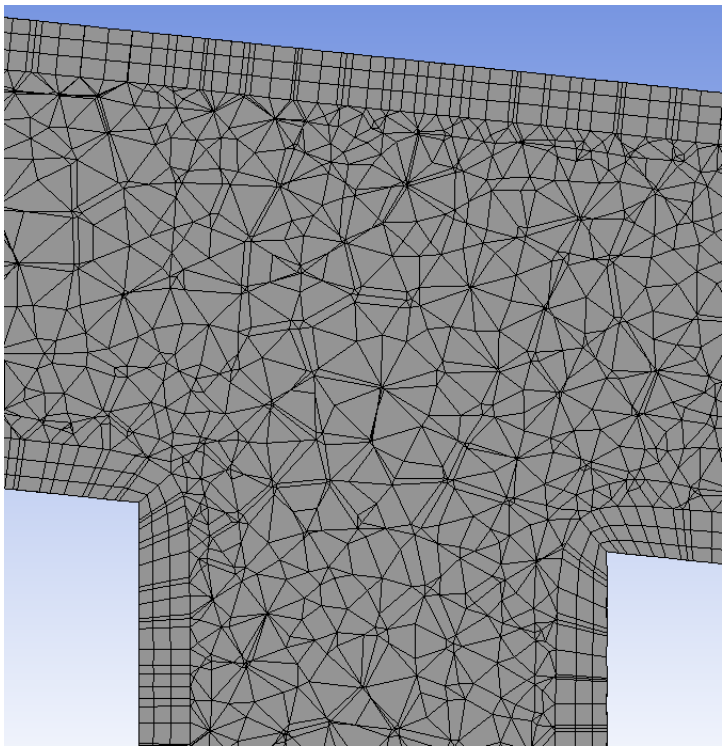

Figure 50. Centerline section plane of the first pipe branch

C. MODEL PHYSICS

The same flow conditions were modeled for each pipe geometry. A saturation temperature of 500 K was chosen, with a corresponding saturation pressure of 2.6389 MPa. The vapor was modeled as a continuous fluid with the liquid phase modeled as a dispersed fluid. Two different set of fluid properties were user-defined for the liquid and vapor phase. The first fluid pair was constant property vapor and liquid phase with properties referenced to the 500 K saturation temperature. Individual fluid properties were generated using an IAPWS IF97 fluid property calculator and provided in Table 14 [17]. The second fluid pair was variable property fluids whose properties were determined using the IAPWS IF97 EOS built into CFX. Table generation for the liquid and vapor phases were set to a temperature of 300 K to 600 K and corresponding pressure range of 0.0035368 MPa to 12.345 MPa with 1000 points. Temperature and pressure extrapolation were both enabled. The CCL file for the implementation of these fluid properties is included in Appendix E.

Table 14. Liquid and Vapor Thermophysical Properties

Property	Liquid	Vapor
Saturation Temperature, T_{sat} (K)	500	500
Density, ρ (kg/m^3)	831.32	13.19
Specific Enthalpy, h (J/kg)	975465	2802590
Specific Entropy, s (J/kg•K)	2581.1	6235.4
Specific Heat Capacity (Constant Pressure), C_p (J/kg•K)	4659.0	3462.6
Viscosity, μ (Pa•s)	1.1790E-04	1.6594E-05
Thermal Conductivity, k (W/m•K)	0.6421	0.044952
Surface Tension, σ (N/m)	0.013472	-

The steam pipe models both utilized a reference pressure of 0 MPa, which would allow the flexibility to use a user-defined expression for the static pressure boundary condition. Gravitational acceleration was added in the negative y-direction and the domain buoyancy model was activated using the density difference option for each phase. A user

variable for calculating the liquid and vapor mass in the pipe was also implemented as discussed in Chapter III. The thermal energy model was used for the domain heat transfer model for both phases. Turbulence was modeled for the vapor phase using the k-epsilon model, while the liquid phase was laminar. Interphase momentum transfer was set to the Schiller-Naumann drag correlation and Legendre-Magnaudet lift model. Mass transfer used the thermal phase change model with a saturation temperature of 500 K. The fluid pair used a two resistance heat transfer model, with the vapor phase set to the Ranz-Marshall option and the liquid phase set to zero resistance.

Inlet and outlet boundary conditions were the same for each geometry, with additional boundary conditions implemented for the steam trap branch outlets. For each model, the inlet boundary condition was a normal speed of 40 m/s and a static temperature of 500 K. Three different inlet qualities were investigated for each geometry: 99.37%, 95.19%, and 84.97%. The required inlet liquid volume fraction was calculated using the inlet area and the known density of the two phases. The inlet volume fractions used for each phase and the resulting inlet quality are provided in Table 15. The outlet boundary condition was an average static pressure of 2.6389 MPa. Wall boundaries were modeled as adiabatic smooth walls with a no slip condition.

Table 15. Inlet volume fractions and corresponding quality

Vapor Volume Fraction	Liquid Volume Fraction	Quality
0.9999	0.0001	99.37%
0.9992	0.0008	95.19%
0.9972	0.0028	84.97%

The choice of droplet size was based on an analysis of the critical Weber number. In order to determine an appropriate droplet size, four different sizes were run using the steam pipe without branches. Droplet sizes chosen used were 1 µm, 10 µm, 100 µm, and 1 mm. The results from each model were then used to determine whether the droplet size would be stable at the chosen flow velocity using a critical Weber number range of 6 to 14.

Droplets which exceeded their maximum stable diameter based on the critical We number would not be included subsequent analyses.

D. CRITICAL WEBER NUMBER ANALYSIS

An analysis was run using 1 mm droplets with an inlet quality of 99%, which was used as an initial guess for the subsequent analyses of different droplet diameters. This first solution was run until the solution met the convergence criteria of root mean square (RMS) residuals below 1×10^{-8}, which took 1056 iterations. Using that initial guess, four subsequent analyses were obtained for droplet diameters of 1 μm, 10 μm, 100 μm, and 1 mm and an inlet vapor volume fraction of 0.9999 using the steam pipe without branches geometry. Each was run for 5000 iterations, for a total of 6056 iterations. Using ParaView for post-processing, the slip velocity for each case was calculated using the difference of the absolute values of the vapor and slip velocities. The result was then plotted as a contour on a centerline plane over the first 8 m, approximately one third of the total pipe length. As expected, the highest slip velocities occurred at the inside radius of the pipe bends. The 1 mm droplets had the highest measured slip velocity, the 1 μm droplets the lowest. Figure 51 is the slip contour for the 1 mm droplets. The greatest slip velocity calculated was then used to determine the largest stable droplet diameter, *D*, for each case using Eq. (2) and critical Weber number of 6 and 14 for a conservative estimate. This resulted a range of stable droplet sizes, provided in Table 16. The 1 mm and 100 μm droplets both exceeded the maximum stable diameter, were not included in subsequent analyses.

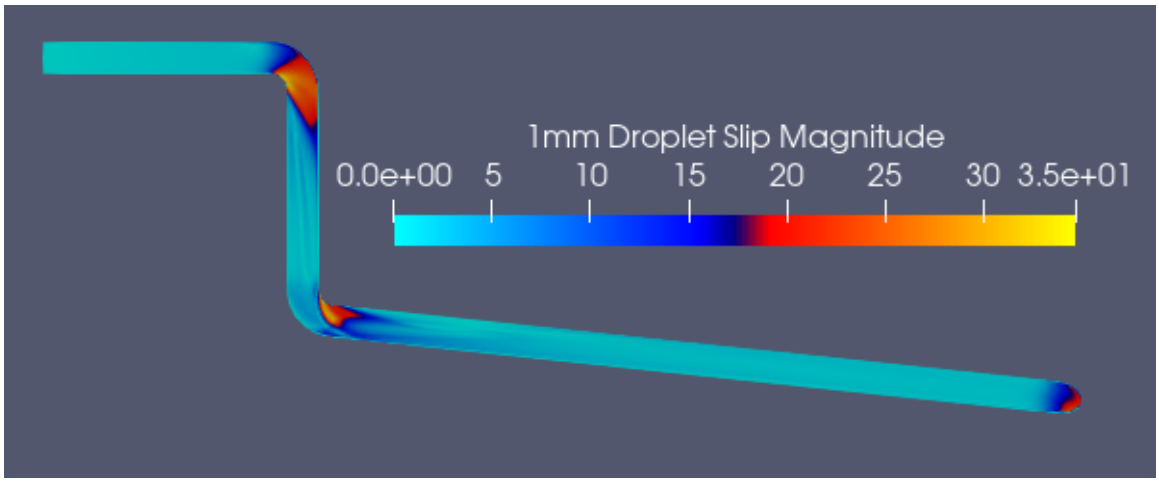

Figure 51. Slip velocity contour for 1 mm droplets in m/s

Table 16. Range of stable droplet diameters

Droplet Diameter (m)	Maximum Slip (m/s)	Min D, We = 6 (m)	Max D, We = 14 (m)
1×10^{-3}	35	5×10^{-6}	1.17×10^{-5}
1×10^{-4}	20	1.53×10^{-5}	3.57×10^{-5}
1×10^{-5}	3.8	4.24×10^{-4}	9.90×10^{-4}
1×10^{-6}	0.085	0.848	1.98

E. LIQUID MASS ANALYSIS

User defined variables and expressions were implemented to quantify the liquid mass in the steam pipe for each model run as an additional means of determining if the solution had reached a steady state. The variable "MassTotal" was added as an additional scalar variable for both the liquid and vapor phases. An expression was then added for each fluid phase which calculated the "MassTotal" on a per-cell basis as the product of the cell volume (Volume of Finite Volumes), the applicable phase density, and the volume fraction of that phase within the cell. An expression "SumLiqMassTotal" was then defined as the sum of the Liquid.MassTotal calculated by the solver and added as a monitor for display

in the solver manager. For a comparison, an estimate of the steady state liquid mass in the pipe was calculated using the equation

$$m_{liq} = V_{pipe} VF_{liq} \rho_{liq}, \tag{10}$$

where V_{pipe} is the pipe volume, VF_{liq} is the liquid volume fraction from the inlet boundary condition, and ρ_{liq} is the liquid phase density from Table 14. The results of the liquid mass predictions for the pipe without branches and the pipe with branches is provided in Table 17.

Table 17. Liquid mass estimation for both pipe geometries with 1 μm droplets

Model	Volume (m^3)	Inlet Liquid Volume Fraction	Estimated Liquid Mass (kg)
Pipe without branches	1.10270	0.0001	0.091669
Pipe without branches	1.10270	0.0008	0.73336
Pipe without branches	1.10270	0.0028	2.5667
Pipe with branches	1.16377	0.0001	0.096746
Pipe with branches	1.16377	0.0008	0.77397
Pipe with branches	1.16377	0.0028	2.7089

F. RESULTS FOR STEAM PIPE WITHOUT BRANCHES

1. Coarse Mesh Results

A total of six different models were run using the steam pipe geometry without the steam traps to text model stability with various combinations of inlet quality and droplet

size. Also tested was the implementation of a user variable to calculate the liquid mass in the pipe and display the result as a monitor point in the CFX solver manager, described in Appendix C. Based on the critical Weber number analysis, only 1 µm and 10 µm droplet diameters were used for each of the inlet vapor volume fractions listed in Table 15. A summary of selected solver information for each model is provided in Table 18. The significant difference in run times between the various models is due to differences in the computers used. The last four were run on Naval Postgraduate School's supercomputer, Hamming. Hamming consists of nodes having either 32 or 64 processors, with the larger nodes resulting in a significantly reduced wall clock time.

Table 18. Solver parameters for steam pipe models without branches

Inlet Vapor VF	$D_{droplet}$ (µm)	Partition Number	Total Time Steps	Clock Time (Hrs:Min)	Memory (Mb)	Memory Allocation (%)	Average Courant Number
0.9999	1	16	5000[a]	32:36	5586.90	2.13	23.56
0.9999	10	16	5000[a]	32:01	5586.90	2.13	23.52
0.9992	1	16	5000	13:51	3172.22	1.23	23.43
0.9992	10	16	5000	13:58	3172.22	1.23	23.06
0.9972	1	16	5000	5:56	3172.22	0.62	22.91
0.9972	10	16	5000	24:18	3172.22	1.23	22.59

a. Completed over two consecutive runs due to convergence of RMS residuals below 1×10^{-12} before reaching 5000 iterations. Excludes the first 1056 iterations which were from a 1mm droplet model used as initial conditions.

Selected parameters for each model were calculated using CFX Post. The inlet and outlet quality were calculated by dividing the vapor phase mass flow rate by the total mass flow rate at the respective boundary. By convention, outlet mass flow rates in CFX are negative, but they are reported as positive values in Table 19. The differential pressure was calculated by subtracting the average inlet pressure from the average outlet pressure. The liquid mass provided is the value calculated by the user expression "SumLiqMassTotal."

Table 19. Select results for the steam pipe without branches

Inlet Vapor VF	$D_{droplet}$ (μm)	X_{inlet}	X_{outlet}	$\dot{m}_{in}$ (kg/s)	$\dot{m}_{out}$ (kg/s)	ΔP (Pa)	Liquid Mass (kg)
0.9999	1	99.37%	99.37%	26.0107	26.0107	-12545	0.09143
0.9999	10	99.37%	99.37%	26.0107	26.0107	-12552	0.09318
0.9992	1	95.19%	95.19%	27.1324	27.1324	-12605	0.73151
0.9992	10	95.1989%	95.1981%	27.1324	27.1326	-12641	0.74442
0.9972	1	84.97%	84.97%	30.3373	30.3373	-12717	2.5602
0.9972	10	84.97%	84.97%	30.3373	30.3373	-13706	2.5943

Reviewing the results of the six solutions, the only one which had not achieved continuity was the model with an inlet vapor volume fraction of 0.9992 and 10 μm droplets. However, the difference was insignificant, with the inlet and outlet mass flow rates differing by less than one thousandth of one percent. Comparing the solver calculated liquid mass to the estimation for each case also showed that further refinement of the model was required to match the liquid mass to the expected value. One consistency among the results was that the larger droplets resulted in increased liquid mass within the pipe and a larger pressure drop for the same inlet vapor volume fraction. Also, the differential pressure was inversely proportional to the vapor volume fraction at the inlet. The lower quality flows also showed more instability in the liquid mass calculation which was only evident upon close inspection of the solver plot.

For each of the six models, the trend in the pipe total liquid mass was conducted and used to determine if a steady-state solution was reached. The models with an inlet vapor volume fraction of 0.9999 reached a constant liquid mass in the pipe relatively quickly, as shown in Figure 52 and Figure 53. The plots for both droplet sizes start at 1056 iterations. The sharp decrease in liquid mass is the result of using a 1mm droplet size solution as the initial conditions for the 1μm and 10μm models. However, in both cases approximately 350 iterations were required for the liquid mass to achieve steady state.

Based on these results, the initial solutions for the steam pipe with branches were run for 2500 iterations before initial evaluation to reduce computational time.

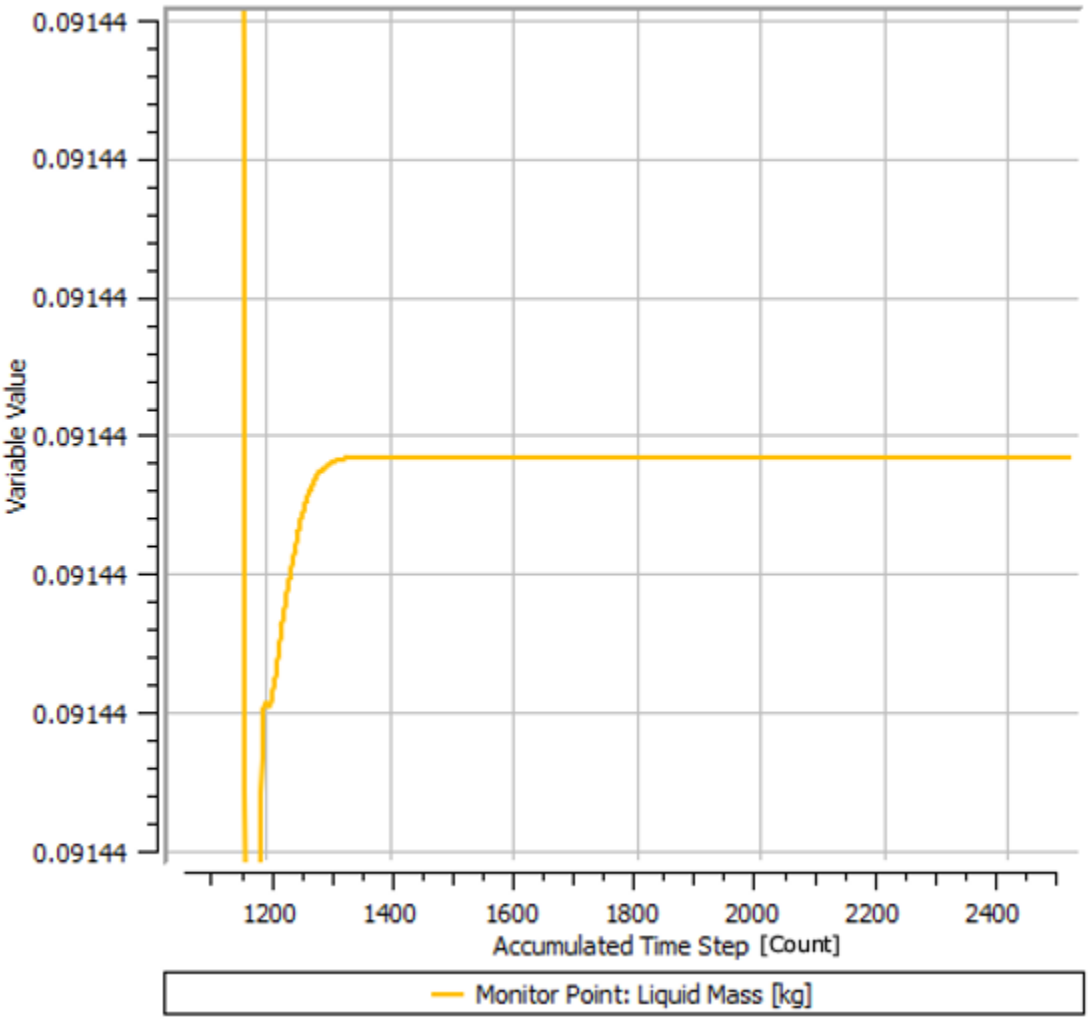

Figure 52. Liquid mass plot for X = 99.37%, $d_{droplet}$ = 1 µm

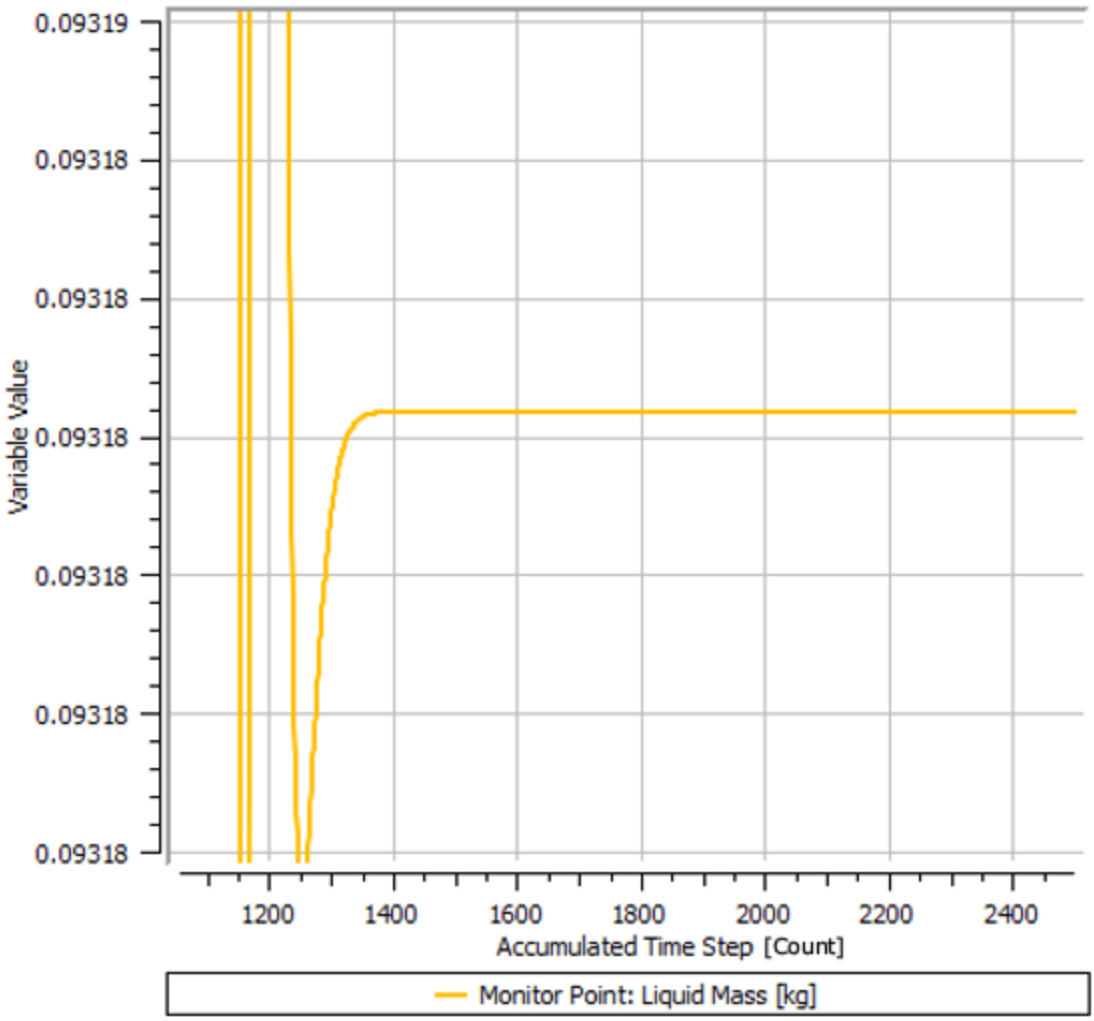

Figure 53. Liquid mass plot for X = 99.37%, $d_{droplet}$ = 10 µm

The solver-determined liquid mass was 0.27% less than the estimated mass for the 99.37% quality model with 1 µm droplets. Increasing to the 10 µm droplets resulted in 1.65% more mass in the pipe than was estimated. In both cases, the accuracy of the result with a coarse mesh and moderate Courant number was excellent.

Results for the 0.9992 inlet vapor volume fraction did not reach a steady-state condition after 5000 iterations. However, like the 0.9999 vapor volume fraction models, less than 500 iterations were required for the liquid mass to reach an approximate steady-state condition. Some instability in the results is still evident, but is overall minimal with the liquid mass varying by less than 1×10^{-4} kg in both cases. This instability resulted from

the combination of using a coarse mesh and a relatively high Courant number. Figure 54 and Figure 55 show the liquid mass plot for the first 2500 iterations for the 1 µm and 10 µm solutions, respectively. Each plot has been scaled to show the variation in liquid mass once the near-steady state condition was reached.

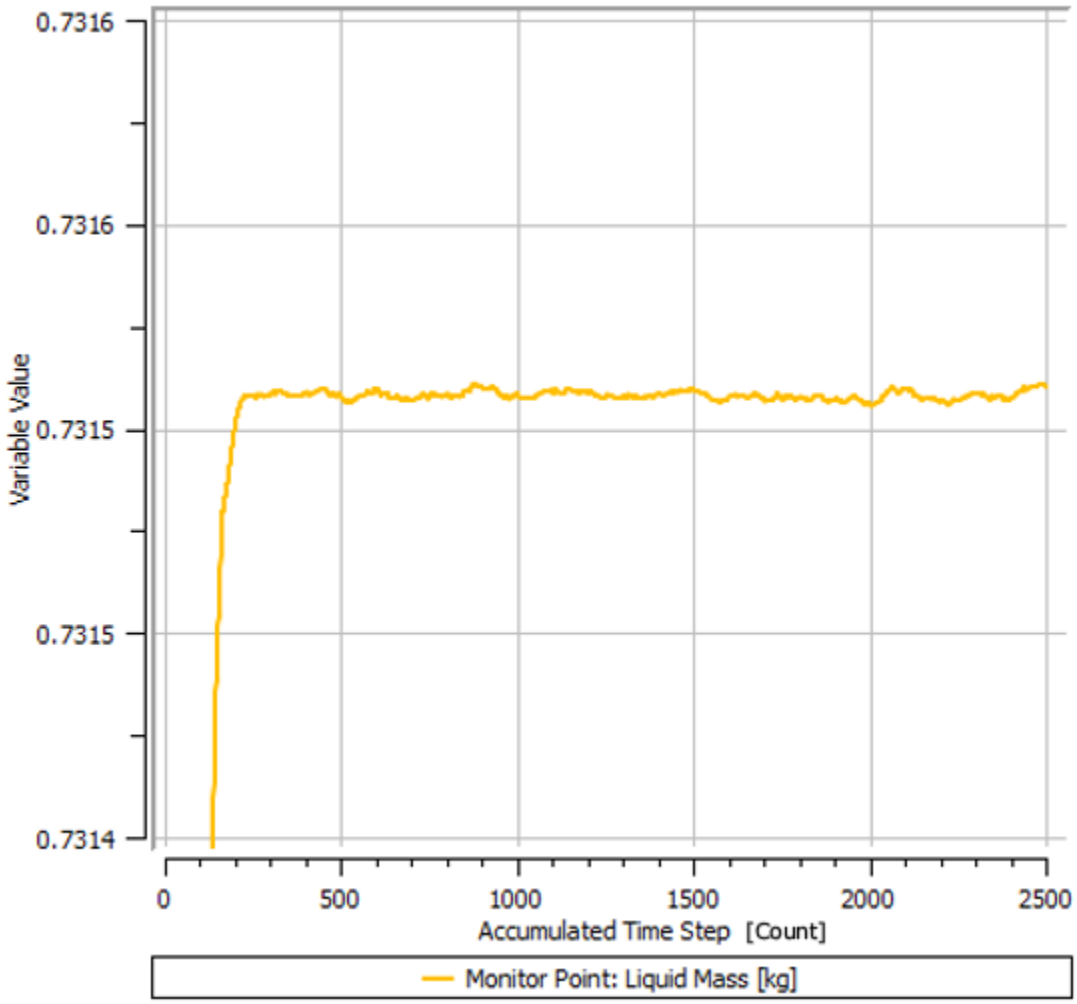

Figure 54. Liquid mass plot for X = 95.19%, $d_{droplet}$ = 1 µm

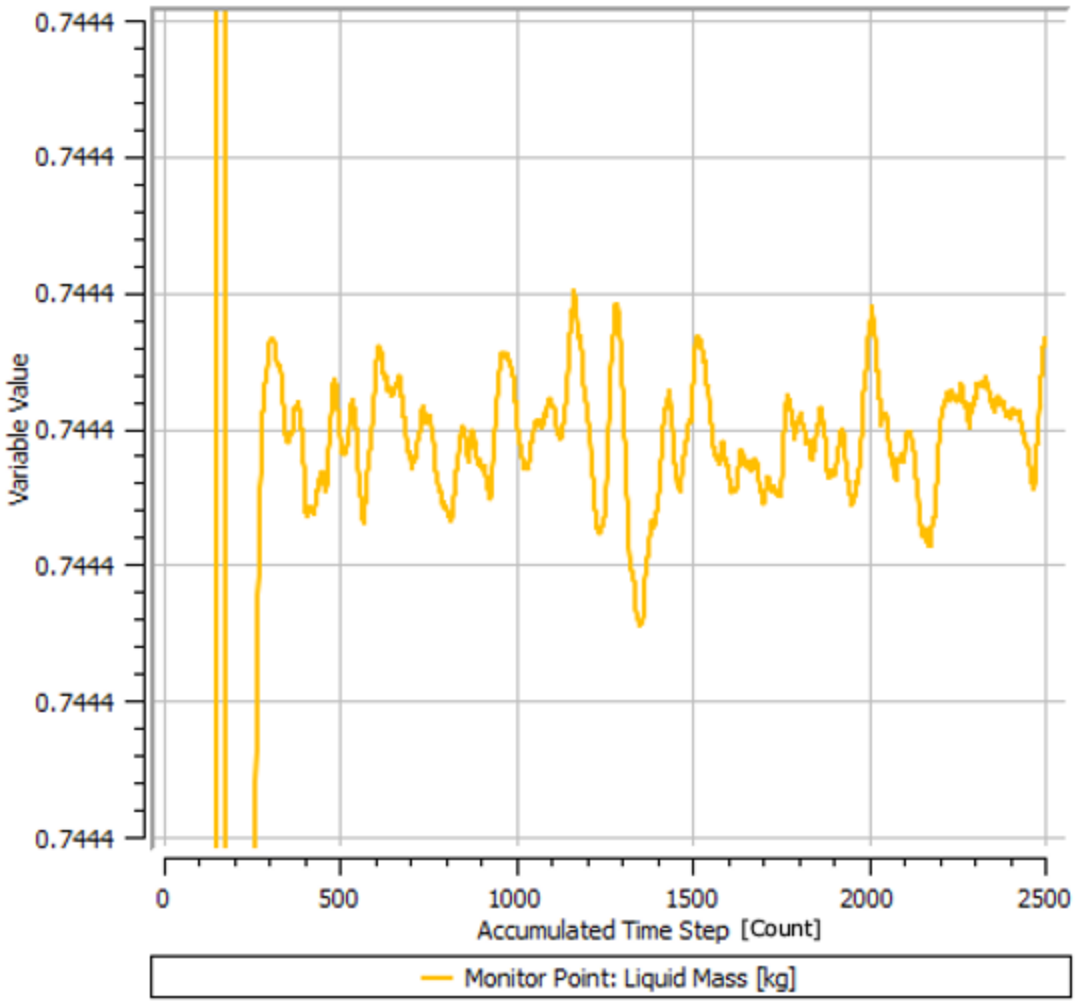

Figure 55. Liquid mass plot for X = 95.19%, $d_{droplet}$ = 10 µm

After 5000 iterations, the solver-determined liquid mass was 0.25% less than the estimated mass for the 95.19% quality model with 1 µm droplets. Increasing to the 10 µm droplets resulted in 1.5% more liquid mass in the pipe. In both cases, the accuracy was similar to the previous solutions for 99.37% quality with the same mesh.

Results for the 0.9972 inlet vapor mass fraction models behaved similarly to the results for the 0.9992 inlet vapor mass fraction models. Again, less than 500 iterations were required to reach a near steady-state solution. Figure 56 and Figure 57 show the liquid mass plots over the first 2500 for the 1 µm and 10 µm models, respectively. The larger droplets did results in slightly more significant oscillation. A refined mesh and lower Courant

number would be required to reach a steady-state condition. However, all six models were stable.

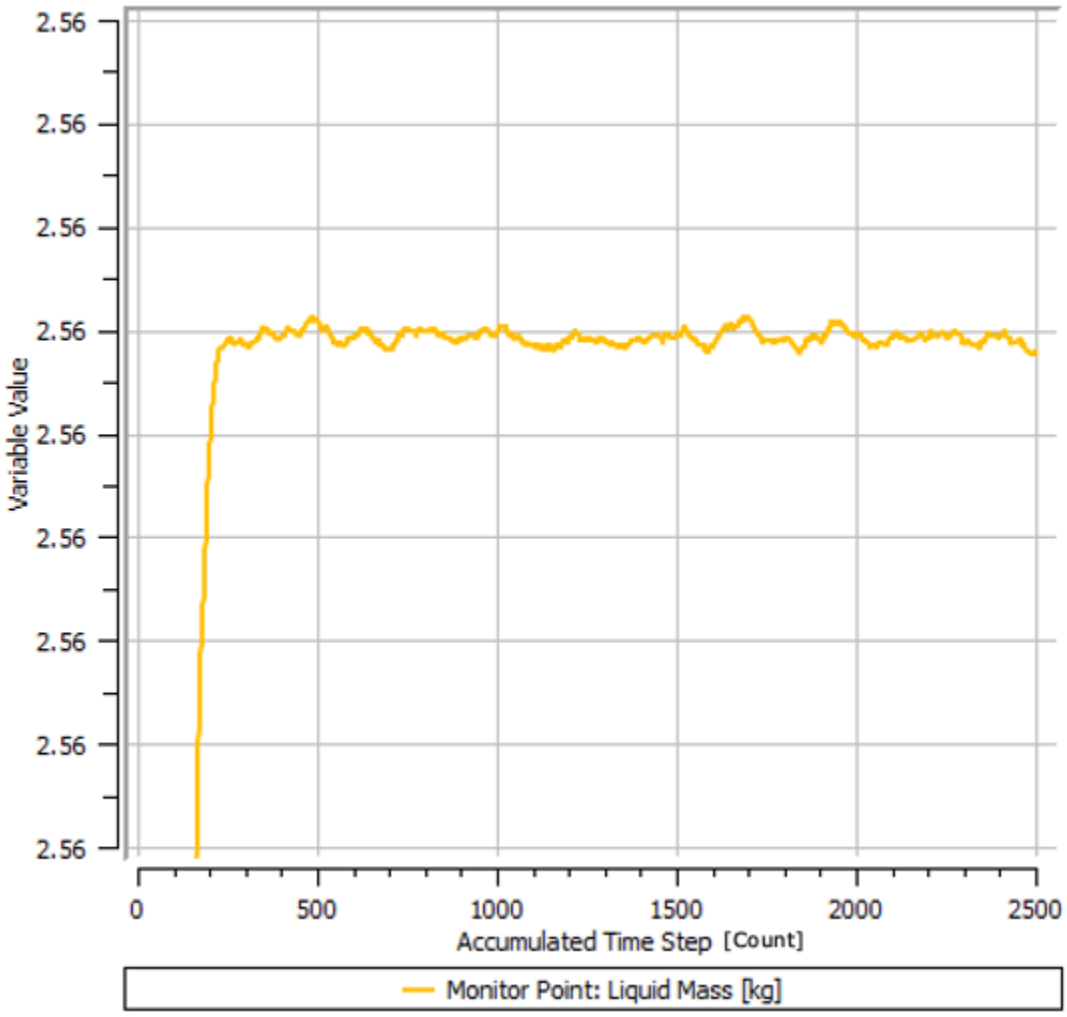

Figure 56. Liquid mass plot for X = 84.97%, $d_{droplet}$ = 1 µm

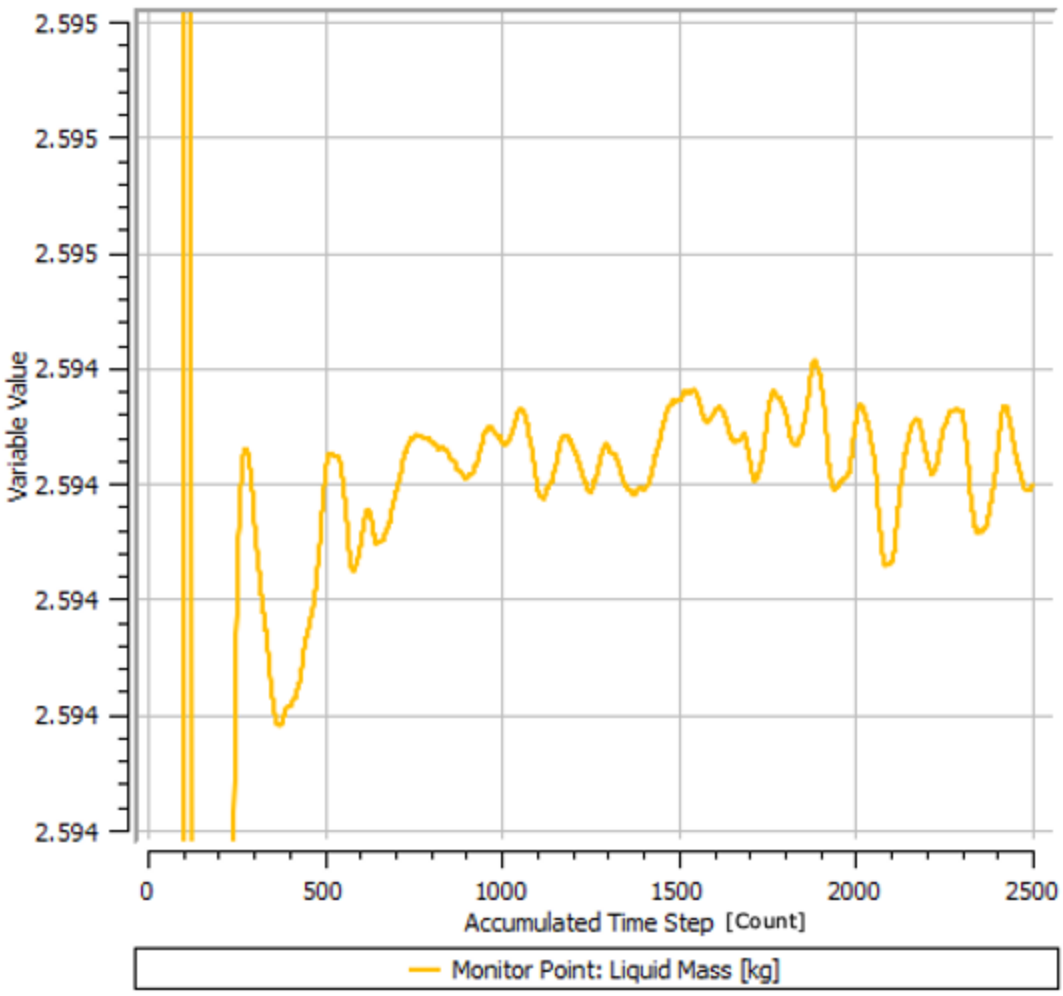

Figure 57. Liquid mass plot for X = 84.97%, $d_{droplet}$ = 10 µm

After 5000 iterations, the solver-determined liquid mass was 0.25% less than the estimated mass for the 84.97% quality model with 1 µm droplets. Increasing to the 10 µm droplets resulted in 1.08% more liquid mass in the pipe. In both cases, the accuracy was similar to the previous solutions.

2. Fine Mesh Results

A solution using the fine mesh was run for the 99.37% quality model with 1 µm and 10 µm droplets using the coarse mesh solutions as initial conditions. A consolidated list of solver parameters is included in Table 20. Significantly greater computational

resources were required to analyze the finer mesh therefore all fine mesh solutions were calculated on Hamming.

Table 20. Solver parameters for steam pipe models without branches

Inlet Vapor VF	$D_{droplet}$ (μm)	Partition Number	Total Time Steps	Clock Time (Hrs:Min)	Memory (Mb)	Memory Allocation (%)	Average Courant Number
0.9999	1	128[b]	257[a]	2:16	145631.6[b]	28.27	64.11
0.9999	1	192[c]	15000	69:29	151009.8[c]	19.54	0.1922
0.9999	10	128[b]	257[a]	2:16	145631.6[b]	28.27	63.95

a. Completed over two consecutive runs due to hardware failure stopping initial solution at 4814 iterations. Second solution started from backup at 4743 iterations (10800 cumulative including initial conditions).

b. Split over two nodes with 64 partitions each.

c. Split over three nodes with 64 partitions each.

The solution for the 1 μm droplet size showed an initial increase in the calculated liquid mass in the pipe compared to the coarse mesh solution, jumping from 0.09143 kg to 0.092 kg after approximately 163 iterations for an increase of 0.6%. The liquid mass remained unsteady for the remainder of the solution. The most notable difference between the coarse and fine mesh solutions was the significant increase in the average Courant number, which nearly tripled due to the smaller element size of the fine mesh. A significant increase of several orders of magnitude in the value of the root mean square residuals was also noted when switching to the fine mesh. Figure 58 shows the liquid mass monitor for the 1 μm droplet solution where the jump in liquid mass is clearly visible. Figure 59 shows the mass and momentum residuals for the same solution. The switch to the fine mesh occurred at 6056 iterations.

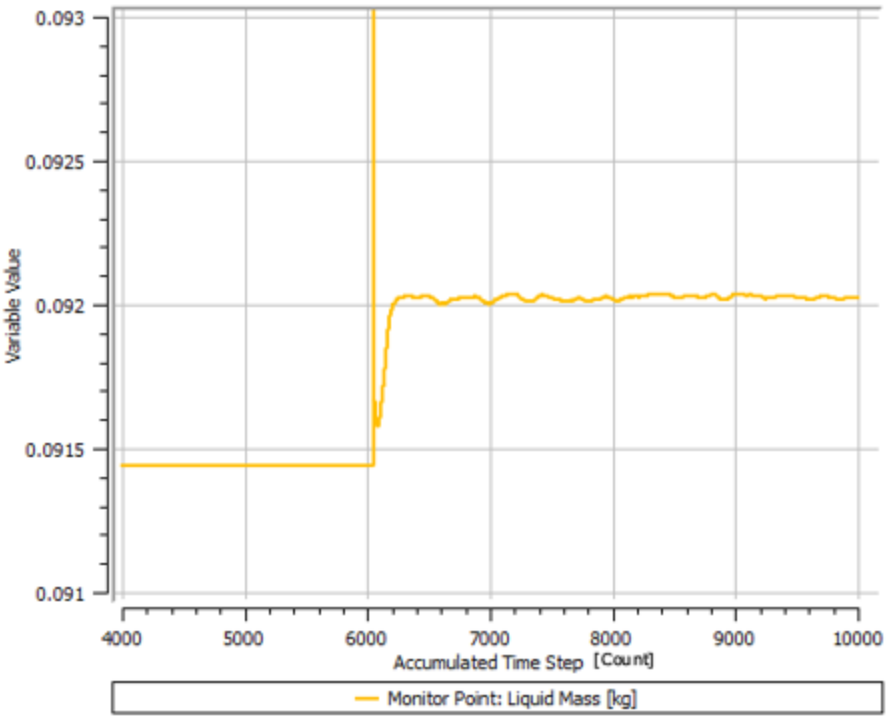

Figure 58. Liquid mass monitor for fine mesh, X = 99.37%, $d_{droplet}$ = 1 µm

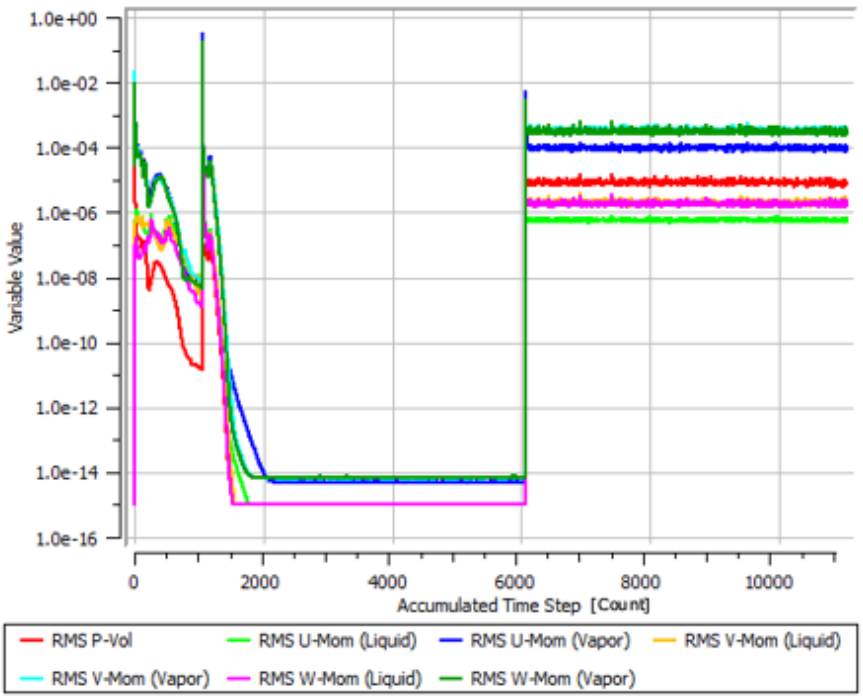

Figure 59. Mass and momentum residuals for fine mesh, X = 99.37%, $d_{droplet}$ = 1 µm

The solution for the 10 µm droplets at 99.37% quality also showed an increase in the liquid mass in the pipe, jumping from 0.09318 kg to 0.10334, an 11% increase in liquid mass as shown in Figure 60. The same increase in Courant number also occurred in the 10 µm droplet solution, as well as the jump in order of magnitude of the mass and momentum residuals.

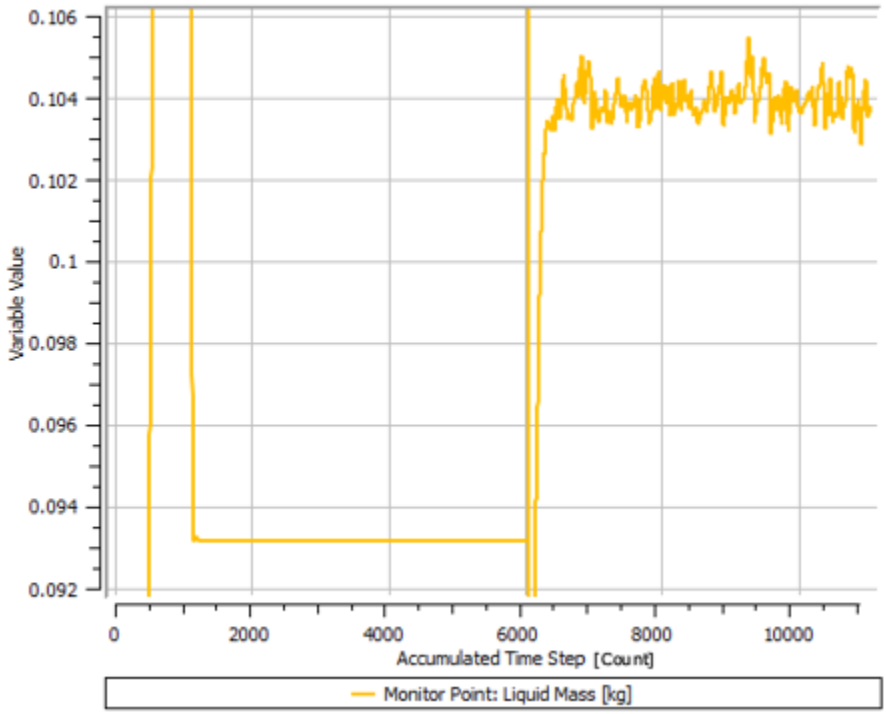

Figure 60. Liquid mass monitor for fine mesh, X = 99.37%, $d_{droplet}$ = 10 µm

The significant increase in the Courant number prompted the investigation of another solution using 1 µm droplets with a reduced timescale factor of 0.003. Using the previous solution as the initial conditions, 15000 additional iterations were run using the reduced timescale. The solution used as the initial conditions had a calculated liquid mass of 0.09196 kg, which had reduced to 0.09180 after 15000 iterations with the reduced timescale factor. The average Courant number after reducing the timescale factor was 0.1922. A review of the liquid mass monitor showed the mass in the pipe steadily decreasing towards the estimated value of 0.091669 from the liquid mass analysis

performed. The stability of the solver was also significantly increased, as evidenced by the change in behavior of the mass and momentum residuals which lowered and smoothed. Figure 61 and Figure 62 shows the changes in the liquid mass calculation and residuals, respectively, after lowering the timescale factor.

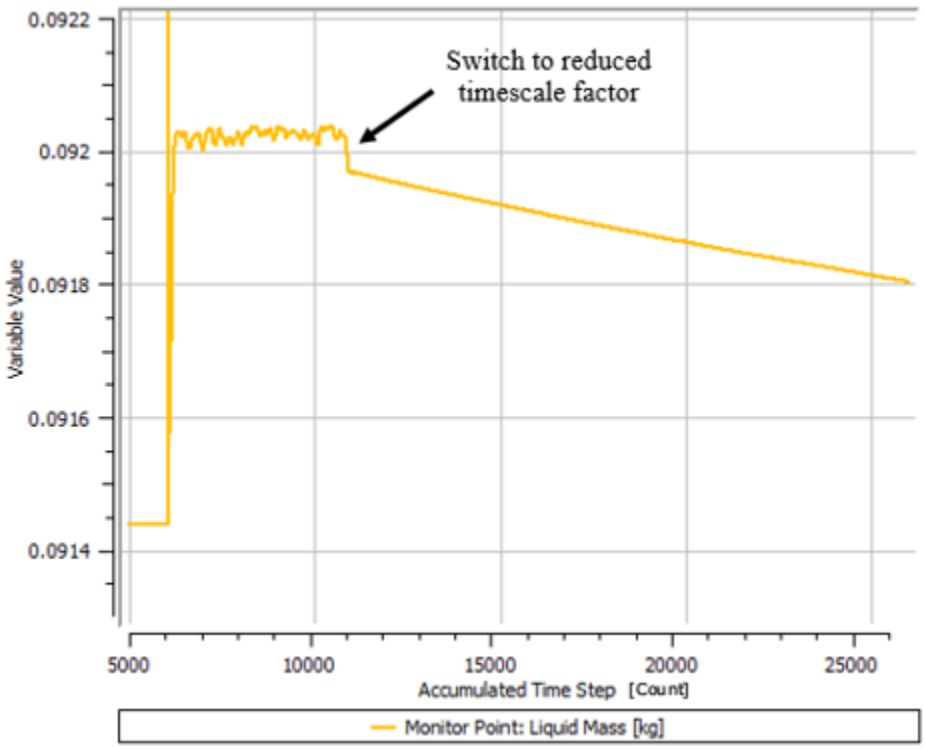

Figure 61. Liquid mass monitor for fine mesh after timescale factor reduction, X = 99.37%, $d_{droplet}$ = 1 µm

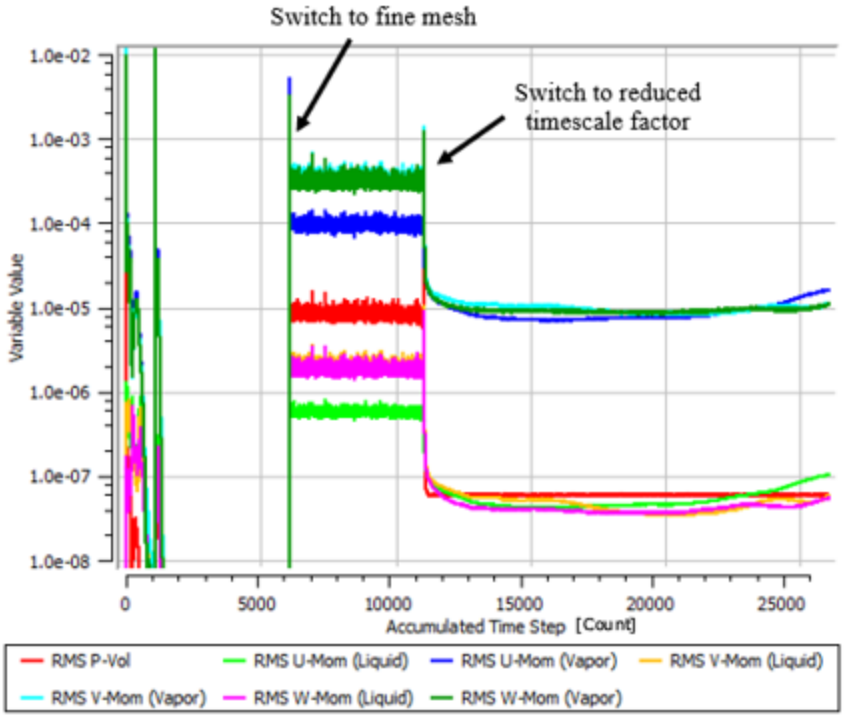

Figure 62. Mass and momentum residuals for fine mesh after timescale factor reduction, X = 99.37%, $d_{droplet}$ = 1 µm

The finer mesh combined with a lowered Courant number resulted in increased stability of the solver, as expected. However, the significant increase in the computational resources required and the minimal increase in accuracy of resolving the liquid mass in the pipe precluded implementing the finer mesh for the remainder of the quality and droplet size combinations. The comparison also showed that the results obtained with the coarse mesh were sufficiently accurate for testing the range of conditions evaluated in this research.

G. RESULTS FOR STEAM PIPE WITH BRANCHES

The steam pipe with branches was modeled using the same six combinations of inlet quality and droplet size as the steam pipe without branches. The first variation on the branch outlet boundary conditions was using a wall boundary to evaluate whether liquid mass collected in the branches. The second variation introduced the dispersed phase zero equation turbulence model for the liquid phase to see what effect, if any, it had on liquid

de-entrainment at the steam traps. Finally, a fluid-specific boundary condition was implemented which set the vapor mass flow rate to zero at the branch outlet and imposed a liquid normal speed boundary condition. The goal was to find a set of boundary conditions that would model the de-entrainment of the liquid droplets in the branch and allow liquid to collect or pass through the outlet boundary. This would allow the mass of liquid de-entrained to be quantified and inform design decisions on the best locations for steam traps. The CCL file for the model with wall boundary conditions is provided in Appendix G. The CCL file for the branch outlet fluid dependent boundary condition is provided in Appendix H.

1. Branch Outlet Wall Boundary Condition Results

a. Laminar Liquid Phase

The six models using the wall boundary condition at the branch outlets were all run on the same computer to better compare the computational resources required for each. The solver parameters are provided in Table 21. The number of partitions and memory allocation were the same for each model, which resulted in an average run time of 22 hours and 58 minutes, ±4 minutes.

Table 21. Solver parameters for steam pipe models with branch outlet wall boundary condition

Inlet Vapor VF	$D_{droplet}$ (μm)	Partition Number	Total Time Steps	Clock Time (Hrs:Min)	Memory (Mb)	Memory Allocation (%)	Average Courant Number
0.9999	1	8	2500	22:55	3760.83	1.44	25.54
0.9999	10	8	2500	22:59	3760.83	1.44	25.54
0.9992	1	8	2500	23:01	3760.83	1.44	25.62
0.9992	10	8	2500	23:02	3760.83	1.44	25.69
0.9972	1	8	2500	23:00	3760.83	1.44	25.64
0.9972	10	8	2500	22:56	3760.83	1.44	25.44

Analysis of the results shows the same trends observed with the steam pipe with no branches. An increase in droplet size resulted in a corresponding increase in the pressure drop from inlet to out for the same quality. Also, decreasing quality resulted in an increased pressure drop. The trend in the liquid mass calculation was different than the steam pipe without the branches. For the steam pipe with the branches, the liquid mass in the pipe was greater than the estimate for each of the six different models. Select parameters for each model are presented in Table 22.

Table 22. Select results for the steam pipe with branch outlet wall boundary condition

Inlet Vapor VF	$D_{droplet}$ (μm)	X_{inlet}	X_{outlet}	$\dot{m}_{in}$ (kg/s)	$\dot{m}_{out}$ (kg/s)	ΔP (Pa)	Liquid Mass (kg)
0.9999	1	99.37%	99.37%	26.0107	26.0106	-12928	0.09677
0.9999	10	99.37%	99.37%	26.0107	26.0103	-13005	0.10032
0.9992	1	95.19%	95.19%	27.1324	27.1324	-13256	0.77421
0.9992	10	95.19%	95.24%	27.1324	27.1201	-13756	0.87692
0.9972	1	84.97%	84.97%	30.3373	30.3376	-14073	2.7098
0.9972	10	84.97%	84.99%	30.3373	30.3286	-14509	3.0399

Using ParaView for post-processing, vertical planes were inserted at the centerline of each leg of the pipe. The vapor mass fraction was plotted on each plane to compare the effects of inlet quality and droplet diameter on liquid concentration within the pipe. Figure 63 through Figure 68 show the cross-sectional views of the inlet and outlet legs of the steam pipe for each inlet quality.

For each variation of inlet quality, the 1 μm diameter droplets showed similar distributions in the first and second branch with slightly higher amounts of liquid in the first branch. The larger 10 μm droplets preferentially deposited in the first branch, which is most evident for the 99.37% quality and 84.97% quality cases. Significant recirculation

occurred in each branch due to the length. The branches were too short to allow the flow to fully develop, and the wall boundary condition resulted in significant swirling of the liquid and vapor. This circulation of flow in the branches also likely led to liquid being removed from the branch which would have otherwise collected. Figure 69 is a side-by-side comparison of liquid velocity vectors in the first pipe branch for the 99.37% quality solution with 1 µm and 10 µm droplets. At the top of the branch, the liquid accelerates as it is re-entrained in the steam flow. This same flow pattern was observed for each individual model.

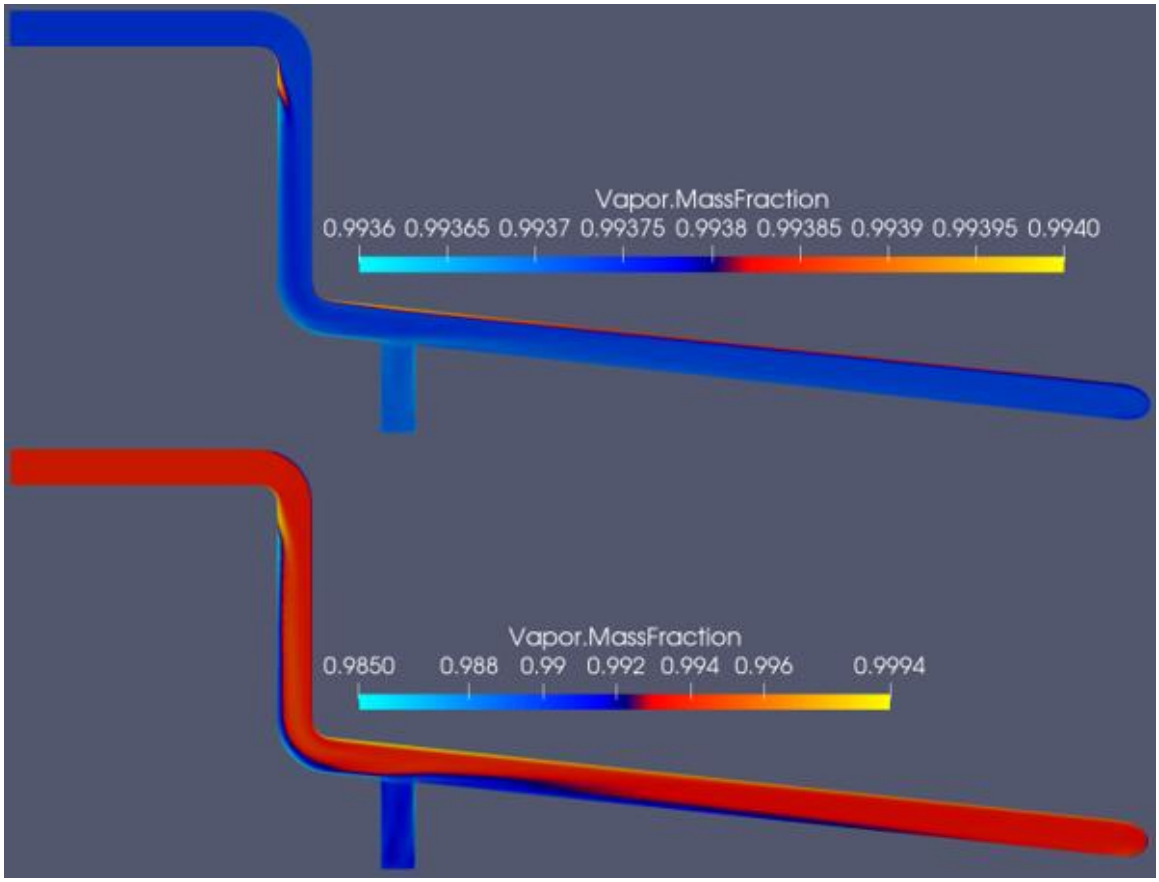

Figure 63. Vapor mass fraction contour X = 99.37%, $d_{droplet}$ = 1 µm (top) and 10 µm (bottom) at inlet

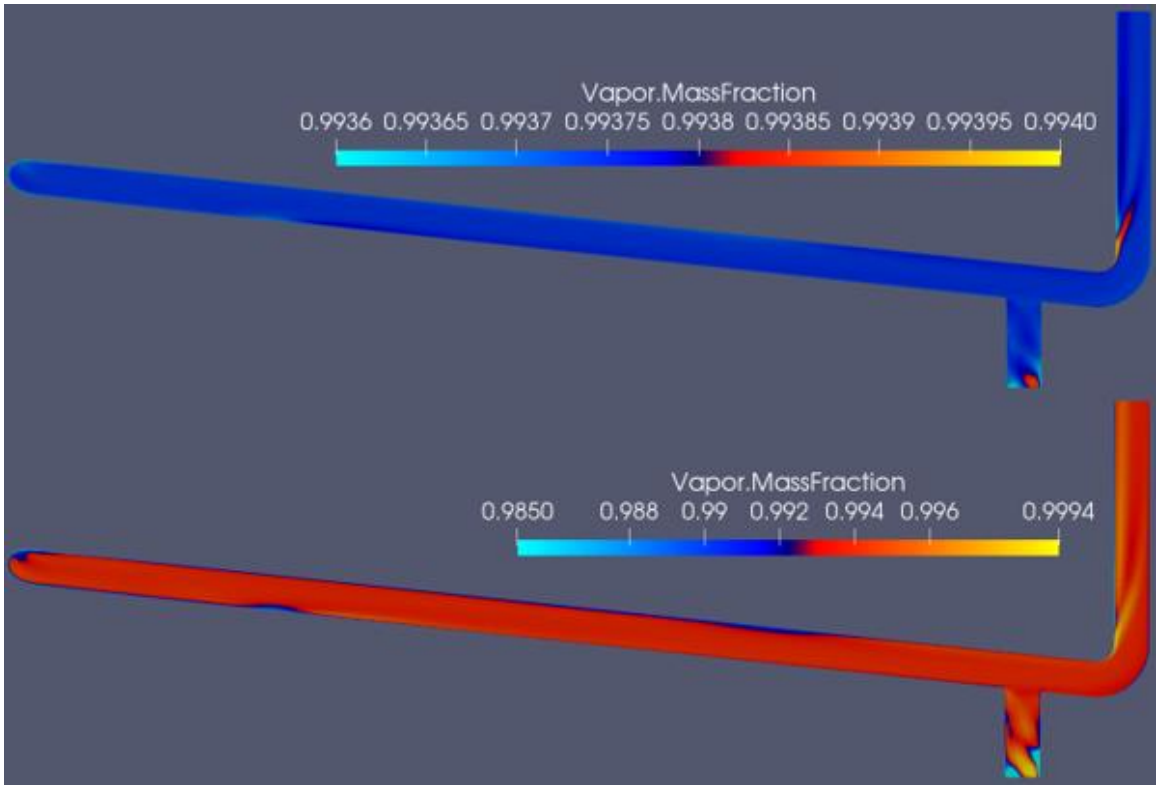

Figure 64. Vapor mass fraction contour for X = 99.37%, $d_{droplet}$ = 1 µm (top) and 10 µm (bottom) at outlet

Figure 65. Vapor mass fraction contour for X = 95.19%, $d_{droplet}$ = 1 µm (top) and 10 µm (bottom) at inlet

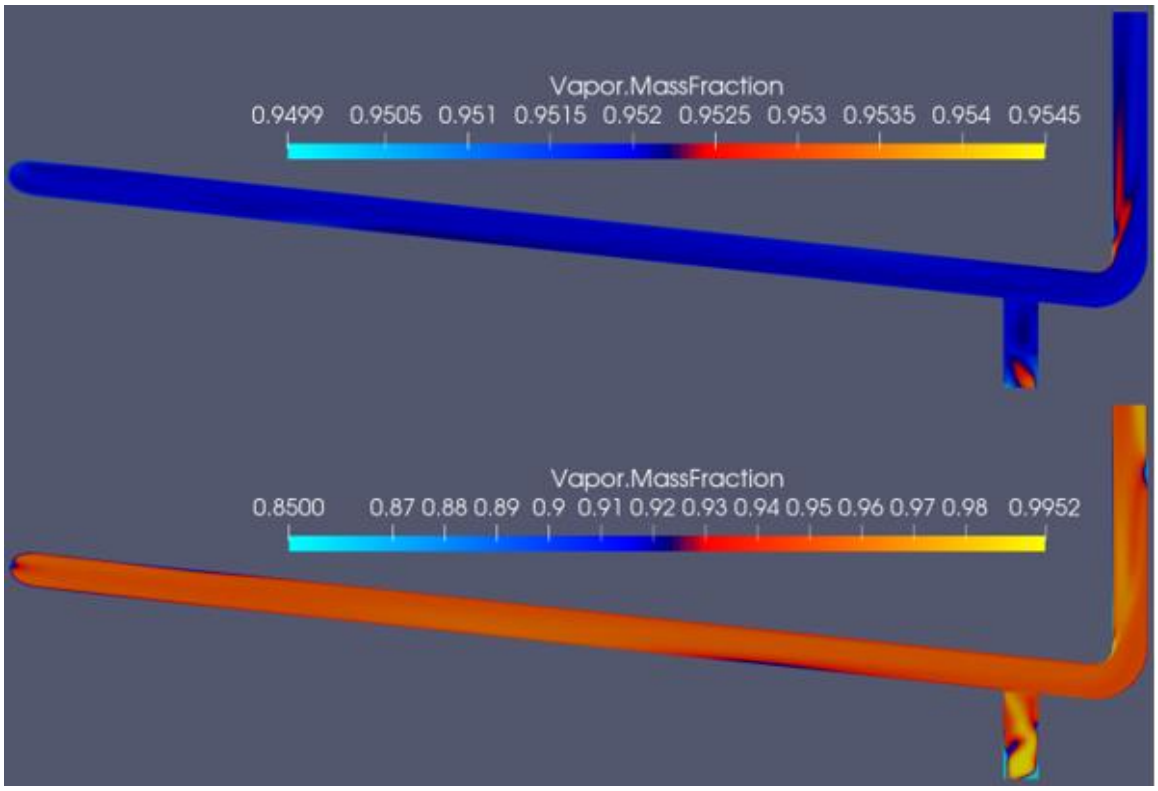

Figure 66. Vapor mass fraction contour for X = 95.19%, $d_{droplet}$ = 1 µm (top) and 10 µm (bottom) at outlet

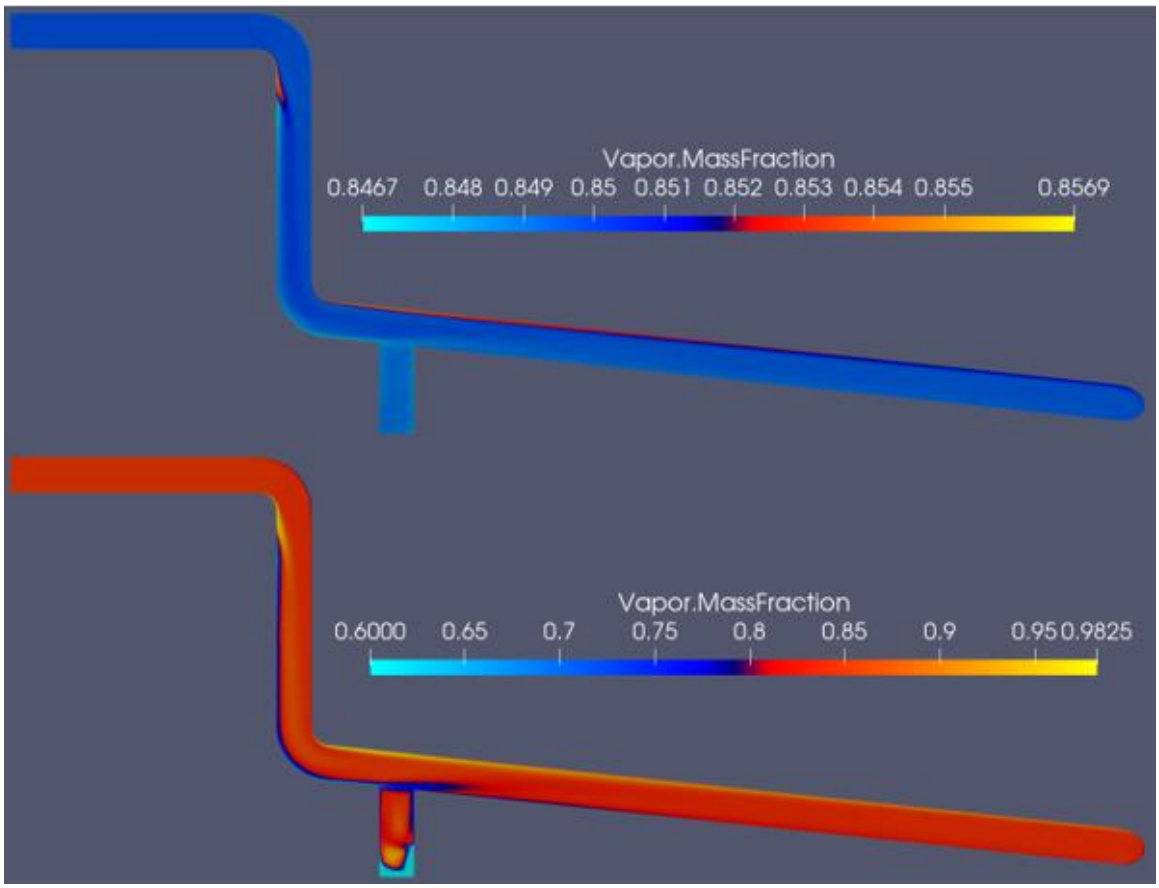

Figure 67. Vapor mass fraction contour for X = 84.97%, $d_{droplet}$ = 1 µm (top) and 10 µm (bottom) at inlet

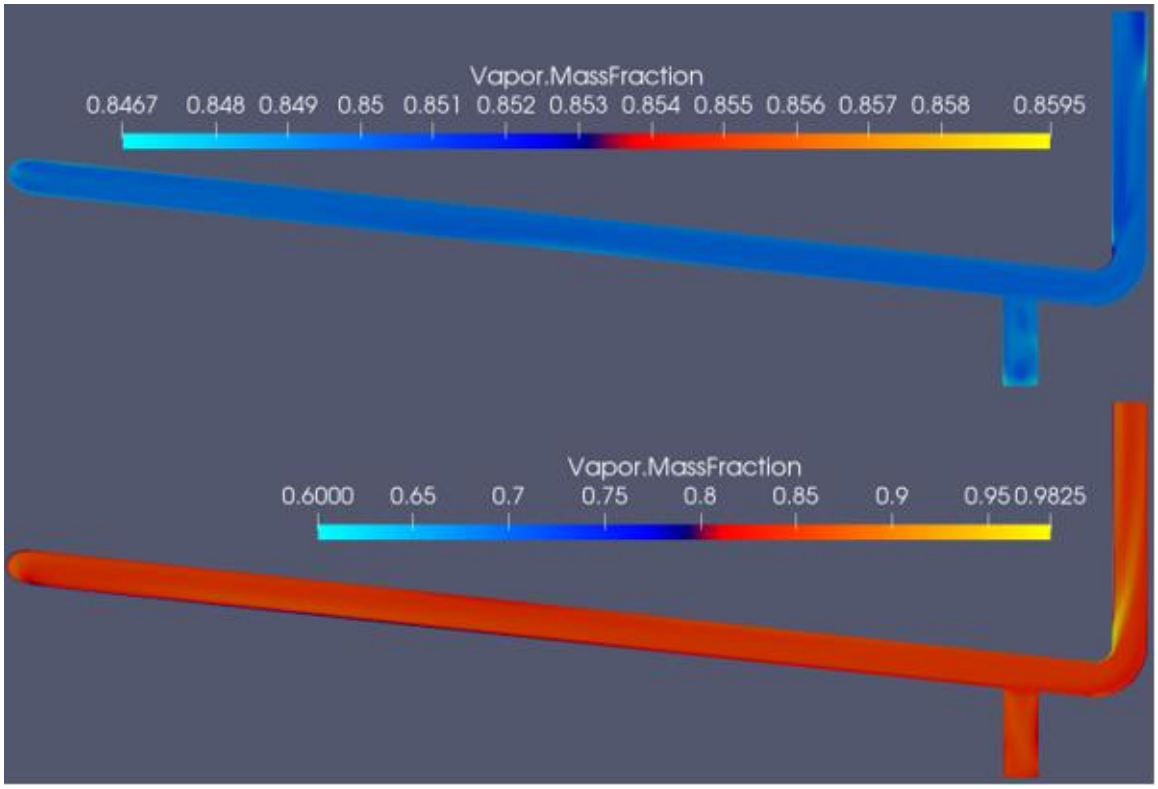

Figure 68. Vapor mass fraction contour for X = 84.97%, $d_{droplet}$ = 1 µm (top) and 10 µm (bottom) at outlet

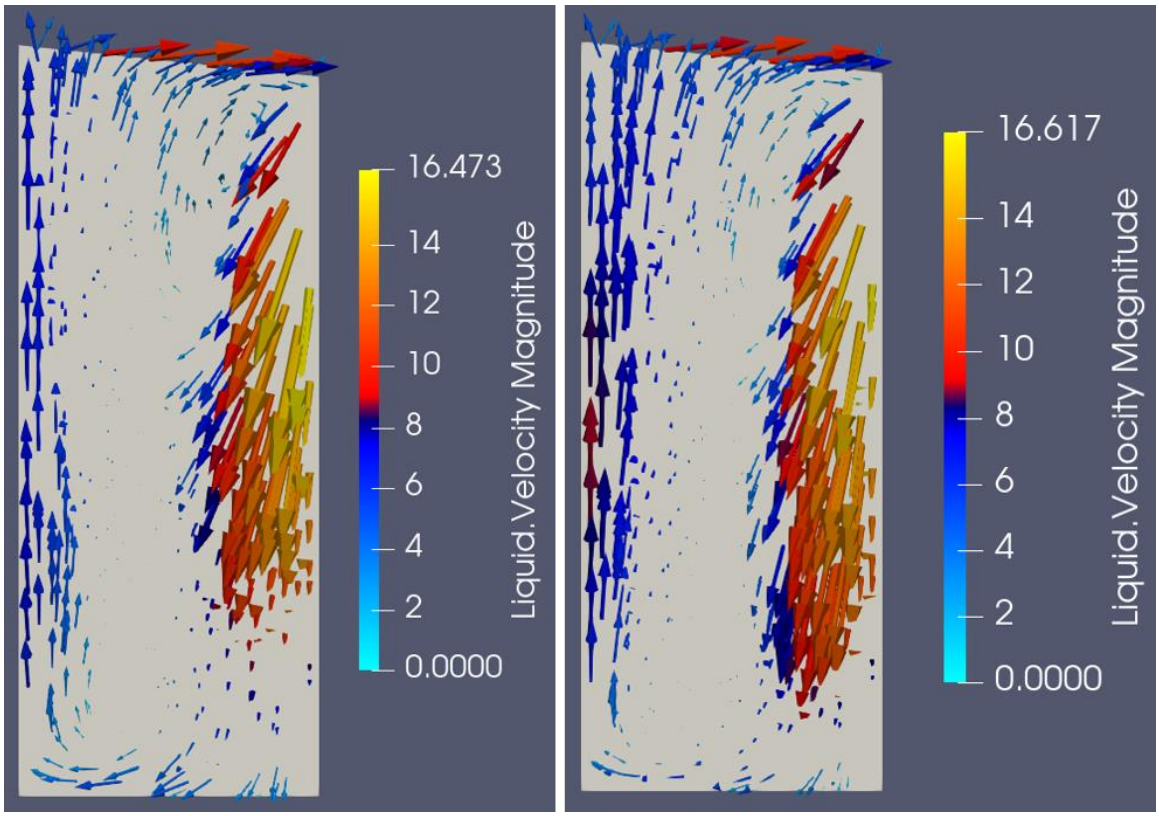

Figure 69. Liquid velocity vectors in the first pipe branch, X = 99.37% and $d_{droplet}$ = 1 µm (left) and 10 µm (right)

Examination of the liquid mass plots for each case showed that none of the six cases had achieved steady-state, including the solutions for 99.37% inlet quality which had achieved steady-state without the branch piping. With the exception of the 95.19% and 84.97% quality solutions with 10 µm droplets, each model had reached a pseudo steady-state condition. The liquid mass for 95.19% and 84.97% solutions with 10 µm droplets were still increasing at the end of 2500 iterations. The 84.97% solution was run for an additional 20000 iterations and a steady-state condition was not reached. The liquid mass continued to increase at a rate of approximately 1 g per 1000 iterations. The 95.19% quality solution with 10 µm droplets was run for an additional 12500 iterations and was also still increasing in steps. The step-wise increases in liquid mass were likely due to the relatively high Courant number. Plots of the liquid mass for the 84.97% and 95.19% quality solutions are provided in Figure 70 and Figure 71 respectively.

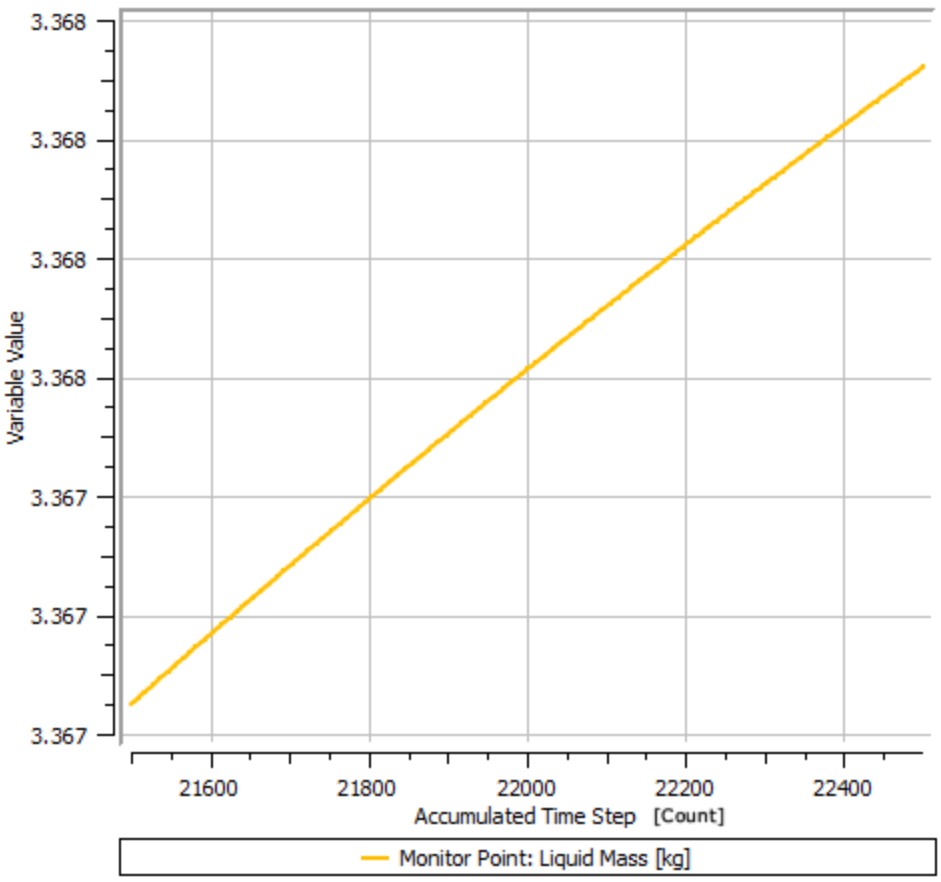

Figure 70. Liquid mass for X = 84.97%, $d_{droplet}$ = 10 µm

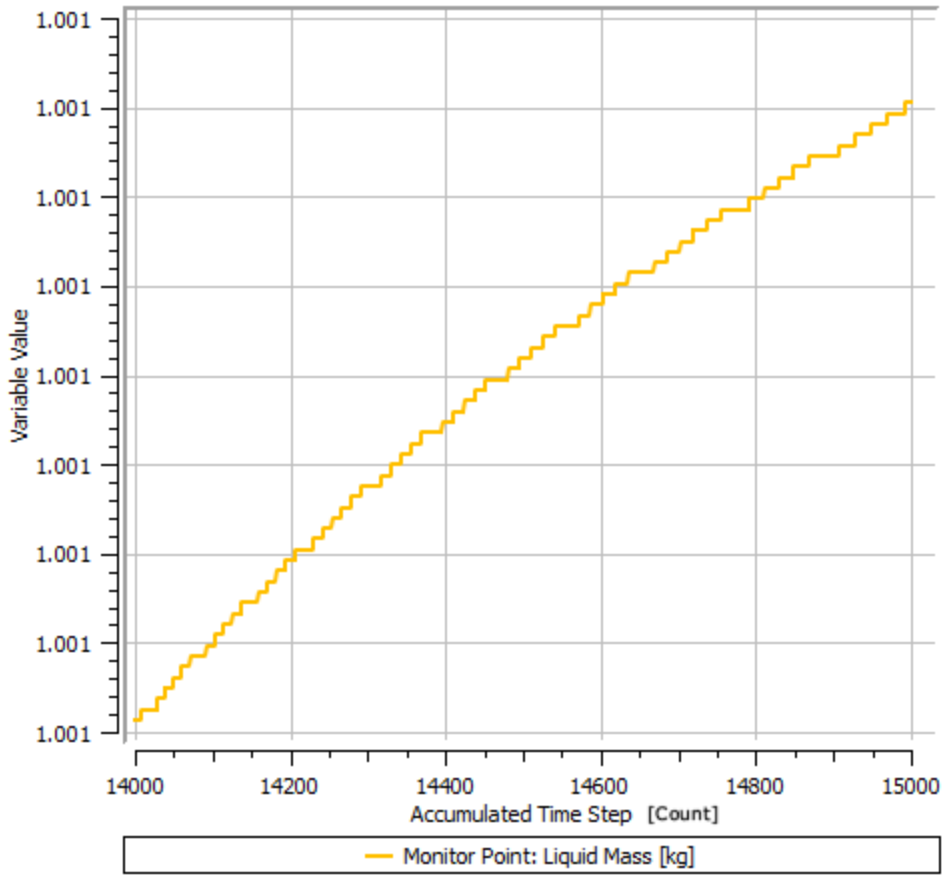

Figure 71. Liquid mass for X = 95.19%, $d_{droplet}$ = 10 µm

b. Turbulent Liquid Phase

The same six variations of the flow were modeled implementing the CFX dispersed phase zero equation turbulence model for the liquid phase. The results were used to compare any difference in computational resources and gross flow parameters including the differential pressure and liquid mass distribution. The solver parameters for the six models are provided in Table 23. Compared to the laminar solutions, 0.5% additional memory was allocated. The calculation times were lower by an average of 40%. The reason for the significantly reduced run time for the 0.9992 vapor volume fraction solutions could not be determined from a review of the solver out file.

Table 23. Solver parameters for branch outlet wall boundary condition and turbulent liquid phase

Inlet Vapor VF	$D_{droplet}$ (μm)	Partition Number	Total Time Steps	Clock Time (Hrs:Min)	Memory (Mb)	Memory Allocation (%)	Average Courant Number
0.9999	1	8	2500	15:12	3778.27	1.44	25.53
0.9999	10	8	2500	15:08	3778.27	1.44	25.54
0.9992	1	8	2500	07:46	3778.27	1.44	25.54
0.9992	10	8	2500	07:47	3778.27	1.44	25.64
0.9972	1	8	2500	15:04	3778.27	1.44	25.54
0.9972	10	8	2500	15:12	3778.27	1.44	25.37

For each of the six cases, the addition of the dispersed phase zero-equation turbulence model for the liquid phase resulted in an increased differential pressure. The increase was relatively low, on the order of 100 Pa, for the first five cases. However, for the last case with 84.97% quality and 10 μm droplets, the increase was more significant, approximately 1700 Pa. A summary of various flow parameters for each case is provided in Table 24.

Table 24. Select results for the steam pipe with branch outlet wall boundary condition

Inlet Vapor VF	$D_{droplet}$ (μm)	X_{inlet}	X_{outlet}	$\dot{m}_{in}$ (kg/s)	$\dot{m}_{out}$ (kg/s)	ΔP (Pa)	Liquid Mass (kg)
0.9999	1	99.37%	99.37%	26.0107	26.0107	-12977	0.09677
0.9999	10	99.37%	99.37%	26.0107	26.0106	-13057	0.10005
0.9992	1	95.19%	95.19%	27.1324	27.1324	-13427	0.77418
0.9992	10	95.19%	95.21%	27.1324	27.1288	-14239	0.85026
0.9972	1	84.97%	84.97%	30.3373	30.3373	-14679	2.7096
0.9972	10	84.97%	84.97%	30.3373	30.3374	-16200	2.9608

Using ParaView, contours were plotted of the difference in the Liquid.MassTotal user variable between the laminar liquid and turbulent liquid solutions. This provided a direct comparison of differences in liquid mass distribution between the two models. The same centerline planes at the inlet and outlet legs of the piping were used. The liquid mass

for the turbulent liquid phase solution was subtracted from the liquid mass for the laminar liquid solution. Therefore, on the resulting contour plots, a positive value indicates a region where the laminar model had a greater liquid mass. Figure 72 through Figure 77 show the difference in liquid mass for at the inlet and outlet cross sections for each inlet quality and droplet size.

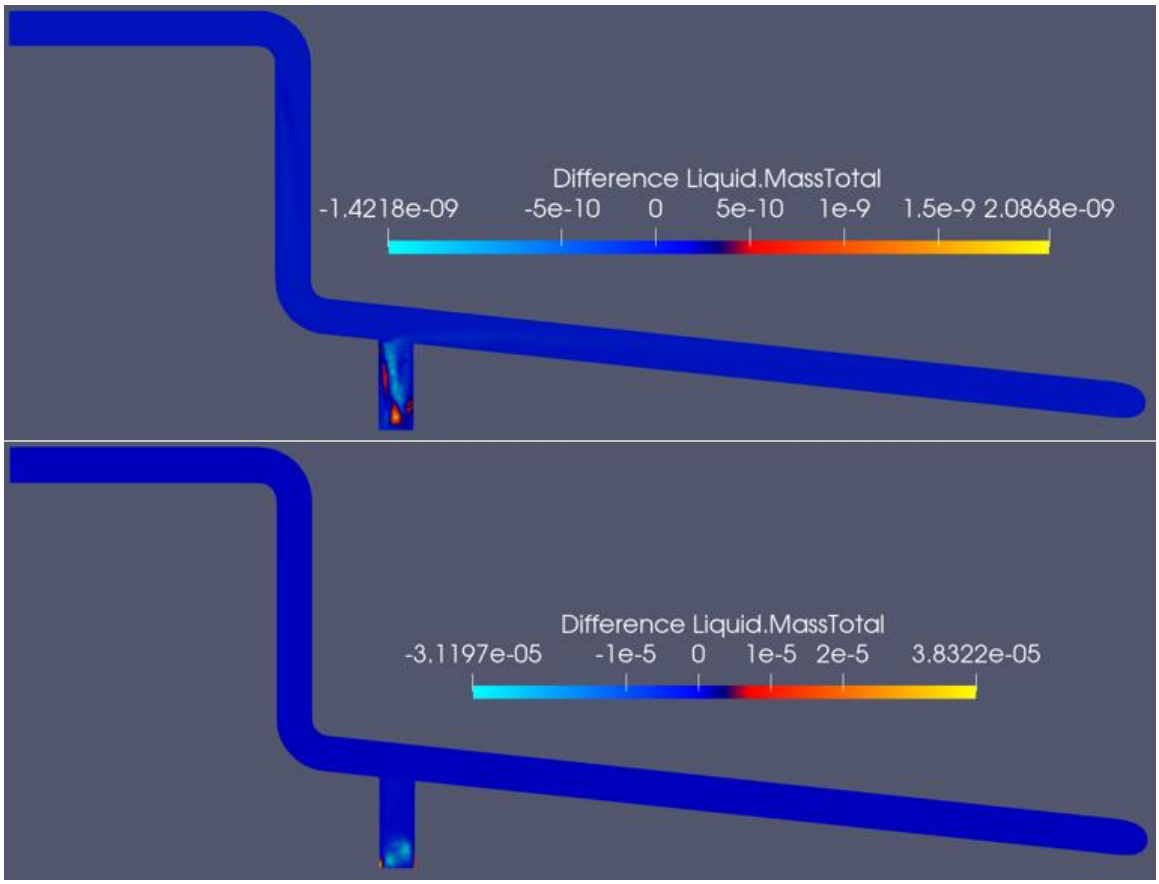

Figure 72. Difference in liquid mass for laminar and turbulent liquid phases, X = 99.37%, $d_{droplet}$ = 1 μm (top) and 10 μm (bottom) at inlet

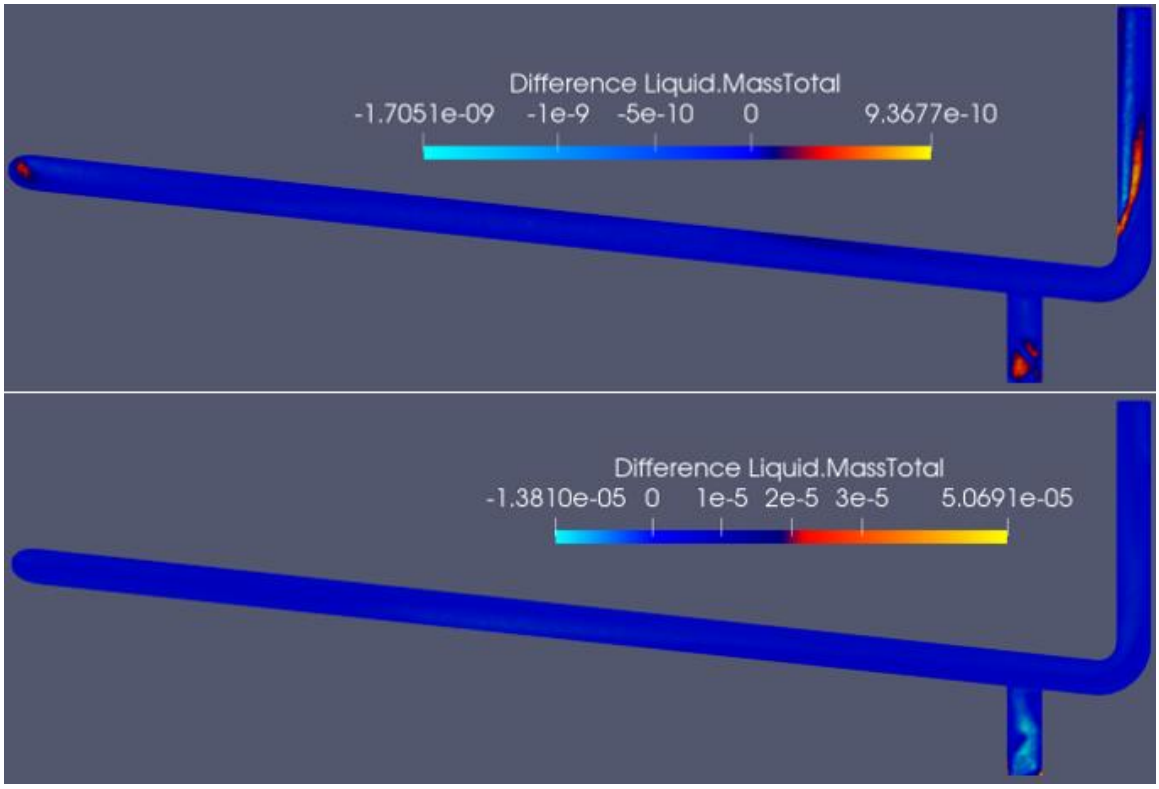

Figure 73. Difference in liquid mass for laminar and turbulent liquid phases, X = 99.37%, $d_{droplet}$ = 1 µm (top) and 10 µm (bottom) at outlet

For the 99.37% inlet quality solutions, there was very little difference in the distribution of liquid mass in the pipe when modeling the liquid phase as turbulent vice laminar. The differences that do exist were on the order of 10^{-9} kg, and are insignificant. Overall, modeling the liquid phase a turbulent did not substantially change the results for the 99.37% quality solutions,

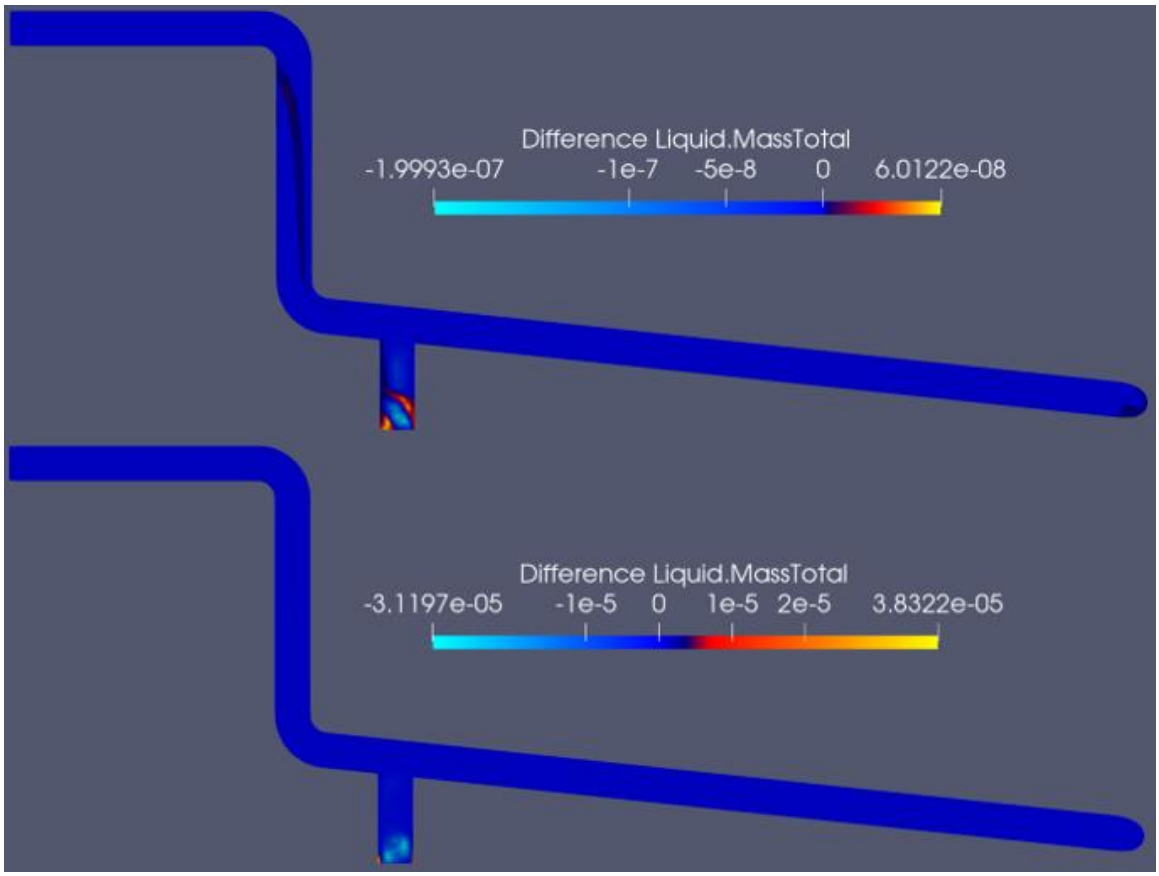

Figure 74. Difference in liquid mass for laminar and turbulent liquid phases, X = 95.19%, $d_{droplet}$ = 1 μm (top) and 10 μm (bottom) at inlet

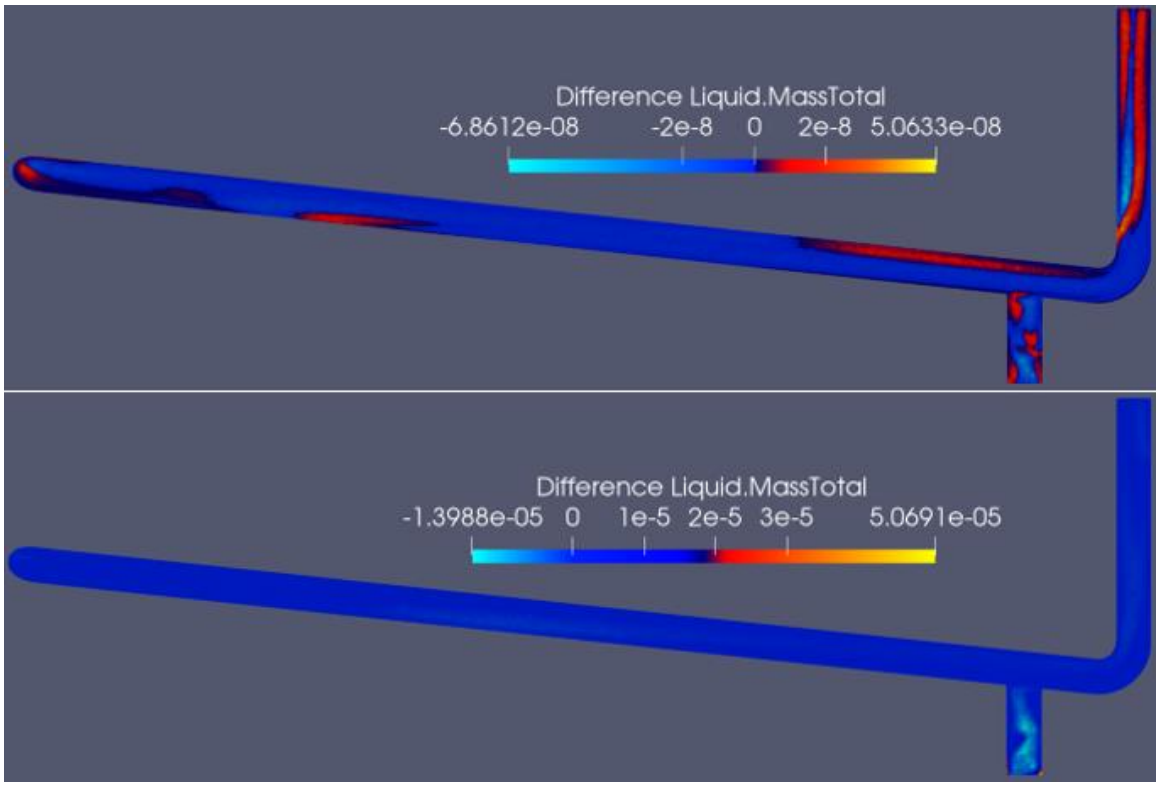

Figure 75. Difference in liquid mass for laminar and turbulent liquid phases, X = 95.19%, $d_{droplet}$ = 1 µm (top) and 10 µm (bottom) at outlet

A similar difference in the liquid mass near the pipe outlet was observed for the 95.19% quality solution with both 1 µm and 10 µm droplets. The numerical differences that were negligible, however the overall shape of the contours was largely the same. Both the 99.37% and 95.19% quality solutions with the 1 µm droplets showed the same tendency for the liquid mass at the inside radius of the outlet bend to be greater for the laminar solution. Likewise, both had a greater concentration of liquid in the second branch, just upstream of the outlet, for the larger turbulent 10 µm droplets.

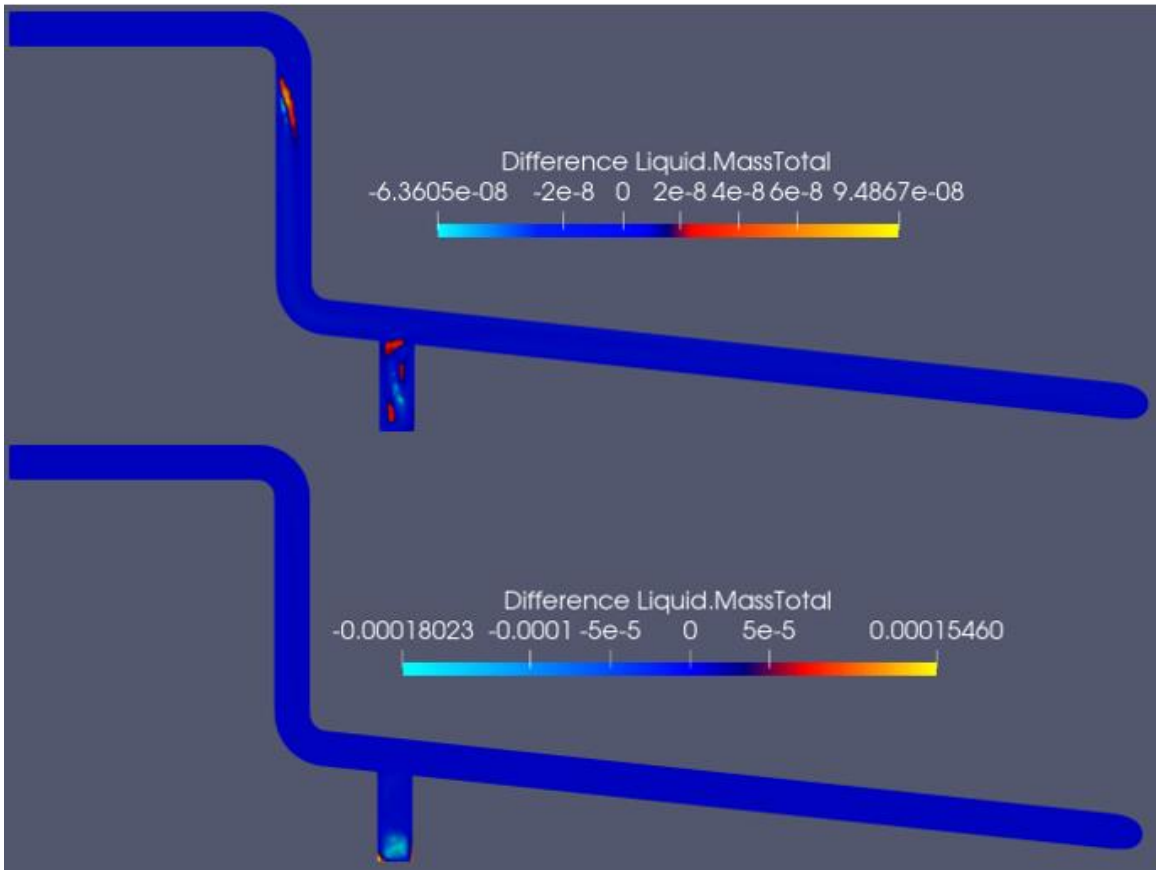

Figure 76. Difference in liquid mass for laminar and turbulent liquid phases, X = 84.97%, $d_{droplet}$ = 1 μm (top) and 10 μm (bottom) at inlet

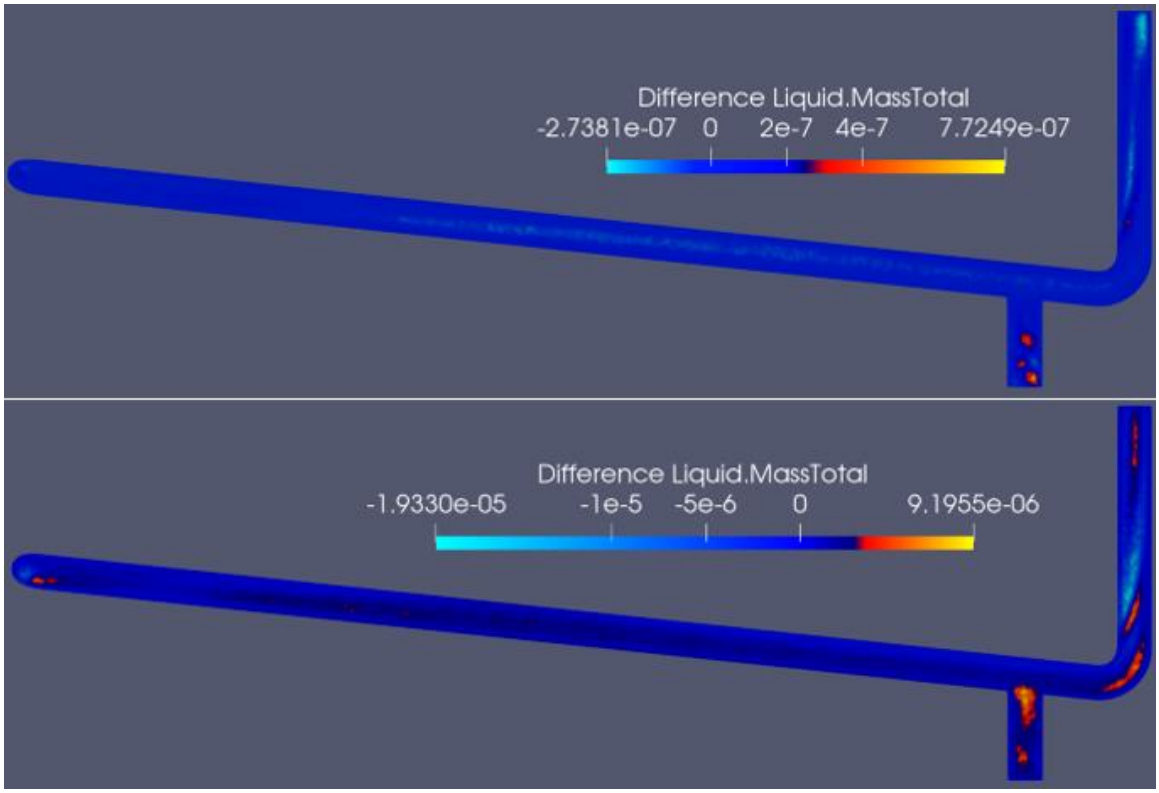

Figure 77. Difference in liquid mass for laminar and turbulent liquid phases, X = 84.97%, $d_{droplet}$ = 1 μm (top) and 10 μm (bottom) at outlet

Finally, the solutions for an 84.97% quality inlet again showed the same trend of minor changes in liquid mass concentration. Overall, for all three inlet qualities the addition of modeling the liquid as turbulent using the dispersed phase zero equation model did not produce any significant changes in distribution of liquid mass. The final variation of the steam pipe with branches model modeled the liquid phase as laminar due to being computationally less expensive to implement.

2. Branch Outlet Fluid Dependent Boundary Condition

The third variation of the steam trap with branches model used fluid dependent boundary conditions at the drain outlet to minimize the recirculation and re-entrainment of liquid that collected in the branches. The branch outlet boundaries were defined as outlets with a vapor mass flow rate of 0 kg/s and a liquid normal speed. The normal speed was chosen by calculating a velocity based on the liquid mass flow rate at the inlet and the

branch outlet flow area. From CFX Post, the liquid mass flow rate at the inlet for 99.37% inlet quality was 0.16283 kg/s. Both branch outlets had a diameter of 0.25 m, for a total outlet area of 0.0982 m^2. Using the known liquid density and Eq. (11) resulted in a calculated liquid velocity of 0.002 m/s. This velocity was used as the liquid normal speed boundary condition for all six models. The liquid mass low rate for the highest quality case was used as a conservative estimate of the liquid speed at the outlet of the branch. The goal was to provide a path for liquid in the branch to flow without implementing a large velocity that would force liquid to the branch outlet. Solver parameters for the two models are provided in Table 25.

$$\dot{m} = \rho V A \tag{11}$$

Table 25. Solver parameters for branch outlet wall boundary condition and turbulent liquid phase

Inlet Vapor VF	$D_{droplet}$ (μm)	Partition Number	Total Time Steps	Clock Time (Hrs:Min)	Memory (Mb)	Memory Allocation (%)	Average Courant Number
0.9999	1	16	5000[a]	09:33[a]	5061.61	1.93	25.50
0.9999	10	16	5000	09:34	5061.61	1.93	25.51

a. Total over two consecutive 2500 iteration runs.

After 5000 iterations, neither solution arrived at a steady-state liquid mass. A reduced timescale factor was implemented for each to determine what effect, if any, it would have on the solution. The 1 μm droplet solution was run for an additional 5000 iterations with a timescale factor of 0.5, while the 10 μm droplet model was run for 5000 iterations with a 0.05 timescale factor. These changes reduced the average Courant number to 12.75 for the 1 μm droplet model and 1.276 for the 10 μm droplet model. Selected flow parameters are provided in Table 26, including the mass flow rate of liquid at each branch outlet. Plots of the liquid mass for each are provided in Figure 78 and Figure 79.

Table 26. Select results for the branch fluid dependent boundary condition

$D_{droplet}$ (μm)	X_{inlet} (%)	$\dot{m}_{in}$ (kg/s)	$\dot{m}_{out}$ (kg/s)	$\dot{m}_{liq,branch1}$ (kg/s)	$\dot{m}_{liq,branch2}$ (kg/s)	ΔP (Pa)	Liquid Mass (kg)
1	99.37	26.0107	26.0106	8.045×10^{-6}	8.095×10^{-6}	-12572	0.09675
10	99.37	26.0107	26.0106	1.042×10^{-4}	1.238×10^{-5}	-12748	0.10179

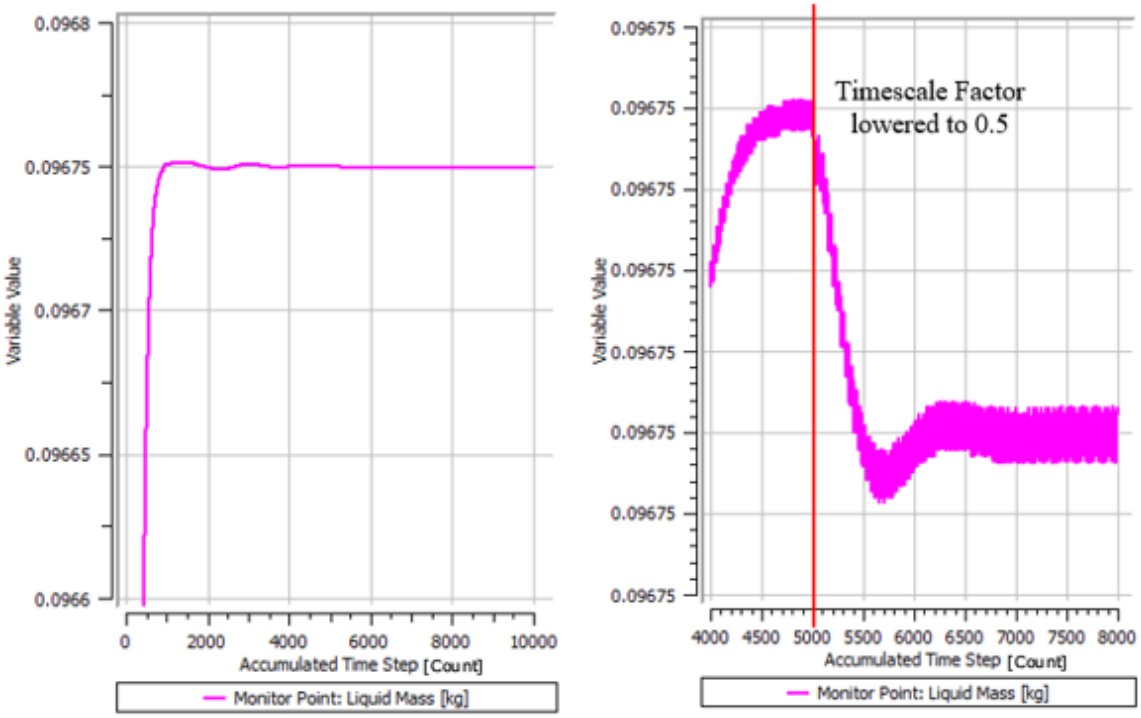

Figure 78. Liquid mass plot, X = 99.37% and $d_{droplet}$ = 1 μm

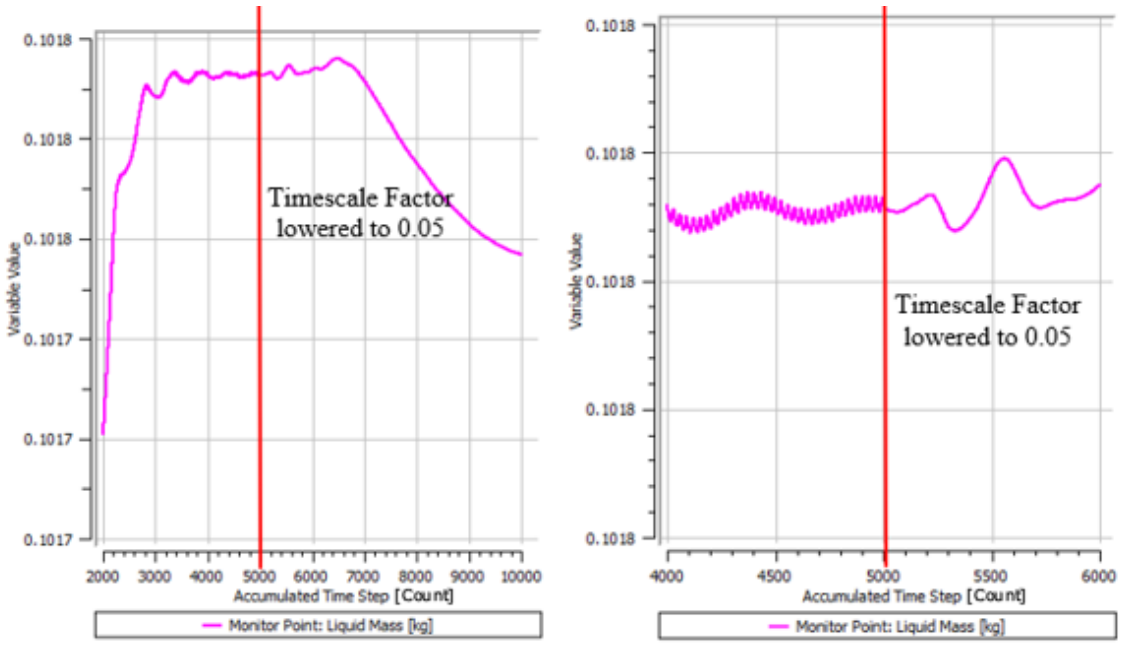

Figure 79. Liquid mass plot, X = 99.37% and $d_{droplet}$ = 10 µm

In both cases, reducing the timescale factor improved the results of the liquid mass calculation performed by the solver. The 1 µm droplet model had achieved a pseudo steady state, with oscillations still occurring. However, the average had converged to 0.09675, within 0.01% of the expected value. The 10 µm droplet model also did not reach steady-state, but the significantly reduced timescale factor did result in greatly improved convergence of the liquid mass. When the timescale factor was lowered to 0.05 at 5002 iterations, the oscillations in the calculation are no longer present. The calculation remained slightly unsteady for approximately 1500 iterations before lowering rapidly. In both cases, lowering the timescale factor and by proxy the Courant number resulted in significant improvements in the solver without mesh refinement.

The fluid dependent branch outlet boundary condition had the desired effect of allowing some liquid flow out of the branch. The chosen velocity was low enough to prevent the solver from forcing liquid to the boundary so that only naturally de-entrained liquid would enter the branch. However, the zero-vapor mass flow rate resulted in the solver placing an artificial wall at approximately 60% of the branch outlet area to prevent vapor flow in both cases. This created similar recirculation of the liquid and vapor to the

previous solutions implementing a wall boundary condition. Figure 80 shows the liquid velocity vectors in the first branch where two recirculation zones are observed.

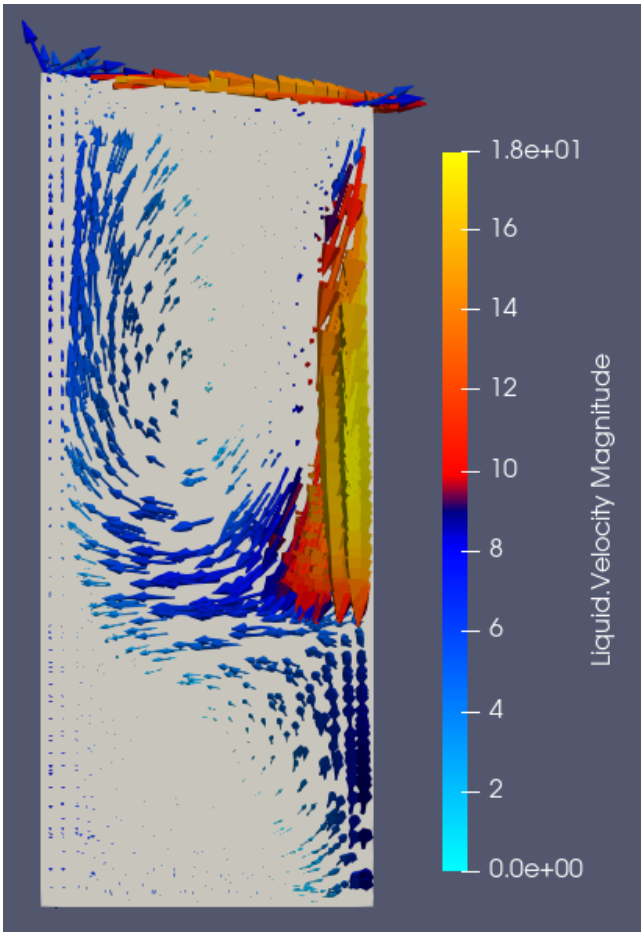

Figure 80. Liquid velocity vectors, X = 99.37%, $d_{droplet}$ = 1 µm

VI. TRACE SYSTEM ANALYSIS

A. TRACE SOLVER DESCRIPTION

TRACE is the latest software developed by the NRC for evaluating nuclear and non-nuclear reactor plant systems. TRACE has numerous capabilities, among which are the ability to model two-phase flows and generalized heat transfer in a one-dimensional model [18]. TRACE simultaneously solves partial differential equations for continuity, energy, and momentum for each phase present in the model, including separate momentum and energy equations for non-condensable gases [18]. This research built one-dimensional models of the condensation case study discussed in Chapter IV and the steam pipe without branches discussed in Chapter V for comparison to CFX to inform model development for transient analysis.

There are three steady-state analysis options in TRACE. This research used the generalized steady-state model. The generalized steady-state model implemented in TRACE "asymptotically evaluates the time-independent steady-state solution" where the state of all components is held at the user-defined conditions [19]. The solver determines when steady-state is reached by evaluating seven flow parameters every five timesteps and calculating the maximum change per second of each one [20]. Steady-state is achieved and the solver returns the results of the model when the fractional change per second of all seven parameters is below the convergence criteria [20]. The seven parameters evaluated by the solver are total pressure, liquid velocity, gas velocity, gas volume fraction, liquid temperature, gas temperature, and non-condensable gas pressure [20].

B. CONDENSATION CASE STUDY

Each case was set up as a steady-state model using the generalized steady-state calculation. The geometry was modeled using a vertical pipe component, with a fill component at the inlet and break at the outlet. The fill and break components in TRACE set the boundary conditions at the inlet and the outlet, respectively. The pipe was divided into six nodes, numbered from inlet to outlet. The initial conditions for all three components were set to saturation conditions at 2.94 MPa. The fill and break volumes were

set to 1 m^3 to provide sufficient volume for a steady-state analysis of the pipe, which had a volume of 0.00377 m^3. The inlet boundary condition was set to constant mass flow rate corresponding to the appropriate value from Table 3 for each of the five cases. The assembled one-dimensional model is provided in Figure 81. The heat flux at the wall boundary was implemented using the "pipe wall" function of the pipe component. The pipe wall was divided into two radial nodes with an inner radius of 0.02 m and a thickness of 1×10^{-4} m. The wall temperature was set to the appropriate temperature from Table 3 and the liquid and vapor heat transfer coefficient set to the corresponding value from Table 2 for each case. TRACE requires setting an outside vapor and liquid temperature, which were set to the wall temperature. This combination of boundary conditions ensured a constant wall temperature, the same as the case study experimental conditions. The smallest wall thickness the solver would recognize was used to minimize the effects of thermal inertia within the pipe wall.

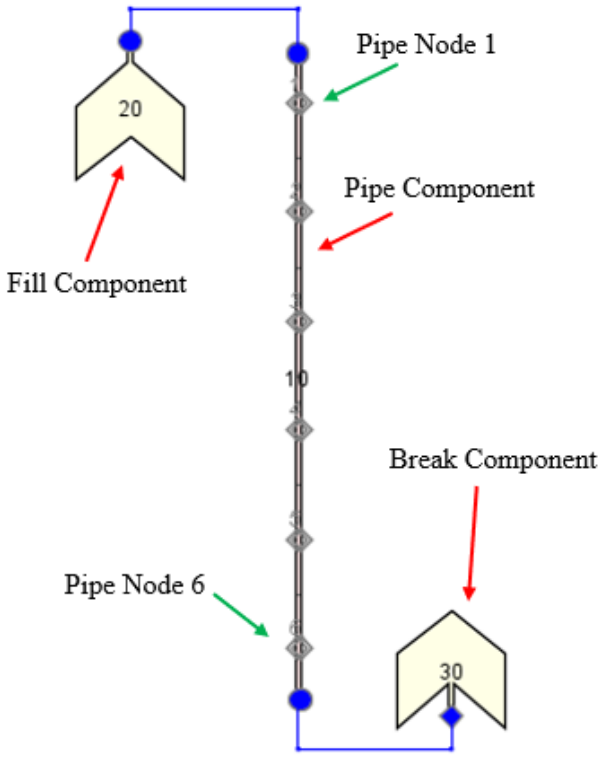

Figure 81. Condensation case study 1-D model in TRACE

A steady state solution was reached for Case 1, Case 5, and Case 25. The solutions for Case 14 and Case 27 did not achieve steady state. TRACE calculated the inner wall power which was compared to the values for total heat in Table 3. TRACE also determines the vapor volume fraction, from which a quality was calculated using the node 6 volume of 1.57×10^{-4} m^3 and the known liquid and vapor densities in Table 1. Results are provided in Table 27.

Table 27. Results of TRACE analysis for condensation case study

Case Number	Time-steps to Reach Steady-State	Inner Wall Surface Power (W)	%Error from Experiment Results	Vapor Volume Fraction	Quality in Node 6
1	305	4580	21.3%	0.9736	40%
5	290	11167	12.1%	0.9603	30%
25	310	4836	23.4%	0.9716	38%

The error in the inner wall power between the TRACE analysis and the steam condensation experiment conducted by Borishanskiy, et. al., likely resulted from the method used to model the pipe wall heat transfer. The experiment results did not include information on the pipe wall thickness or the outer wall temperature so an exact model could not be built in TRACE. Rather, the model was built to around achieving the derived inner wall temperature for each case, which resulted in non-physical wall thickness and boundary conditions. This difference in the wall boundary contributed to the results obtained in TRACE.

Case 14 and Case 27, the two cases with heat flux density on the order of 1×10^6, did not reach steady state. TRACE completed 4229 time steps with a time step size of 0.25 s for Case 14, and 1300 time steps with a time step size of 1 s for Case 27. For Case 14, none of the seven monitored parameters met the convergence criteria of 10^{-4} fractional change. For the Case 27 model, vapor velocity was the only parameter that did not meet convergence criteria.

C. STEAM PIPING SYSTEM

The steam pipe without branches was modeled using TRACE to compare with the results from CFX and to establish steady-state conditions for use as the initial conditions for follow-on transient analysis. The steam pipe model used the generalized steady-state calculation. A total of six individual pipe components were used. The same 0.33 m node length was used for each pipe component for consistency in node size. A six-degree downward slope for the four center pipe components was used to match the geometry of the model used in CFX. TRACE is a one-dimensional code, so losses in the pipe bends were modeled as loss factors inserted at the inlet and outlet plane of each pipe component that corresponds to a bend. The loss factor of 0.22 was determined by linearly interpolating the values for a flanged 90-degree regular radius pipe [6]. A fill and break were inserted at the inlet and outlet, respectively, each with a volume of 10 m^3. The fill boundary condition was set to inlet velocity with the vapor and liquid velocity both set to 40 m/s. A schematic of the overall model is provided in Figure 82.

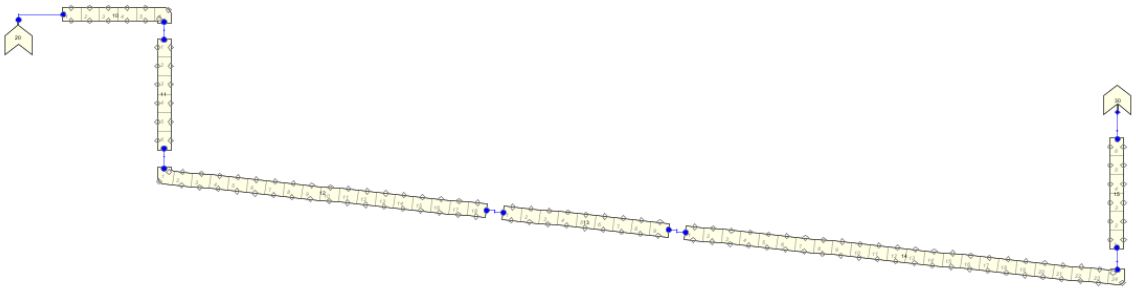

Figure 82. TRACE model for the steam pipe without branches

Steady-state was reached after 245 time steps with a step size of 0.148 s. The results from TRACE showed good agreement with the CFX results for the 0.9999 volume fraction case. The vapor volume fraction at the outlet was fractionally greater than the inlet vapor volume fraction, 0.999902. The pressure drop from the inlet to the outlet was 19540 Pa, compared to approximately 13000 Pa for the CFX solution. A comparison of selected parameters from TRACE to results from CFX are provided in Table 28. Overall, the results

from TRACE showed excellent agreeance with the results obtained from CFX for a steady-state analysis.

Table 28. Comparison of results from TRACE and CFX

Solver	$D_{droplet}$ (μm)	Inlet Vapor VF	Outlet Vapor VF	P_{inlet} (MPa)	P_{outlet} (MPa)	ΔP (MPa)	$V_{in,vap}$ (m/s)	$V_{out,vap}$ (m/s)
TRACE	-	0.9999	0.9999	2.64810	2.62860	-0.01950	39.94	40.17
CFX	1	0.9999	0.9999	2.65142	2.63887	-0.01255	39.99	40.58
CFX	10	0.9999	0.9998	2.65143	2.63888	-0.01255	39.99	40.55

THIS PAGE INTENTIONALLY LEFT BLANK

VII. CONCLUSIONS AND RECOMMENDATIONS

This research was the first step in conducting a future transient analysis of a saturated steam system using CFX and TRACE. An examination of CFX's ability to model conjugate heat transfer and wall condensation using the thermal energy model was conducted which showed that the choice of boundary conditions can significantly impact the model and prevent non-physical results. A two-phase saturated steam flow model was implemented in CFX for analysis of liquid droplet de-entrainment at pipe branches at steady-state conditions. The stability of the model was shown for an inlet quality as low as 84.97% and for constant diameter droplets up to 10 µm. A CEL expression was implemented for calculating the liquid mass in the pipe and monitoring the convergence of the model to steady-state conditions. A corresponding one-dimensional model was built in TRACE for rapid system analysis and to serve as the initial conditions for transient modeling.

Future work can improve the results obtained by conducting a mesh refinement study for the steam pipe model. A mesh refinement study is crucial for further validation of stability of the two-phase model built through this effort. Variable property fluid models using the IAPWS IF-97 EOS should be implemented for the steam pipe model under steady-state condition following mesh refinement to validate the solver's ability to perform the transient analysis. Also, an effort should be made to measure the liquid mass in the pipe in TRACE to provide another point of comparison with CFX.

THIS PAGE INTENTIONALLY LEFT BLANK

APPENDIX A. FLUID PROPERTY CCL FILE FOR CONDENSATION CASE STUDY

```
LIBRARY:
  MATERIAL: LiquidConst
    Material Group = Constant Property Liquids,Wet Steam
    Option = Pure Substance
    Thermodynamic State = Liquid
    PROPERTIES:
      Option = General Material
      EQUATION OF STATE:
        Density = 823.42 [kg m^-3]
        Molar Mass = 18.02 [kg kmol^-1]
        Option = Value
      END
      SPECIFIC HEAT CAPACITY:
        Option = Value
        Specific Heat Capacity = 4.7094 [J g^-1 K^-1]
        Specific Heat Type = Constant Pressure
      END
      REFERENCE STATE:
        Option = Specified Point
        Reference Pressure = 2.94 [MPa]
        Reference Specific Enthalpy = 1003100 [J kg^-1]
        Reference Specific Entropy = 2.6353 [J g^-1 K^-1]
        Reference Temperature = 505.89 [K]
      END
      DYNAMIC VISCOSITY:
        Dynamic Viscosity = 0.00011475 [Pa s]
        Option = Value
      END
      THERMAL CONDUCTIVITY:
        Option = Value
        Thermal Conductivity = 0.63412 [W m^-1 K^-1]
      END
    END
  END
  MATERIAL: LiquidVar
    Material Group = Wet Steam,IAPWS IF97
    Option = Pure Substance
    Thermodynamic State = Liquid
    PROPERTIES:
      Option = IAPWS Library
      REFERENCE STATE:
        Option = Automatic
      END
      TABLE GENERATION:
        Maximum Absolute Pressure = 12.345 [MPa]
        Maximum Points = 1000
        Maximum Temperature = 600 [K]
        Minimum Absolute Pressure = 0.0035368 [MPa]
        Minimum Temperature = 300 [K]
        Pressure Extrapolation = On
        Temperature Extrapolation = Yes
      END
    END
  END
  MATERIAL: VaporConst
    Material Group = Wet Steam,Constant Property Gases
```

```
    Option = Pure Substance
    Thermodynamic State = Gas
    PROPERTIES:
      Option = General Material
      EQUATION OF STATE:
        Density = 14.7 [kg m^-3]
        Molar Mass = 18.02 [kg kmol^-1]
        Option = Value
      END
      SPECIFIC HEAT CAPACITY:
        Option = Value
        Specific Heat Capacity = 3.5873 [J g^-1 K^-1]
        Specific Heat Type = Constant Pressure
      END
      REFERENCE STATE:
        Option = Specified Point
        Reference Pressure = 2.94 [MPa]
        Reference Specific Enthalpy = 2803100 [J kg^-1]
        Reference Specific Entropy = 6.1935 [J g^-1 K^-1]
        Reference Temperature = 505.89 [K]
      END
      DYNAMIC VISCOSITY:
        Dynamic Viscosity = 1.6802e-5 [Pa s]
        Option = Value
      END
      THERMAL CONDUCTIVITY:
        Option = Value
        Thermal Conductivity = 0.045639 [W m^-1 K^-1]
      END
    END
  END
  MATERIAL: VaporVar
    Material Group = IAPWS IF97,Wet Steam
    Option = Pure Substance
    Thermodynamic State = Gas
    PROPERTIES:
      Option = IAPWS Library
      REFERENCE STATE:
        Option = Automatic
      END
      TABLE GENERATION:
        Maximum Absolute Pressure = 12.345 [MPa]
        Maximum Points = 1000
        Maximum Temperature = 600 [K]
        Minimum Absolute Pressure = 0.0035368 [MPa]
        Minimum Temperature = 300 [K]
        Pressure Extrapolation = On
        Temperature Extrapolation = Yes
      END
    END
  END
END
COMMAND FILE:
  Version = 20.2
END
```

APPENDIX B. USER EXPRESSIONS FOR CONDENSATION CASE STUDY

```
LIBRARY:
  CEL:
    EXPRESSIONS:
      InletPress = areaAve(Pressure)@Inlet
      LiquidVelInlet = massFlowAve(Liquid.Velocity)@Inlet
      LiquidVelOutlet = massFlowAve(Liquid.Velocity)@Outlet
      MassFlowInlet = massFlow()@Inlet
      MassFlowOutlet = -massFlow()@Outlet
      OutletPress = areaAve(Pressure)@Outlet
      Press = 2.94[MPa]
      QualityInlet = \
        massFlow(Vapor)@Inlet/(massFlow(Vapor)@Inlet+massFlow(Liquid)@Inlet)
      QualityOutlet = \
        massFlow(Vapor)@Outlet/(massFlow(Vapor)@Outlet+massFlow(Liquid)@Outlet)
      Tsat = \
        1[K]*(0.5*(650.17534844798+((2*((-724213.16703206*((Press/1[MPa])^0.25\
        )^2)+(-3232555.0322333*((Press/1[MPa])^0.25))+405113.40542057))/(-((11\
        67.0521452767*((Press/1[MPa])^0.25)^2)+(12020.824702470*((Press/1[MPa]\
        )^0.25))-4823.2657361591)-(((1167.0521452767*((Press/1[MPa])^0.25)^2)+\
        (12020.824702470*((Press/1[MPa])^0.25))-4823.2657361591)^2-(4*(((Press\
        /1[MPa])^0.25)^2+(-17.073846940092*((Press/1[MPa])^0.25))+14.915108613\
        530)*((-724213.16703206*((Press/1[MPa])^0.25)^2)+(-3232555.0322333*((P\
        ress/1[MPa])^0.25))+405113.40542057)))^0.5))-((650.17534844798+((2*((-\
        724213.16703206*((Press/1[MPa])^0.25)^2)+(-3232555.0322333*((Press/1[M\
        Pa])^0.25))+405113.40542057))/(-((1167.0521452767*((Press/1[MPa])^0.25\
        )^2)+(12020.824702470*((Press/1[MPa])^0.25))-4823.2657361591)-(((1167.\
        0521452767*((Press/1[MPa])^0.25)^2)+(12020.824702470*((Press/1[MPa])^0\
        .25))-4823.2657361591)^2-(4*(((Press/1[MPa])^0.25)^2+(-17.073846940092\
        *((Press/1[MPa])^0.25))+14.915108613530)*((-724213.16703206*((Press/1[\
        MPa])^0.25)^2)+(-3232555.0322333*((Press/1[MPa])^0.25))+405113.4054205\
        7)))^0.5)))^2-4*(-0.23855557567849+(650.17534844798*((2*((-724213.1670\
        3206*((Press/1[MPa])^0.25)^2)+(-3232555.0322333*((Press/1[MPa])^0.25))\
        +405113.40542057))/(-((1167.0521452767*((Press/1[MPa])^0.25)^2)+(12020\
        .824702470*((Press/1[MPa])^0.25))-4823.2657361591)-(((1167.0521452767*\
        ((Press/1[MPa])^0.25)^2)+(12020.824702470*((Press/1[MPa])^0.25))-4823.\
        2657361591)^2-(4*(((Press/1[MPa])^0.25)^2+(-17.073846940092*((Press/1[\
        MPa])^0.25))+14.915108613530)*((-724213.16703206*((Press/1[MPa])^0.25)\
        ^2)+(-3232555.0322333*((Press/1[MPa])^0.25))+405113.40542057)))^0.5)))\
        ))^0.5))
      VaporVelInlet = massFlowAve(Vapor.Velocity)@Inlet
      VaporVelOutlet = massFlowAve(Vapor.Velocity)@Outlet
      WallHeatFlux = if(Accumulated Iteration Number <=250, \
        0[W/m^2]-(Accumulated Iteration Number*123.6)[W/m^2], -30900[W/m^2])
      WallTemp = if(Accumulated Iteration Number <=250, \
        505.89[K]-(Accumulated Iteration Number*0.0128)[K], 502.69[K])
    END
  END
END
COMMAND FILE:
  Version = 20.2
END
```

THIS PAGE INTENTIONALLY LEFT BLANK

APPENDIX C. CCL FILE FOR IMPLEMENTATION OF TOTAL MASS VARIABLE

```
LIBRARY:
  CEL:
    EXPRESSIONS:
      SumLiqMassTotal = sum(Liquid.MassTotal)@Default Domain
    END
  END
  ADDITIONAL VARIABLE: MassTotal
    Option = Definition
    Tensor Type = SCALAR
    Units = [kg]
    Variable Type = Specific
  END
END
FLOW: Flow Analysis 1
  DOMAIN: Default Domain
    FLUID MODELS:
      ADDITIONAL VARIABLE: MassTotal
        Option = Fluid Dependent
      END
      FLUID: Liquid
        ADDITIONAL VARIABLE: MassTotal
          Additional Variable Value = Volume of Finite Volumes *Density \
            *Volume Fraction
          Option = Algebraic Equation
        END
      END
      FLUID: Vapor
        ADDITIONAL VARIABLE: MassTotal
          Additional Variable Value = Volume of Finite Volumes *Density \
            *Volume Fraction
          Option = Algebraic Equation
        END
      END
    END
  OUTPUT CONTROL:
    MONITOR OBJECTS:
      MONITOR POINT: Liquid Mass
        Coord Frame = Coord 0
        Expression Value = SumLiqMassTotal
        Option = Expression
      END
    END
  END
END
COMMAND FILE:
  Version = 20.2
END
```

THIS PAGE INTENTIONALLY LEFT BLANK

APPENDIX D. MATLAB SCRIPT FOR STEAM PIPE MESH CALCULATION

```
% 23m total pipe length, 0.25m diameter
% Not accoutning for steam traps

clear all
clc

a = 0.005; % Element size, m
L = 23; % Pipe length, m
d = 0.25; % pipe diameter, m

A_xs = pi/4*d^2; % Pipe cross-sectional area, m^2
V_tet = a^3/(6*sqrt(2)); % Tetrahedral volume, m^3
A_facesize = (a/4)^2;
V_domain = 1.1027; % domain volume, m^3
y1 = 0.0001; % First layer thickness, m
AR = sqrt(A_facesize)/y1

% Number of mesh elements calculations
N_bulk = V_domain/V_hex
N_inflation = 20*(1/A_facesize)*pi*d*L
N_total = N_bulk+N_inflation
```

THIS PAGE INTENTIONALLY LEFT BLANK

APPENDIX E. CCL FILE FOR STEAM PIPE FLUID PROPERTIES

```
LIBRARY:
  MATERIAL: LiquidConst
    Material Group = Constant Property Liquids,Wet Steam
    Option = Pure Substance
    Thermodynamic State = Liquid
    PROPERTIES:
      Option = General Material
      EQUATION OF STATE:
        Density = 831.318 [kg m^-3]
        Molar Mass = 18.02 [kg kmol^-1]
        Option = Value
      END
      SPECIFIC HEAT CAPACITY:
        Option = Value
        Specific Heat Capacity = 4659 [J kg^-1 K^-1]
        Specific Heat Type = Constant Pressure
      END
      REFERENCE STATE:
        Option = Specified Point
        Reference Pressure = 2.6389 [MPa]
        Reference Specific Enthalpy = 975465 [J kg^-1]
        Reference Specific Entropy = 2581.1 [J kg^-1 K^-1]
        Reference Temperature = 500 [K]
      END
      DYNAMIC VISCOSITY:
        Dynamic Viscosity = 0.0001179 [Pa s]
        Option = Value
      END
      THERMAL CONDUCTIVITY:
        Option = Value
        Thermal Conductivity = 0.6421 [W m^-1 K^-1]
      END
    END
  END
  MATERIAL: LiquidVar
    Material Group = IAPWS IF97,Wet Steam
    Option = Pure Substance
    Thermodynamic State = Liquid
    PROPERTIES:
      Option = IAPWS Library
      REFERENCE STATE:
        Option = Automatic
      END
      TABLE GENERATION:
        Maximum Absolute Pressure = 12.345 [MPa]
        Maximum Points = 100
        Maximum Temperature = 600 [K]
        Minimum Absolute Pressure = 0.0035368 [MPa]
        Minimum Temperature = 300 [K]
        Pressure Extrapolation = On
        Temperature Extrapolation = Yes
      END
    END
  END
  MATERIAL: VaporConst
    Material Group = Wet Steam,Constant Property Gases
    Option = Pure Substance
```

```
    Thermodynamic State = Gas
    PROPERTIES:
      Option = General Material
      EQUATION OF STATE:
        Density = 13.1976 [kg m^-3]
        Molar Mass = 18.02 [kg kmol^-1]
        Option = Value
      END
      SPECIFIC HEAT CAPACITY:
        Option = Value
        Specific Heat Capacity = 3462.6 [J kg^-1 K^-1]
        Specific Heat Type = Constant Pressure
      END
      REFERENCE STATE:
        Option = Specified Point
        Reference Pressure = 2.6389 [MPa]
        Reference Specific Enthalpy = 2802590 [J kg^-1]
        Reference Specific Entropy = 6235.4 [J kg^-1 K^-1]
        Reference Temperature = 500 [K]
      END
      DYNAMIC VISCOSITY:
        Dynamic Viscosity = 1.6594e-5 [Pa s]
        Option = Value
      END
      THERMAL CONDUCTIVITY:
        Option = Value
        Thermal Conductivity = 0.044952 [W m^-1 K^-1]
      END
      THERMAL EXPANSIVITY:
        Option = Value
        Thermal Expansivity = 0.001686 [K^-1]
      END
    END
  END
  MATERIAL: VaporVar
    Material Group = IAPWS IF97,Wet Steam
    Option = Pure Substance
    Thermodynamic State = Gas
    PROPERTIES:
      Option = IAPWS Library
      REFERENCE STATE:
        Option = Automatic
      END
      TABLE GENERATION:
        Maximum Absolute Pressure = 12.345 [MPa]
        Maximum Points = 1000
        Maximum Temperature = 600 [K]
        Minimum Absolute Pressure = 0.0035368 [MPa]
        Minimum Temperature = 300 [K]
        Pressure Extrapolation = On
        Temperature Extrapolation = Yes
      END
    END
  END
END
COMMAND FILE:
  Version = 20.2
END
```

APPENDIX F. CCL FILE FOR STEAM PIPE MODEL WITHOUT BRANCHES

```
LIBRARY:
  CEL:
    EXPRESSIONS:
      LiquidVFInlet = 1-VaporVFInlet
      LiquidVelInlet = massFlowAve(Liquid.Velocity)@Inlet
      LiquidVelOutlet = massFlowAve(Liquid.Velocity)@Outlet
      MassFlowInlet = massFlow()@Inlet
      MassFlowOutlet = -massFlow()@Outlet
      Press = 2.6389[MPa]
      QualityEquilInlet = \
        ((massFlowAve(Liquid.enthalpy*Liquid.mf+Vapor.enthalpy*Vapor.mf)@Inle\
        t ) - 975465[J kg^-1])/(2.80259e+6 [J kg^-1] -975465[J kg^-1] )
      QualityEquilOutlet = \
        ((massFlowAve(Liquid.enthalpy*Liquid.mf+Vapor.enthalpy*Vapor.mf)@Outle\
        t ) - 975465[J kg^-1])/(2.80259e+6 [J kg^-1] -975465[J kg^-1] )
      QualityInlet = \
        Vapor.massFlow()@Inlet/(Vapor.massFlow()@Inlet+Liquid.massFlow()@Inlet)
      QualityOutlet = \
        Vapor.massFlow()@Outlet/(Vapor.massFlow()@Outlet+Liquid.massFlow()@Out\
        let)
      SumLiqMassTotal = sum(Liquid.MassTotal)@Default Domain
      Tsat = \
        1[K]*(0.5*(650.17534844798+((2*((-724213.16703206*((Press/1[MPa])^0.25\
        )^2)+(-3232555.0322333*((Press/1[MPa])^0.25))+405113.40542057))/(-((11\
        67.0521452767*((Press/1[MPa])^0.25)^2)+(12020.824702470*((Press/1[MPa]\
        )^0.25))-4823.2657361591)-(((1167.0521452767*((Press/1[MPa])^0.25)^2)+\
        (12020.824702470*((Press/1[MPa])^0.25))-4823.2657361591)^2-(4*(((Press\
        /1[MPa])^0.25)^2+(-17.073846940092*((Press/1[MPa])^0.25))+14.915108613\
        530)*((-724213.16703206*((Press/1[MPa])^0.25)^2)+(-3232555.0322333*((P\
        ress/1[MPa])^0.25))+405113.40542057)))^0.5))-((650.17534844798+((2*((-\
        724213.16703206*((Press/1[MPa])^0.25)^2)+(-3232555.0322333*((Press/1[M\
        Pa])^0.25))+405113.40542057))/(-((1167.0521452767*((Press/1[MPa])^0.25\
        )^2)+(12020.824702470*((Press/1[MPa])^0.25))-4823.2657361591)-(((1167.\
        0521452767*((Press/1[MPa])^0.25)^2)+(12020.824702470*((Press/1[MPa])^0\
        .25))-4823.2657361591)^2-(4*(((Press/1[MPa])^0.25)^2+(-17.073846940092\
        *((Press/1[MPa])^0.25))+14.915108613530)*((-724213.16703206*((Press/1[\
        MPa])^0.25)^2)+(-3232555.0322333*((Press/1[MPa])^0.25))+405113.4054205\
        7)))^0.5)))^2-4*(-0.23855557567849+(650.17534844798*((2*((-724213.1670\
        3206*((Press/1[MPa])^0.25)^2)+(-3232555.0322333*((Press/1[MPa])^0.25))\
        +405113.40542057))/(-((1167.0521452767*((Press/1[MPa])^0.25)^2)+(12020\
        .824702470*((Press/1[MPa])^0.25))-4823.2657361591)-(((1167.0521452767*\
        ((Press/1[MPa])^0.25)^2)+(12020.824702470*((Press/1[MPa])^0.25))-4823.\
        2657361591)^2-(4*(((Press/1[MPa])^0.25)^2+(-17.073846940092*((Press/1[\
        MPa])^0.25))+14.915108613530)*((-724213.16703206*((Press/1[MPa])^0.25)\
        ^2)+(-3232555.0322333*((Press/1[MPa])^0.25))+405113.40542057)))^0.5)))\
        ))^0.5))
      VaporVFInlet = if(Accumulated Iteration Number <= 100, \
        .9999-((Accumulated Iteration Number-300)*0.000007), 0.9992)
      VaporVelInlet = massFlowAve(Vapor.Velocity)@Inlet
      VaporVelOutlet = massFlowAve(Vapor.Velocity)@Outlet
      WallHeatFlux = if(Accumulated Iteration Number <=250, \
        0[W/m^2]-(Accumulated Iteration Number*123.6)[W/m^2], -30900[W/m^2])
      WallTemp = if(Accumulated Iteration Number <=250, 500[K]-(Accumulated \
        Iteration Number*0.008)[K], 498[K])
    END
  END
```

```
ADDITIONAL VARIABLE: MassTotal
  Option = Definition
  Tensor Type = SCALAR
  Units = [kg]
  Variable Type = Specific
END
MATERIAL: LiquidConst
  Material Group = Constant Property Liquids,Wet Steam
  Option = Pure Substance
  Thermodynamic State = Liquid
  PROPERTIES:
    Option = General Material
    EQUATION OF STATE:
      Density = 831.318 [kg m^-3]
      Molar Mass = 18.02 [kg kmol^-1]
      Option = Value
    END
    SPECIFIC HEAT CAPACITY:
      Option = Value
      Specific Heat Capacity = 4659 [J kg^-1 K^-1]
      Specific Heat Type = Constant Pressure
    END
    REFERENCE STATE:
      Option = Specified Point
      Reference Pressure = 2.6389 [MPa]
      Reference Specific Enthalpy = 975465 [J kg^-1]
      Reference Specific Entropy = 2581.1 [J kg^-1 K^-1]
      Reference Temperature = 500 [K]
    END
    DYNAMIC VISCOSITY:
      Dynamic Viscosity = 0.0001179 [Pa s]
      Option = Value
    END
    THERMAL CONDUCTIVITY:
      Option = Value
      Thermal Conductivity = 0.6421 [W m^-1 K^-1]
    END
  END
END
MATERIAL: LiquidVar
  Material Group = IAPWS IF97,Wet Steam
  Option = Pure Substance
  Thermodynamic State = Liquid
  PROPERTIES:
    Option = IAPWS Library
    REFERENCE STATE:
      Option = Automatic
    END
    TABLE GENERATION:
      Maximum Absolute Pressure = 12.345 [MPa]
      Maximum Points = 100
      Maximum Temperature = 600 [K]
      Minimum Absolute Pressure = 0.0035368 [MPa]
      Minimum Temperature = 300 [K]
      Pressure Extrapolation = On
      Temperature Extrapolation = Yes
    END
  END
END
MATERIAL: VaporConst
  Material Group = Wet Steam,Constant Property Gases
  Option = Pure Substance
```

```
    Thermodynamic State = Gas
    PROPERTIES:
      Option = General Material
      EQUATION OF STATE:
        Density = 13.1976 [kg m^-3]
        Molar Mass = 18.02 [kg kmol^-1]
        Option = Value
      END
      SPECIFIC HEAT CAPACITY:
        Option = Value
        Specific Heat Capacity = 3462.6 [J kg^-1 K^-1]
        Specific Heat Type = Constant Pressure
      END
      REFERENCE STATE:
        Option = Specified Point
        Reference Pressure = 2.6389 [MPa]
        Reference Specific Enthalpy = 2802590 [J kg^-1]
        Reference Specific Entropy = 6235.4 [J kg^-1 K^-1]
        Reference Temperature = 500 [K]
      END
      DYNAMIC VISCOSITY:
        Dynamic Viscosity = 1.6594e-5 [Pa s]
        Option = Value
      END
      THERMAL CONDUCTIVITY:
        Option = Value
        Thermal Conductivity = 0.044952 [W m^-1 K^-1]
      END
      THERMAL EXPANSIVITY:
        Option = Value
        Thermal Expansivity = 0.001686 [K^-1]
      END
    END
  END
  MATERIAL: VaporVar
    Material Group = IAPWS IF97,Wet Steam
    Option = Pure Substance
    Thermodynamic State = Gas
    PROPERTIES:
      Option = IAPWS Library
      REFERENCE STATE:
        Option = Automatic
      END
      TABLE GENERATION:
        Maximum Absolute Pressure = 12.345 [MPa]
        Maximum Points = 1000
        Maximum Temperature = 600 [K]
        Minimum Absolute Pressure = 0.0035368 [MPa]
        Minimum Temperature = 300 [K]
        Pressure Extrapolation = On
        Temperature Extrapolation = Yes
      END
    END
  END
END
FLOW: Flow Analysis 1
  SOLUTION UNITS:
    Angle Units = [rad]
    Length Units = [m]
    Mass Units = [kg]
    Solid Angle Units = [sr]
    Temperature Units = [K]
```

```
  Time Units = [s]
END
ANALYSIS TYPE:
  Option = Steady State
  EXTERNAL SOLVER COUPLING:
    Option = None
  END
END
DOMAIN: Default Domain
  Coord Frame = Coord 0
  Domain Type = Fluid
  Location = B4
  BOUNDARY MODELS:
    WALL BOILING MODEL:
      Option = None
    END
  END
  BOUNDARY: Inlet
    Boundary Type = INLET
    Location = Inlet
    BOUNDARY CONDITIONS:
      FLOW REGIME:
        Option = Subsonic
      END
      HEAT TRANSFER:
        Option = Static Temperature
        Static Temperature = 500 [K]
      END
      MASS AND MOMENTUM:
        Normal Speed = 40 [m s^-1]
        Option = Normal Speed
      END
      TURBULENCE:
        Option = Medium Intensity and Eddy Viscosity Ratio
      END
    END
    FLUID: Liquid
      BOUNDARY CONDITIONS:
        VOLUME FRACTION:
          Option = Value
          Volume Fraction = 0.0001
        END
      END
    END
    FLUID: Vapor
      BOUNDARY CONDITIONS:
        VOLUME FRACTION:
          Option = Value
          Volume Fraction = 0.9999
        END
      END
    END
  END
  BOUNDARY: Outlet
    Boundary Type = OUTLET
    Location = Outlet
    BOUNDARY CONDITIONS:
      FLOW REGIME:
        Option = Subsonic
      END
      MASS AND MOMENTUM:
        Option = Average Static Pressure
```

```
      Pressure Profile Blend = 0.05
      Relative Pressure = 2.6389 [MPa]
    END
    PRESSURE AVERAGING:
      Option = Average Over Whole Outlet
    END
  END
END
BOUNDARY: Wall
  Boundary Type = WALL
  Location = Wall
  BOUNDARY CONDITIONS:
    HEAT TRANSFER:
      Option = Adiabatic
    END
    MASS AND MOMENTUM:
      Option = No Slip Wall
    END
    WALL CONTACT MODEL:
      Option = Use Volume Fraction
    END
    WALL ROUGHNESS:
      Option = Smooth Wall
    END
  END
END
DOMAIN MODELS:
  BUOYANCY MODEL:
    Buoyancy Reference Density = 0 [kg m^-3]
    Gravity X Component = 0 [m s^-2]
    Gravity Y Component = -9.81 [m s^-2]
    Gravity Z Component = 0 [m s^-2]
    Option = Buoyant
    BUOYANCY REFERENCE LOCATION:
      Option = Automatic
    END
  END
  DOMAIN MOTION:
    Option = Stationary
  END
  MESH DEFORMATION:
    Option = None
  END
  REFERENCE PRESSURE:
    Reference Pressure = 0 [MPa]
  END
END
FLUID DEFINITION: Liquid
  Material = LiquidConst
  Option = Material Library
  MORPHOLOGY:
    Mean Diameter = 1 [micron]
    Minimum Volume Fraction = 1e-9
    Option = Dispersed Fluid
  END
END
FLUID DEFINITION: Vapor
  Material = VaporConst
  Option = Material Library
  MORPHOLOGY:
    Minimum Volume Fraction = 1e-9
    Option = Continuous Fluid
```

```
  END
END
FLUID MODELS:
  ADDITIONAL VARIABLE: MassTotal
    Option = Fluid Dependent
  END
  COMBUSTION MODEL:
    Option = None
  END
  FLUID: Liquid
    ADDITIONAL VARIABLE: MassTotal
      Additional Variable Value = Volume of Finite Volumes *Density \
        *Volume Fraction
      Option = Algebraic Equation
    END
    FLUID BUOYANCY MODEL:
      Option = Density Difference
    END
    HEAT TRANSFER MODEL:
      Option = Thermal Energy
    END
    TURBULENCE MODEL:
      Option = Laminar
    END
  END
  FLUID: Vapor
    ADDITIONAL VARIABLE: MassTotal
      Additional Variable Value = Volume of Finite Volumes *Density \
        *Volume Fraction
      Option = Algebraic Equation
    END
    FLUID BUOYANCY MODEL:
      Option = Density Difference
    END
    HEAT TRANSFER MODEL:
      Option = Thermal Energy
    END
    TURBULENCE MODEL:
      Option = k epsilon
      BUOYANCY TURBULENCE:
        Option = None
      END
    END
    TURBULENT WALL FUNCTIONS:
      Option = Scalable
    END
  END
  HEAT TRANSFER MODEL:
    Homogeneous Model = False
    Option = Fluid Dependent
  END
  THERMAL RADIATION MODEL:
    Option = None
  END
  TURBULENCE MODEL:
    Homogeneous Model = False
    Option = Fluid Dependent
  END
END
FLUID PAIR: Liquid | Vapor
  Surface Tension Coefficient = 0.013472 [N m^-1]
  INTERPHASE HEAT TRANSFER:
```

```
      Option = Two Resistance
      FLUID1 INTERPHASE HEAT TRANSFER:
        Option = Zero Resistance
      END
      FLUID2 INTERPHASE HEAT TRANSFER:
        Option = Ranz Marshall
      END
    END
    INTERPHASE TRANSFER MODEL:
      Option = Particle Model
    END
    MASS TRANSFER:
      Option = Phase Change
      PHASE CHANGE MODEL:
        Option = Thermal Phase Change
        Saturation Temperature = 500 [K]
      END
    END
    MOMENTUM TRANSFER:
      DRAG FORCE:
        Option = Ishii Zuber
      END
      LIFT FORCE:
        Option = Legendre Magnaudet
      END
      TURBULENT DISPERSION FORCE:
        Option = None
      END
      VIRTUAL MASS FORCE:
        Option = None
      END
      WALL LUBRICATION FORCE:
        Option = None
      END
    END
    TURBULENCE TRANSFER:
      ENHANCED TURBULENCE PRODUCTION MODEL:
        Option = None
      END
    END
  END
  MULTIPHASE MODELS:
    Homogeneous Model = False
    FREE SURFACE MODEL:
      Option = None
    END
  END
END
OUTPUT CONTROL:
  BACKUP DATA RETENTION:
    Option = Keep All Files
  END
  BACKUP RESULTS: Backup Results 1
    File Compression Level = Default
    Option = Standard
    Output Equation Residuals = All
    OUTPUT FREQUENCY:
      Iteration Interval = 100
      Option = Iteration Interval
    END
  END
  MONITOR OBJECTS:
```

```
MONITOR BALANCES:
  Option = Full
END
MONITOR FORCES:
  Option = Full
END
MONITOR PARTICLES:
  Option = Full
END
MONITOR POINT: Inlet Pressure
  Coord Frame = Coord 0
  Expression Value = areaAve(Pressure)@Inlet
  Option = Expression
END
MONITOR POINT: Inlet Quality
  Coord Frame = Coord 0
  Expression Value = QualityInlet
  Option = Expression
END
MONITOR POINT: Liquid Inlet Velocity
  Coord Frame = Coord 0
  Expression Value = LiquidVelInlet
  Option = Expression
END
MONITOR POINT: Liquid Mass
  Coord Frame = Coord 0
  Expression Value = SumLiqMassTotal
  Option = Expression
END
MONITOR POINT: Liquid Outlet Velocity
  Coord Frame = Coord 0
  Expression Value = LiquidVelOutlet
  Option = Expression
END
MONITOR POINT: Mass Flow Rate In
  Coord Frame = Coord 0
  Expression Value = MassFlowInlet
  Option = Expression
END
MONITOR POINT: Mass Flow Rate Out
  Coord Frame = Coord 0
  Expression Value = MassFlowOutlet
  Option = Expression
END
MONITOR POINT: Outlet Pressure
  Coord Frame = Coord 0
  Expression Value = areaAve(Pressure)@Outlet
  Option = Expression
END
MONITOR POINT: Outlet Quality
  Coord Frame = Coord 0
  Expression Value = QualityOutlet
  Option = Expression
END
MONITOR POINT: Outlet Temperature
  Coord Frame = Coord 0
  Expression Value = massFlowAve(Temperature)@Outlet
  Option = Expression
END
MONITOR POINT: Saturation Temp
  Coord Frame = Coord 0
  Expression Value = massFlowAve(Liquid | Vapor.Saturation \
```

```
          Temperature)@Outlet
        Option = Expression
      END
      MONITOR POINT: Vapor Inlet Velocity
        Coord Frame = Coord 0
        Expression Value = VaporVelInlet
        Option = Expression
      END
      MONITOR POINT: Vapor Outlet Velocity
        Coord Frame = Coord 0
        Expression Value = VaporVelOutlet
        Option = Expression
      END
      MONITOR RESIDUALS:
        Option = Full
      END
      MONITOR TOTALS:
        Option = Full
      END
    END
    RESULTS:
      File Compression Level = Default
      Option = Standard
      Output Equation Residuals = All
    END
  END
  SOLVER CONTROL:
    Turbulence Numerics = First Order
    ADVECTION SCHEME:
      Option = High Resolution
    END
    CONVERGENCE CONTROL:
      Length Scale Option = Conservative
      Maximum Number of Iterations = 5000
      Minimum Number of Iterations = 1
      Timescale Control = Auto Timescale
      Timescale Factor = 1.0
    END
    CONVERGENCE CRITERIA:
      Residual Target = 1e-15
      Residual Type = RMS
    END
    DYNAMIC MODEL CONTROL:
      Global Dynamic Model Control = On
    END
    INTERRUPT CONTROL:
      Option = Any Interrupt
      CONVERGENCE CONDITIONS:
        Option = Default Conditions
      END
    END
  END
END
COMMAND FILE:
  Version = 20.2
```

THIS PAGE INTENTIONALLY LEFT BLANK

APPENDIX G. CCL FILE FOR STEAM PIPE MODEL WITH BRANCHES AND BRANCH OUTLET WALL BOUNDARY

```
LIBRARY:
  CEL:
    EXPRESSIONS:
      Drain1Quality = Vapor.massFlow()@Drain 1 Outlet/(Vapor.massFlow()@Drain \
        1 Outlet+Liquid.massFlow()@Drain 1 Outlet)
      Drain2Quality = Vapor.massFlow()@Drain 2 Outlet/(Vapor.massFlow()@Drain \
        2 Outlet+Liquid.massFlow()@Drain 2 Outlet)
      LiquidVFInlet = 1-VaporVFInlet
      LiquidVelInlet = massFlowAve(Liquid.Velocity)@Inlet
      LiquidVelOutlet = massFlowAve(Liquid.Velocity)@Outlet
      Press = 2.6389[MPa]
      QualityEquilInlet = \
        ((massFlowAve(Liquid.enthalpy*Liquid.mf+Vapor.enthalpy*Vapor.mf)@Inle\
        t ) - 975465[J kg^-1])/(2.80259e+6 [J kg^-1] -975465[J kg^-1] )
      QualityEquilOutlet = \
        ((massFlowAve(Liquid.enthalpy*Liquid.mf+Vapor.enthalpy*Vapor.mf)@Outle\
        t ) - 975465[J kg^-1])/(2.80259e+6 [J kg^-1] -975465[J kg^-1] )
      QualityInlet = \
        Vapor.massFlow()@Inlet/(Vapor.massFlow()@Inlet+Liquid.massFlow()@Inlet)
      QualityOutlet = \
        Vapor.massFlow()@Outlet/(Vapor.massFlow()@Outlet+Liquid.massFlow()@Out\
        let)
      SumLiqMassTotal = sum(Liquid.MassTotal)@Default Domain
      Tsat = \
        1[K]*(0.5*(650.17534844798+((2*((-724213.16703206*((Press/1[MPa])^0.25\
        )^2)+(-3232555.0322333*((Press/1[MPa])^0.25))+405113.40542057))/(-((11\
        67.0521452767*((Press/1[MPa])^0.25)^2)+(12020.824702470*((Press/1[MPa]\
        )^0.25))-4823.2657361591)-(((1167.0521452767*((Press/1[MPa])^0.25)^2)+\
        (12020.824702470*((Press/1[MPa])^0.25))-4823.2657361591)^2-(4*(((Press\
        /1[MPa])^0.25)^2+(-17.073846940092*((Press/1[MPa])^0.25))+14.915108613\
        530)*((-724213.16703206*((Press/1[MPa])^0.25)^2)+(-3232555.0322333*((P\
        ress/1[MPa])^0.25))+405113.40542057)))^0.5))-((650.17534844798+((2*((-\
        724213.16703206*((Press/1[MPa])^0.25)^2)+(-3232555.0322333*((Press/1[M\
        Pa])^0.25))+405113.40542057))/(-((1167.0521452767*((Press/1[MPa])^0.25\
        )^2)+(12020.824702470*((Press/1[MPa])^0.25))-4823.2657361591)-(((1167.\
        0521452767*((Press/1[MPa])^0.25)^2)+(12020.824702470*((Press/1[MPa])^0\
        .25))-4823.2657361591)^2-(4*(((Press/1[MPa])^0.25)^2+(-17.073846940092\
        *((Press/1[MPa])^0.25))+14.915108613530)*((-724213.16703206*((Press/1[\
        MPa])^0.25)^2)+(-3232555.0322333*((Press/1[MPa])^0.25))+405113.4054205\
        7)))^0.5)))^2-4*(-0.23855557567849+(650.17534844798*((2*((-724213.1670\
        3206*((Press/1[MPa])^0.25)^2)+(-3232555.0322333*((Press/1[MPa])^0.25))\
        +405113.40542057))/(-((1167.0521452767*((Press/1[MPa])^0.25)^2)+(12020\
        .824702470*((Press/1[MPa])^0.25))-4823.2657361591)-(((1167.0521452767*\
        ((Press/1[MPa])^0.25)^2)+(12020.824702470*((Press/1[MPa])^0.25))-4823.\
        2657361591)^2-(4*(((Press/1[MPa])^0.25)^2+(-17.073846940092*((Press/1[\
        MPa])^0.25))+14.915108613530)*((-724213.16703206*((Press/1[MPa])^0.25)\
        ^2)+(-3232555.0322333*((Press/1[MPa])^0.25))+405113.40542057)))^0.5)))\
        ))^0.5))
      VaporVFInlet = if(Accumulated Iteration Number <= 100, \
        .9999-((Accumulated Iteration Number-300)*0.000007), 0.9992)
      VaporVelInlet = massFlowAve(Vapor.Velocity)@Inlet
      VaporVelOutlet = massFlowAve(Vapor.Velocity)@Outlet
    END
  END
  ADDITIONAL VARIABLE: MassTotal
    Option = Definition
```

```
  Tensor Type = SCALAR
  Units = [kg]
  Variable Type = Specific
END
MATERIAL: LiquidConst
  Material Group = Constant Property Liquids,Wet Steam
  Option = Pure Substance
  Thermodynamic State = Liquid
  PROPERTIES:
    Option = General Material
    EQUATION OF STATE:
      Density = 831.318 [kg m^-3]
      Molar Mass = 18.02 [kg kmol^-1]
      Option = Value
    END
    SPECIFIC HEAT CAPACITY:
      Option = Value
      Specific Heat Capacity = 4659 [J kg^-1 K^-1]
      Specific Heat Type = Constant Pressure
    END
    REFERENCE STATE:
      Option = Specified Point
      Reference Pressure = 2.6389 [MPa]
      Reference Specific Enthalpy = 975465 [J kg^-1]
      Reference Specific Entropy = 2581.1 [J kg^-1 K^-1]
      Reference Temperature = 500 [K]
    END
    DYNAMIC VISCOSITY:
      Dynamic Viscosity = 0.0001179 [Pa s]
      Option = Value
    END
    THERMAL CONDUCTIVITY:
      Option = Value
      Thermal Conductivity = 0.6421 [W m^-1 K^-1]
    END
  END
END
MATERIAL: LiquidVar
  Material Group = IAPWS IF97,Wet Steam
  Option = Pure Substance
  Thermodynamic State = Liquid
  PROPERTIES:
    Option = IAPWS Library
    REFERENCE STATE:
      Option = Automatic
    END
    TABLE GENERATION:
      Maximum Absolute Pressure = 12.345 [MPa]
      Maximum Points = 100
      Maximum Temperature = 600 [K]
      Minimum Absolute Pressure = 0.0035368 [MPa]
      Minimum Temperature = 300 [K]
      Pressure Extrapolation = On
      Temperature Extrapolation = Yes
    END
  END
END
MATERIAL: VaporConst
  Material Group = Wet Steam,Constant Property Gases
  Option = Pure Substance
  Thermodynamic State = Gas
  PROPERTIES:
```

```
      Option = General Material
      EQUATION OF STATE:
        Density = 13.1976 [kg m^-3]
        Molar Mass = 18.02 [kg kmol^-1]
        Option = Value
      END
      SPECIFIC HEAT CAPACITY:
        Option = Value
        Specific Heat Capacity = 3462.6 [J kg^-1 K^-1]
        Specific Heat Type = Constant Pressure
      END
      REFERENCE STATE:
        Option = Specified Point
        Reference Pressure = 2.6389 [MPa]
        Reference Specific Enthalpy = 2802590 [J kg^-1]
        Reference Specific Entropy = 6235.4 [J kg^-1 K^-1]
        Reference Temperature = 500 [K]
      END
      DYNAMIC VISCOSITY:
        Dynamic Viscosity = 1.6594e-5 [Pa s]
        Option = Value
      END
      THERMAL CONDUCTIVITY:
        Option = Value
        Thermal Conductivity = 0.044952 [W m^-1 K^-1]
      END
      THERMAL EXPANSIVITY:
        Option = Value
        Thermal Expansivity = 0.001686 [K^-1]
      END
    END
  END
  MATERIAL: VaporVar
    Material Group = IAPWS IF97,Wet Steam
    Option = Pure Substance
    Thermodynamic State = Gas
    PROPERTIES:
      Option = IAPWS Library
      REFERENCE STATE:
        Option = Automatic
      END
      TABLE GENERATION:
        Maximum Absolute Pressure = 12.345 [MPa]
        Maximum Points = 1000
        Maximum Temperature = 600 [K]
        Minimum Absolute Pressure = 0.0035368 [MPa]
        Minimum Temperature = 300 [K]
        Pressure Extrapolation = On
        Temperature Extrapolation = Yes
      END
    END
  END
END
FLOW: Flow Analysis 1
  SOLUTION UNITS:
    Angle Units = [rad]
    Length Units = [m]
    Mass Units = [kg]
    Solid Angle Units = [sr]
    Temperature Units = [K]
    Time Units = [s]
  END
```

```
ANALYSIS TYPE:
  Option = Steady State
  EXTERNAL SOLVER COUPLING:
    Option = None
  END
END
DOMAIN: Default Domain
  Coord Frame = Coord 0
  Domain Type = Fluid
  Location = B4
  BOUNDARY MODELS:
    WALL BOILING MODEL:
      Option = None
    END
  END
  BOUNDARY: Drain 1 Outlet
    Boundary Type = WALL
    Location = Drain 1 Outlet
    BOUNDARY CONDITIONS:
      HEAT TRANSFER:
        Option = Adiabatic
      END
      MASS AND MOMENTUM:
        Option = No Slip Wall
      END
      WALL CONTACT MODEL:
        Option = Use Volume Fraction
      END
      WALL ROUGHNESS:
        Option = Smooth Wall
      END
    END
  END
  BOUNDARY: Drain 1 Wall
    Boundary Type = WALL
    Location = Drain 1 Wall
    BOUNDARY CONDITIONS:
      HEAT TRANSFER:
        Option = Adiabatic
      END
      MASS AND MOMENTUM:
        Option = No Slip Wall
      END
      WALL CONTACT MODEL:
        Option = Use Volume Fraction
      END
      WALL ROUGHNESS:
        Option = Smooth Wall
      END
    END
  END
  BOUNDARY: Drain 2 Outlet
    Boundary Type = WALL
    Location = Drain 2 Outlet
    BOUNDARY CONDITIONS:
      HEAT TRANSFER:
        Option = Adiabatic
      END
      MASS AND MOMENTUM:
        Option = No Slip Wall
      END
      WALL CONTACT MODEL:
```

```
      Option = Use Volume Fraction
    END
    WALL ROUGHNESS:
      Option = Smooth Wall
    END
  END
END
BOUNDARY: Drain 2 Wall
  Boundary Type = WALL
  Location = Drain 2 Wall
  BOUNDARY CONDITIONS:
    HEAT TRANSFER:
      Option = Adiabatic
    END
    MASS AND MOMENTUM:
      Option = No Slip Wall
    END
    WALL CONTACT MODEL:
      Option = Use Volume Fraction
    END
    WALL ROUGHNESS:
      Option = Smooth Wall
    END
  END
END
BOUNDARY: Inlet
  Boundary Type = INLET
  Location = Inlet
  BOUNDARY CONDITIONS:
    FLOW REGIME:
      Option = Subsonic
    END
    HEAT TRANSFER:
      Option = Static Temperature
      Static Temperature = 500 [K]
    END
    MASS AND MOMENTUM:
      Normal Speed = 40 [m s^-1]
      Option = Normal Speed
    END
    TURBULENCE:
      Option = Medium Intensity and Eddy Viscosity Ratio
    END
  END
  FLUID: Liquid
    BOUNDARY CONDITIONS:
      VOLUME FRACTION:
        Option = Value
        Volume Fraction = 0.0001
      END
    END
  END
  FLUID: Vapor
    BOUNDARY CONDITIONS:
      VOLUME FRACTION:
        Option = Value
        Volume Fraction = 0.9999
      END
    END
  END
END
BOUNDARY: Outlet
```

```
  Boundary Type = OUTLET
  Location = Outlet
  BOUNDARY CONDITIONS:
    FLOW REGIME:
      Option = Subsonic
    END
    MASS AND MOMENTUM:
      Option = Average Static Pressure
      Pressure Profile Blend = 0.05
      Relative Pressure = 2.6389 [MPa]
    END
    PRESSURE AVERAGING:
      Option = Average Over Whole Outlet
    END
  END
END
BOUNDARY: Wall
  Boundary Type = WALL
  Location = Wall
  BOUNDARY CONDITIONS:
    HEAT TRANSFER:
      Option = Adiabatic
    END
    MASS AND MOMENTUM:
      Option = No Slip Wall
    END
    WALL CONTACT MODEL:
      Option = Use Volume Fraction
    END
    WALL ROUGHNESS:
      Option = Smooth Wall
    END
  END
END
DOMAIN MODELS:
  BUOYANCY MODEL:
    Buoyancy Reference Density = 0 [kg m^-3]
    Gravity X Component = 0 [m s^-2]
    Gravity Y Component = -9.81 [m s^-2]
    Gravity Z Component = 0 [m s^-2]
    Option = Buoyant
    BUOYANCY REFERENCE LOCATION:
      Option = Automatic
    END
  END
  DOMAIN MOTION:
    Option = Stationary
  END
  MESH DEFORMATION:
    Option = None
  END
  REFERENCE PRESSURE:
    Reference Pressure = 0 [MPa]
  END
END
FLUID DEFINITION: Liquid
  Material = LiquidConst
  Option = Material Library
  MORPHOLOGY:
    Mean Diameter = 1 [micron]
    Minimum Volume Fraction = 1e-9
    Option = Dispersed Fluid
```

```
  END
END
FLUID DEFINITION: Vapor
  Material = VaporConst
  Option = Material Library
  MORPHOLOGY:
    Minimum Volume Fraction = 1e-9
    Option = Continuous Fluid
  END
END
FLUID MODELS:
  ADDITIONAL VARIABLE: MassTotal
    Option = Fluid Dependent
  END
  COMBUSTION MODEL:
    Option = None
  END
  FLUID: Liquid
    ADDITIONAL VARIABLE: MassTotal
      Additional Variable Value = Volume of Finite Volumes *Density \
        *Volume Fraction
      Option = Algebraic Equation
    END
    FLUID BUOYANCY MODEL:
      Option = Density Difference
    END
    HEAT TRANSFER MODEL:
      Option = Thermal Energy
    END
    TURBULENCE MODEL:
      Option = Laminar
    END
  END
  FLUID: Vapor
    ADDITIONAL VARIABLE: MassTotal
      Additional Variable Value = Volume of Finite Volumes *Density \
        *Volume Fraction
      Option = Algebraic Equation
    END
    FLUID BUOYANCY MODEL:
      Option = Density Difference
    END
    HEAT TRANSFER MODEL:
      Option = Thermal Energy
    END
    TURBULENCE MODEL:
      Option = k epsilon
      BUOYANCY TURBULENCE:
        Option = None
      END
    END
    TURBULENT WALL FUNCTIONS:
      Option = Scalable
    END
  END
  HEAT TRANSFER MODEL:
    Homogeneous Model = False
    Option = Fluid Dependent
  END
  THERMAL RADIATION MODEL:
    Option = None
  END
```

```
    TURBULENCE MODEL:
      Homogeneous Model = False
      Option = Fluid Dependent
    END
  END
  FLUID PAIR: Liquid | Vapor
    Surface Tension Coefficient = 0.013472 [N m^-1]
    INTERPHASE HEAT TRANSFER:
      Option = Two Resistance
      FLUID1 INTERPHASE HEAT TRANSFER:
        Option = Zero Resistance
      END
      FLUID2 INTERPHASE HEAT TRANSFER:
        Option = Ranz Marshall
      END
    END
    INTERPHASE TRANSFER MODEL:
      Option = Particle Model
    END
    MASS TRANSFER:
      Option = Phase Change
      PHASE CHANGE MODEL:
        Option = Thermal Phase Change
        Saturation Temperature = 500 [K]
      END
    END
    MOMENTUM TRANSFER:
      DRAG FORCE:
        Option = Schiller Naumann
      END
      LIFT FORCE:
        Option = Legendre Magnaudet
      END
      TURBULENT DISPERSION FORCE:
        Option = None
      END
      VIRTUAL MASS FORCE:
        Option = None
      END
      WALL LUBRICATION FORCE:
        Option = None
      END
    END
    TURBULENCE TRANSFER:
      ENHANCED TURBULENCE PRODUCTION MODEL:
        Option = None
      END
    END
  END
  MULTIPHASE MODELS:
    Homogeneous Model = False
    FREE SURFACE MODEL:
      Option = None
    END
  END
END
OUTPUT CONTROL:
  BACKUP DATA RETENTION:
    Option = Keep All Files
  END
  BACKUP RESULTS: Backup Results 1
    File Compression Level = Default
```

```
  Option = Standard
  Output Equation Residuals = All
  OUTPUT FREQUENCY:
    Iteration Interval = 500
    Option = Iteration Interval
  END
END
MONITOR OBJECTS:
  MONITOR BALANCES:
    Option = Full
  END
  MONITOR FORCES:
    Option = Full
  END
  MONITOR PARTICLES:
    Option = Full
  END
  MONITOR POINT: Inlet Pressure
    Coord Frame = Coord 0
    Expression Value = areaAve(Pressure)@Inlet
    Option = Expression
  END
  MONITOR POINT: Inlet Quality
    Coord Frame = Coord 0
    Expression Value = QualityInlet
    Option = Expression
  END
  MONITOR POINT: Liquid Inlet Velocity
    Coord Frame = Coord 0
    Expression Value = LiquidVelInlet
    Option = Expression
  END
  MONITOR POINT: Liquid Mass
    Coord Frame = Coord 0
    Expression Value = SumLiqMassTotal
    Option = Expression
  END
  MONITOR POINT: Liquid Mass Flow In
    Coord Frame = Coord 0
    Expression Value = Liquid.massFlow()@Inlet
    Option = Expression
  END
  MONITOR POINT: Liquid Mass Flow Outlet
    Coord Frame = Coord 0
    Expression Value = Liquid.massFlow()@Outlet
    Option = Expression
  END
  MONITOR POINT: Liquid Outlet Velocity
    Coord Frame = Coord 0
    Expression Value = LiquidVelOutlet
    Option = Expression
  END
  MONITOR POINT: Outlet Pressure
    Coord Frame = Coord 0
    Expression Value = areaAve(Pressure)@Outlet
    Option = Expression
  END
  MONITOR POINT: Outlet Quality
    Coord Frame = Coord 0
    Expression Value = QualityOutlet
    Option = Expression
  END
```

```
    MONITOR POINT: Outlet Temperature
      Coord Frame = Coord 0
      Expression Value = massFlowAve(Temperature)@Outlet
      Option = Expression
    END
    MONITOR POINT: Saturation Temp
      Coord Frame = Coord 0
      Expression Value = massFlowAve(Liquid | Vapor.Saturation \
        Temperature)@Outlet
      Option = Expression
    END
    MONITOR POINT: Vapor Inlet Velocity
      Coord Frame = Coord 0
      Expression Value = VaporVelInlet
      Option = Expression
    END
    MONITOR POINT: Vapor Mass Flow In
      Coord Frame = Coord 0
      Expression Value = Vapor.massFlow()@Inlet
      Option = Expression
    END
    MONITOR POINT: Vapor Mass Flow Outlet
      Coord Frame = Coord 0
      Expression Value = Vapor.massFlow()@Outlet
      Option = Expression
    END
    MONITOR POINT: Vapor Outlet Velocity
      Coord Frame = Coord 0
      Expression Value = VaporVelOutlet
      Option = Expression
    END
    MONITOR RESIDUALS:
      Option = Full
    END
    MONITOR TOTALS:
      Option = Full
    END
  END
  RESULTS:
    File Compression Level = Default
    Option = Standard
    Output Equation Residuals = All
  END
END
SOLVER CONTROL:
  Turbulence Numerics = First Order
  ADVECTION SCHEME:
    Option = High Resolution
  END
  CONVERGENCE CONTROL:
    Length Scale Option = Conservative
    Maximum Number of Iterations = 5000
    Minimum Number of Iterations = 1
    Timescale Control = Auto Timescale
    Timescale Factor = 1.0
  END
  CONVERGENCE CRITERIA:
    Residual Target = 1e-15
    Residual Type = RMS
  END
  DYNAMIC MODEL CONTROL:
    Global Dynamic Model Control = On
```

```
    END
    INTERRUPT CONTROL:
      Option = Any Interrupt
      CONVERGENCE CONDITIONS:
        Option = Default Conditions
      END
    END
  END
END
COMMAND FILE:
  Version = 20.2
```

THIS PAGE INTENTIONALLY LEFT BLANK

APPENDIX H. CCL FILE FOR STEAM PIPE MODEL WITH BRANCHES AND FLUID DEPENDENT BOUNDARY

```
LIBRARY:
  CEL:
    EXPRESSIONS:
      Drain1Quality = Vapor.massFlow()@Drain 1 Outlet/(Vapor.massFlow()@Drain \
        1 Outlet+Liquid.massFlow()@Drain 1 Outlet)
      Drain2Quality = Vapor.massFlow()@Drain 2 Outlet/(Vapor.massFlow()@Drain \
        2 Outlet+Liquid.massFlow()@Drain 2 Outlet)
      LiquidVFInlet = 1-VaporVFInlet
      LiquidVelInlet = massFlowAve(Liquid.Velocity)@Inlet
      LiquidVelOutlet = massFlowAve(Liquid.Velocity)@Outlet
      Press = 2.6389[MPa]
      QualityEquilInlet = \
        ((massFlowAve(Liquid.enthalpy*Liquid.mf+Vapor.enthalpy*Vapor.mf)@Inle\
        t ) - 975465[J kg^-1])/(2.80259e+6 [J kg^-1] -975465[J kg^-1] )
      QualityEquilOutlet = \
        ((massFlowAve(Liquid.enthalpy*Liquid.mf+Vapor.enthalpy*Vapor.mf)@Outle\
        t ) - 975465[J kg^-1])/(2.80259e+6 [J kg^-1] -975465[J kg^-1] )
      QualityInlet = \
        Vapor.massFlow()@Inlet/(Vapor.massFlow()@Inlet+Liquid.massFlow()@Inlet)
      QualityOutlet = \
        Vapor.massFlow()@Outlet/(Vapor.massFlow()@Outlet+Liquid.massFlow()@Out\
        let)
      SumLiqMassTotal = sum(Liquid.MassTotal)@Default Domain
      Tsat = \
        1[K]*(0.5*(650.17534844798+((2*((-724213.16703206*((Press/1[MPa])^0.25\
        )^2)+(-3232555.0322333*((Press/1[MPa])^0.25))+405113.40542057))/(-((11\
        67.0521452767*((Press/1[MPa])^0.25)^2)+(12020.824702470*((Press/1[MPa]\
        )^0.25))-4823.2657361591)-(((1167.0521452767*((Press/1[MPa])^0.25)^2)+\
        (12020.824702470*((Press/1[MPa])^0.25))-4823.2657361591)^2-(4*(((Press\
        /1[MPa])^0.25)^2+(-17.073846940092*((Press/1[MPa])^0.25))+14.915108613\
        530)*((-724213.16703206*((Press/1[MPa])^0.25)^2)+(-3232555.0322333*((P\
        ress/1[MPa])^0.25))+405113.40542057)))^0.5))-((650.17534844798+((2*((-\
        724213.16703206*((Press/1[MPa])^0.25)^2)+(-3232555.0322333*((Press/1[M\
        Pa])^0.25))+405113.40542057))/(-((1167.0521452767*((Press/1[MPa])^0.25\
        )^2)+(12020.824702470*((Press/1[MPa])^0.25))-4823.2657361591)-(((1167.\
        0521452767*((Press/1[MPa])^0.25)^2)+(12020.824702470*((Press/1[MPa])^0\
        .25))-4823.2657361591)^2-(4*(((Press/1[MPa])^0.25)^2+(-17.073846940092\
        *((Press/1[MPa])^0.25))+14.915108613530)*((-724213.16703206*((Press/1[\
        MPa])^0.25)^2)+(-3232555.0322333*((Press/1[MPa])^0.25))+405113.4054205\
        7)))^0.5)))^2-4*(-0.23855557567849+(650.17534844798*((2*((-724213.1670\
        3206*((Press/1[MPa])^0.25)^2)+(-3232555.0322333*((Press/1[MPa])^0.25))\
        +405113.40542057))/(-((1167.0521452767*((Press/1[MPa])^0.25)^2)+(12020\
        .824702470*((Press/1[MPa])^0.25))-4823.2657361591)-(((1167.0521452767*\
        ((Press/1[MPa])^0.25)^2)+(12020.824702470*((Press/1[MPa])^0.25))-4823.\
        2657361591)^2-(4*(((Press/1[MPa])^0.25)^2+(-17.073846940092*((Press/1[\
        MPa])^0.25))+14.915108613530)*((-724213.16703206*((Press/1[MPa])^0.25)\
        ^2)+(-3232555.0322333*((Press/1[MPa])^0.25))+405113.40542057)))^0.5)))\
        ))^0.5))
      VaporVFInlet = if(Accumulated Iteration Number <= 100, \
        .9999-((Accumulated Iteration Number-300)*0.000007), 0.9992)
      VaporVelInlet = massFlowAve(Vapor.Velocity)@Inlet
      VaporVelOutlet = massFlowAve(Vapor.Velocity)@Outlet
    END
  END
  ADDITIONAL VARIABLE: MassTotal
    Option = Definition
```

```
  Tensor Type = SCALAR
  Units = [kg]
  Variable Type = Specific
END
MATERIAL: LiquidConst
  Material Group = Constant Property Liquids,Wet Steam
  Option = Pure Substance
  Thermodynamic State = Liquid
  PROPERTIES:
    Option = General Material
    EQUATION OF STATE:
      Density = 831.318 [kg m^-3]
      Molar Mass = 18.02 [kg kmol^-1]
      Option = Value
    END
    SPECIFIC HEAT CAPACITY:
      Option = Value
      Specific Heat Capacity = 4659 [J kg^-1 K^-1]
      Specific Heat Type = Constant Pressure
    END
    REFERENCE STATE:
      Option = Specified Point
      Reference Pressure = 2.6389 [MPa]
      Reference Specific Enthalpy = 975465 [J kg^-1]
      Reference Specific Entropy = 2581.1 [J kg^-1 K^-1]
      Reference Temperature = 500 [K]
    END
    DYNAMIC VISCOSITY:
      Dynamic Viscosity = 0.0001179 [Pa s]
      Option = Value
    END
    THERMAL CONDUCTIVITY:
      Option = Value
      Thermal Conductivity = 0.6421 [W m^-1 K^-1]
    END
  END
END
MATERIAL: LiquidVar
  Material Group = IAPWS IF97,Wet Steam
  Option = Pure Substance
  Thermodynamic State = Liquid
  PROPERTIES:
    Option = IAPWS Library
    REFERENCE STATE:
      Option = Automatic
    END
    TABLE GENERATION:
      Maximum Absolute Pressure = 12.345 [MPa]
      Maximum Points = 100
      Maximum Temperature = 600 [K]
      Minimum Absolute Pressure = 0.0035368 [MPa]
      Minimum Temperature = 300 [K]
      Pressure Extrapolation = On
      Temperature Extrapolation = Yes
    END
  END
END
MATERIAL: VaporConst
  Material Group = Wet Steam,Constant Property Gases
  Option = Pure Substance
  Thermodynamic State = Gas
  PROPERTIES:
```

```
      Option = General Material
      EQUATION OF STATE:
        Density = 13.1976 [kg m^-3]
        Molar Mass = 18.02 [kg kmol^-1]
        Option = Value
      END
      SPECIFIC HEAT CAPACITY:
        Option = Value
        Specific Heat Capacity = 3462.6 [J kg^-1 K^-1]
        Specific Heat Type = Constant Pressure
      END
      REFERENCE STATE:
        Option = Specified Point
        Reference Pressure = 2.6389 [MPa]
        Reference Specific Enthalpy = 2802590 [J kg^-1]
        Reference Specific Entropy = 6235.4 [J kg^-1 K^-1]
        Reference Temperature = 500 [K]
      END
      DYNAMIC VISCOSITY:
        Dynamic Viscosity = 1.6594e-5 [Pa s]
        Option = Value
      END
      THERMAL CONDUCTIVITY:
        Option = Value
        Thermal Conductivity = 0.044952 [W m^-1 K^-1]
      END
      THERMAL EXPANSIVITY:
        Option = Value
        Thermal Expansivity = 0.001686 [K^-1]
      END
    END
  END
  MATERIAL: VaporVar
    Material Group = IAPWS IF97,Wet Steam
    Option = Pure Substance
    Thermodynamic State = Gas
    PROPERTIES:
      Option = IAPWS Library
      REFERENCE STATE:
        Option = Automatic
      END
      TABLE GENERATION:
        Maximum Absolute Pressure = 12.345 [MPa]
        Maximum Points = 1000
        Maximum Temperature = 600 [K]
        Minimum Absolute Pressure = 0.0035368 [MPa]
        Minimum Temperature = 300 [K]
        Pressure Extrapolation = On
        Temperature Extrapolation = Yes
      END
    END
  END
END
FLOW: Flow Analysis 1
  SOLUTION UNITS:
    Angle Units = [rad]
    Length Units = [m]
    Mass Units = [kg]
    Solid Angle Units = [sr]
    Temperature Units = [K]
    Time Units = [s]
  END
```

```
ANALYSIS TYPE:
  Option = Steady State
  EXTERNAL SOLVER COUPLING:
    Option = None
  END
END
DOMAIN: Default Domain
  Coord Frame = Coord 0
  Domain Type = Fluid
  Location = B4
  BOUNDARY MODELS:
    WALL BOILING MODEL:
      Option = None
    END
  END
  BOUNDARY: Drain 1 Outlet
    Boundary Type = OUTLET
    Location = Drain 1 Outlet
    BOUNDARY CONDITIONS:
      FLOW REGIME:
        Option = Subsonic
      END
      MASS AND MOMENTUM:
        Option = Fluid Velocity
      END
    END
    FLUID: Liquid
      BOUNDARY CONDITIONS:
        VELOCITY:
          Normal Speed = 2e-3 [m s^-1]
          Option = Normal Speed
        END
      END
    END
    FLUID: Vapor
      BOUNDARY CONDITIONS:
        VELOCITY:
          Mass Flow Rate = 0 [kg s^-1]
          Option = Mass Flow Rate
        END
      END
    END
  END
  BOUNDARY: Drain 1 Wall
    Boundary Type = WALL
    Location = Drain 1 Wall
    BOUNDARY CONDITIONS:
      HEAT TRANSFER:
        Option = Adiabatic
      END
      MASS AND MOMENTUM:
        Option = No Slip Wall
      END
      WALL CONTACT MODEL:
        Option = Use Volume Fraction
      END
      WALL ROUGHNESS:
        Option = Smooth Wall
      END
    END
  END
  BOUNDARY: Drain 2 Outlet
```

```
  Boundary Type = OUTLET
  Location = Drain 2 Outlet
  BOUNDARY CONDITIONS:
    FLOW REGIME:
      Option = Subsonic
    END
    MASS AND MOMENTUM:
      Option = Fluid Velocity
    END
  END
  FLUID: Liquid
    BOUNDARY CONDITIONS:
      VELOCITY:
        Normal Speed = 0.002 [m s^-1]
        Option = Normal Speed
      END
    END
  END
  FLUID: Vapor
    BOUNDARY CONDITIONS:
      VELOCITY:
        Mass Flow Rate = 0 [kg s^-1]
        Option = Mass Flow Rate
      END
    END
  END
END
BOUNDARY: Drain 2 Wall
  Boundary Type = WALL
  Location = Drain 2 Wall
  BOUNDARY CONDITIONS:
    HEAT TRANSFER:
      Option = Adiabatic
    END
    MASS AND MOMENTUM:
      Option = No Slip Wall
    END
    WALL CONTACT MODEL:
      Option = Use Volume Fraction
    END
    WALL ROUGHNESS:
      Option = Smooth Wall
    END
  END
END
BOUNDARY: Inlet
  Boundary Type = INLET
  Location = Inlet
  BOUNDARY CONDITIONS:
    FLOW REGIME:
      Option = Subsonic
    END
    HEAT TRANSFER:
      Option = Static Temperature
      Static Temperature = 500 [K]
    END
    MASS AND MOMENTUM:
      Normal Speed = 40 [m s^-1]
      Option = Normal Speed
    END
    TURBULENCE:
      Option = Medium Intensity and Eddy Viscosity Ratio
```

```
    END
  END
  FLUID: Liquid
    BOUNDARY CONDITIONS:
      VOLUME FRACTION:
        Option = Value
        Volume Fraction = 0.0001
      END
    END
  END
  FLUID: Vapor
    BOUNDARY CONDITIONS:
      VOLUME FRACTION:
        Option = Value
        Volume Fraction = 0.9999
      END
    END
  END
END
BOUNDARY: Outlet
  Boundary Type = OUTLET
  Location = Outlet
  BOUNDARY CONDITIONS:
    FLOW REGIME:
      Option = Subsonic
    END
    MASS AND MOMENTUM:
      Option = Average Static Pressure
      Pressure Profile Blend = 0.05
      Relative Pressure = 2.6389 [MPa]
    END
    PRESSURE AVERAGING:
      Option = Average Over Whole Outlet
    END
  END
END
BOUNDARY: Wall
  Boundary Type = WALL
  Location = Wall
  BOUNDARY CONDITIONS:
    HEAT TRANSFER:
      Option = Adiabatic
    END
    MASS AND MOMENTUM:
      Option = No Slip Wall
    END
    WALL CONTACT MODEL:
      Option = Use Volume Fraction
    END
    WALL ROUGHNESS:
      Option = Smooth Wall
    END
  END
END
DOMAIN MODELS:
  BUOYANCY MODEL:
    Buoyancy Reference Density = 0 [kg m^-3]
    Gravity X Component = 0 [m s^-2]
    Gravity Y Component = -9.81 [m s^-2]
    Gravity Z Component = 0 [m s^-2]
    Option = Buoyant
    BUOYANCY REFERENCE LOCATION:
```

```
      Option = Automatic
    END
  END
  DOMAIN MOTION:
    Option = Stationary
  END
  MESH DEFORMATION:
    Option = None
  END
  REFERENCE PRESSURE:
    Reference Pressure = 0 [MPa]
  END
END
FLUID DEFINITION: Liquid
  Material = LiquidConst
  Option = Material Library
  MORPHOLOGY:
    Mean Diameter = 1 [micron]
    Minimum Volume Fraction = 1e-9
    Option = Dispersed Fluid
  END
END
FLUID DEFINITION: Vapor
  Material = VaporConst
  Option = Material Library
  MORPHOLOGY:
    Minimum Volume Fraction = 1e-9
    Option = Continuous Fluid
  END
END
FLUID MODELS:
  ADDITIONAL VARIABLE: MassTotal
    Option = Fluid Dependent
  END
  COMBUSTION MODEL:
    Option = None
  END
  FLUID: Liquid
    ADDITIONAL VARIABLE: MassTotal
      Additional Variable Value = Volume of Finite Volumes *Density \
        *Volume Fraction
      Option = Algebraic Equation
    END
    FLUID BUOYANCY MODEL:
      Option = Density Difference
    END
    HEAT TRANSFER MODEL:
      Option = Thermal Energy
    END
    TURBULENCE MODEL:
      Option = Laminar
    END
  END
  FLUID: Vapor
    ADDITIONAL VARIABLE: MassTotal
      Additional Variable Value = Volume of Finite Volumes *Density \
        *Volume Fraction
      Option = Algebraic Equation
    END
    FLUID BUOYANCY MODEL:
      Option = Density Difference
    END
```

```
    HEAT TRANSFER MODEL:
      Option = Thermal Energy
    END
    TURBULENCE MODEL:
      Option = k epsilon
      BUOYANCY TURBULENCE:
        Option = None
      END
    END
    TURBULENT WALL FUNCTIONS:
      Option = Scalable
    END
  END
  HEAT TRANSFER MODEL:
    Homogeneous Model = False
    Option = Fluid Dependent
  END
  THERMAL RADIATION MODEL:
    Option = None
  END
  TURBULENCE MODEL:
    Homogeneous Model = False
    Option = Fluid Dependent
  END
END
FLUID PAIR: Liquid | Vapor
  Surface Tension Coefficient = 0.013472 [N m^-1]
  INTERPHASE HEAT TRANSFER:
    Option = Two Resistance
    FLUID1 INTERPHASE HEAT TRANSFER:
      Option = Zero Resistance
    END
    FLUID2 INTERPHASE HEAT TRANSFER:
      Option = Ranz Marshall
    END
  END
  INTERPHASE TRANSFER MODEL:
    Option = Particle Model
  END
  MASS TRANSFER:
    Option = Phase Change
    PHASE CHANGE MODEL:
      Option = Thermal Phase Change
      Saturation Temperature = 500 [K]
    END
  END
  MOMENTUM TRANSFER:
    DRAG FORCE:
      Option = Schiller Naumann
    END
    LIFT FORCE:
      Option = Legendre Magnaudet
    END
    TURBULENT DISPERSION FORCE:
      Option = None
    END
    VIRTUAL MASS FORCE:
      Option = None
    END
    WALL LUBRICATION FORCE:
      Option = None
    END
```

```
    END
    TURBULENCE TRANSFER:
      ENHANCED TURBULENCE PRODUCTION MODEL:
        Option = None
      END
    END
  END
  MULTIPHASE MODELS:
    Homogeneous Model = False
    FREE SURFACE MODEL:
      Option = None
    END
  END
END
OUTPUT CONTROL:
  BACKUP DATA RETENTION:
    Option = Keep All Files
  END
  BACKUP RESULTS: Backup Results 1
    File Compression Level = Default
    Option = Standard
    Output Equation Residuals = All
    OUTPUT FREQUENCY:
      Iteration Interval = 500
      Option = Iteration Interval
    END
  END
  MONITOR OBJECTS:
    MONITOR BALANCES:
      Option = Full
    END
    MONITOR FORCES:
      Option = Full
    END
    MONITOR PARTICLES:
      Option = Full
    END
    MONITOR POINT: Drain 1 Quality
      Coord Frame = Coord 0
      Expression Value = Drain1Quality
      Option = Expression
    END
    MONITOR POINT: Drain 2 Quality
      Coord Frame = Coord 0
      Expression Value = Drain2Quality
      Option = Expression
    END
    MONITOR POINT: Inlet Pressure
      Coord Frame = Coord 0
      Expression Value = areaAve(Pressure)@Inlet
      Option = Expression
    END
    MONITOR POINT: Inlet Quality
      Coord Frame = Coord 0
      Expression Value = QualityInlet
      Option = Expression
    END
    MONITOR POINT: Liquid Inlet Velocity
      Coord Frame = Coord 0
      Expression Value = LiquidVelInlet
      Option = Expression
    END
```

```
MONITOR POINT: Liquid Mass
  Coord Frame = Coord 0
  Expression Value = SumLiqMassTotal
  Option = Expression
END
MONITOR POINT: Liquid Mass Flow Drain 1
  Coord Frame = Coord 0
  Expression Value = Liquid.massFlow()@Drain 1 Outlet
  Option = Expression
END
MONITOR POINT: Liquid Mass Flow Drain 2
  Coord Frame = Coord 0
  Expression Value = Liquid.massFlow()@Drain 2 Outlet
  Option = Expression
END
MONITOR POINT: Liquid Mass Flow In
  Coord Frame = Coord 0
  Expression Value = Liquid.massFlow()@Inlet
  Option = Expression
END
MONITOR POINT: Liquid Mass Flow Outlet
  Coord Frame = Coord 0
  Expression Value = Liquid.massFlow()@Outlet
  Option = Expression
END
MONITOR POINT: Liquid Outlet Velocity
  Coord Frame = Coord 0
  Expression Value = LiquidVelOutlet
  Option = Expression
END
MONITOR POINT: Outlet Pressure
  Coord Frame = Coord 0
  Expression Value = areaAve(Pressure)@Outlet
  Option = Expression
END
MONITOR POINT: Outlet Quality
  Coord Frame = Coord 0
  Expression Value = QualityOutlet
  Option = Expression
END
MONITOR POINT: Outlet Temperature
  Coord Frame = Coord 0
  Expression Value = massFlowAve(Temperature)@Outlet
  Option = Expression
END
MONITOR POINT: Saturation Temp
  Coord Frame = Coord 0
  Expression Value = massFlowAve(Liquid | Vapor.Saturation \
    Temperature)@Outlet
  Option = Expression
END
MONITOR POINT: Vapor Inlet Velocity
  Coord Frame = Coord 0
  Expression Value = VaporVelInlet
  Option = Expression
END
MONITOR POINT: Vapor Mass Flow Drain 1
  Coord Frame = Coord 0
  Expression Value = Vapor.massFlow()@Drain 1 Outlet
  Option = Expression
END
MONITOR POINT: Vapor Mass Flow Drain 2
```

```
        Coord Frame = Coord 0
        Expression Value = Vapor.massFlow()@Drain 2 Outlet
        Option = Expression
      END
      MONITOR POINT: Vapor Mass Flow In
        Coord Frame = Coord 0
        Expression Value = Vapor.massFlow()@Inlet
        Option = Expression
      END
      MONITOR POINT: Vapor Mass Flow Outlet
        Coord Frame = Coord 0
        Expression Value = Vapor.massFlow()@Outlet
        Option = Expression
      END
      MONITOR POINT: Vapor Outlet Velocity
        Coord Frame = Coord 0
        Expression Value = VaporVelOutlet
        Option = Expression
      END
      MONITOR RESIDUALS:
        Option = Full
      END
      MONITOR TOTALS:
        Option = Full
      END
    END
    RESULTS:
      File Compression Level = Default
      Option = Standard
      Output Equation Residuals = All
    END
  END
  SOLVER CONTROL:
    Turbulence Numerics = First Order
    ADVECTION SCHEME:
      Option = High Resolution
    END
    CONVERGENCE CONTROL:
      Length Scale Option = Conservative
      Maximum Number of Iterations = 5000
      Minimum Number of Iterations = 1
      Timescale Control = Auto Timescale
      Timescale Factor = 0.5
    END
    CONVERGENCE CRITERIA:
      Residual Target = 1e-15
      Residual Type = RMS
    END
    DYNAMIC MODEL CONTROL:
      Global Dynamic Model Control = On
    END
    INTERRUPT CONTROL:
      Option = Any Interrupt
      CONVERGENCE CONDITIONS:
        Option = Default Conditions
      END
    END
  END
END
COMMAND FILE:
  Version = 20.2
END
```

THIS PAGE INTENTIONALLY LEFT BLANK

LIST OF REFERENCES

[1] B. J. Azzopardi, "The effect of the side arm diameter on the two-phase flow split at a "T" junction," *International Journal of Multiphase Flow*, vol. 10, no. 4, pp. 509-512, 1984.

[2] B. J. Azzopardi and P. B. Whalley, "The effect of flow patterns on two-phase flow in a T junction," *International Journal of Multiphase Flow*, vol. 8, no. 5, pp. 491-507, 1982.

[3] W. Seeger, J. Reimann and U. Muller, "Two-phase flow in a T-junction with a horizontal inlet Part I: phase separation," *International Journal of Multiphase Flow*, vol. 12, no. 4, pp. 575-585, 1986.

[4] J. D. Ballyk, M. Shoukri and A. M. Chan, "Steam-water annular flow in a horizontal dividing T-junction," *International Journal of Multiphase Flow*, vol. 14, no. 3, pp. 265-285, 1988.

[5] G. Caruso, F. Gianetti and A. Naviglio, "Experimental investigation on pure steam and steam-air mixture condensation inside tubes," *International Journal of Heat and Technology*, vol. 30, no. 2, pp. 77-84, 2012.

[6] F. M. White, Fluid Mechanics, 7th ed., New York, NY: McGraw-Hill, 2011.

[7] M. T. Rubel, B. D. Timmerman, H. M. Soliman, G. E. Sims and M. A. Ebadian, "Phase distribution of high-pressure steam-water flow at large-diameter tee junctions," *Transactions of the ASME*, vol. 116, pp. 592-596, 1994.

[8] F. Peng, M. Shoukri and A. M. C. Chan, "Effect of branch orientation on annular two-phase flow in T-junctions," *Transactions of the ASME Journal of Fluids Engineering*, vol. 118, pp. 166-171, 1996.

[9] T. W. Alger, "Droplet phase characteristics in liquid-dominated steam-water nozzle flow," Lawrence Livermore Laboratory, University of California, Livermore, CA, 1978.

[10] V. M. Borishanskiy, D. I. Volkov, N. I. Ivashchenko, L. A. Vorontsova, Y. T. Illarionov, O. P. Kretunov, A. P. Borkov, G. A. Makarova and I. A. Alekseyev, "Heat transfer from steam condensing inside vertical pipes and coils," *Heat Transfer Soviet Research*, vol. 10, no. 4, pp. 44-58, 1978.

[11] Ansys, Inc., *Ansys CFX-Pre User's Guide 2021R2,* Canonsburg, PA: Ansys, Inc., 2021.

[12] Ansys, Inc., *Ansys CFX-Solver Modeling Guide 2021R2*, Canonsburg, PA: Ansys, Inc., 2021.

[13] Ansys, Inc., *Ansys CFX-Solver Theory Guide 2021R2,* Canonsburg, PA: Ansys, Inc., 2021.

[14] The International Association for the Properties of Water and Steam, *Revised release on the IAPWS Industrial Formulation 1997 for the thermodynamic properties of water and steam, revision 7,* Lucerne, 2012.

[15] National Institute of Standards and Technology, "Thermophysical Properties of Fluid Systems," [Online]. Available: https://webbook.nist.gov/chemistry/fluid/. [Accessed 2022].

[16] Z. Yang, X. Ma, Y. Duan and Y. Chen, "Internal flow and heat transfer of a condensing water droplet in steam flow," *Chemical Engineering Science,* vol. 94, pp. 54-59, 2013.

[17] Zittau/Goerlitz University of Applied Sciences, "Fluid Property Calculator," [Online]. Available: https://web1.hszg.de/thermo_fpc/. [Accessed July 2022].

[18] U.S. Nuclear Regulatory Commission, *TRACE V5.0 Patch 5 Theory Manual: Field equations, solution methods, and physical models,* Washington, D.C., 2017.

[19] U.S. Nuclear Regulatory Commission, *TRACE V5.0 Patch 6 User's Guide, Volume 2: Modeling Guidelines*, Washington, D.C., 2019.

[20] U.S. Nuclear Regulatory Commission, *TRACE V5.0 Patch 6 User's Guide, Volume 1: Input Specification,* Washington, D.C., 2020.

INITIAL DISTRIBUTION LIST

1. Defense Technical Information Center
   Ft. Belvoir, Virginia

2. Dudley Knox Library
   Naval Postgraduate School
   Monterey, California